W. T. Webber

WADC TR - 59-50

R-1421

ASTIA AD-228 500

59

EFFECTS OF GAS MOTION ON HETEROGENEOUS COMBUSTION; NATURAL CONVECTION, STEADY FORCED CONVECTION, STANDING ACOUSTIC WAVES, AND SHOCK WAVES FINAL SUMMARY REPORT

WILLIAM T. WEBBER
ROCKETDYNE ENGINEERING

CONTRACT AF 33(616)-3556

APRIL 1959

PROPULSION LABORATORY
WRIGHT AIR DEVELOPMENT CENTER
AIR RESEARCH AND DEVELOPMENT COMMAND
UNITED STATES AIR FORCE
WRIGHT-PATTERSON AIR FORCE BASE
DAYTON, OHIO

PB 161128 $2.25
office of Technical Services
U.S. Dept. of Commerce
Washington 25, D.C.

FOREWORD

This report is a final summarization of heterogeneous combustion studies conducted at the Rocketdyne Propulsion Field Laboratory by the Physics and Processes Group of the Research Subdivision from June 1956 through December 1958 and is submitted in partial fulfillment of the requirements under Contract AF33(616)-3556.

The research was performed as WADC Project Number 6-(2-3058), WADC Task Number 70175. This task was administered under the direction of the Aeronautical Research Laboratory, Wright Air Development Center, Wright-Patterson Air Force Base, Ohio, with Mr. Everett Stephens acting as task scientist.

The author acknowledges the valuable assistance of the following persons: Frank B. Cramer for experimental and analytical work on the quartz fibre studies; Henry Friedman in programing the numerical model of combustion for the IBM 704 Data Processing Machine; Dr. R. B. Lawhead (Project Supervisor) and Dr. R. S. Levine (Group Leader) for helpful discussions and criticism throughout the project.

This report has been reviewed and approved by R. J. Thompson, Jr. (Manager Research). The technical editor was William C. Kaysing.

ABSTRACT

Two experimental techniques have been used to determine the effects of gas motion upon the combustion of liquid fuels under extremes of conditions resembling those found in liquid rocket combustion chambers.

In the first technique methanol was burned as it flowed down a vertical quartz fibre mounted in a pressure vessel containing pure oxygen at pressures from 1.0 to 10.2 atmospheres. The combustion rate was determined under conditions of natural convection, with steady forced flow transverse to the fibre; and with the fibre held at the velocity loop of a very strong standing acoustic field. The application of conventional heat and mass transfer correlations for cylinders give theoretical values for combustion rate which are in fairly close agreement with the experimentally observed data. Reynolds number (based on fuel element diameter) was varied from 340.0 to 5300.0. Grashof number was varied from 1.3 million to 340.0 million. In the acoustic field the Reynolds number was derived from the mean gas particle velocity.

The second technique was to burn sprays of liquid fuel in an oxygen atmosphere in the channel of a shock tube through which a pressure pulse was passed. Here the pressure, velocity, and temperature perturbations of the wave affect the combustion rate at the location of, and in the wake of the wave, and thus can act to sustain or augment the wave to the point where it resembles a detonation. Some experiments were conducted to determine which combinations of droplet size, initiating pulse amplitude, pulse duration, extent of combustion completed before introduction of the pulse, etc., cause the wave to grow to detonation strength, and which allow it to decay. Other experiments were conducted to quantitatively infer combustion rates as functions of wave strength, by measuring pressure histories at several positions along the tube. In these experiments, Reynolds numbers per centimeter ranged from about 150,000 to 1,500,000. Combustion rates increase with Reynolds number at about the proper slope to agree with classical correlations for heat and mass transfer up to Reynolds numbers per centimeter of about 450,000. Beyond this point there appears to be a sudden increase in rate.

PUBLICATION REVIEW

This report has been reviewed and is approved.

FOR THE COMMANDER:

TABLE OF CONTENTS

LIST OF ILLUSTRATIONS

SUMMARY

Basic combustion researches were conducted under Air Force Contract AF33(616)-3556, directed toward determining the effects of gas motion upon heterogeneous combustion. The researches were performed in two consecutive time periods and employed two principal types of experimental techniques. The first technique used was to burn methanol flowing down a quartz fibre in a pressurized vessel. The second technique was to burn sprays of liquid fuel in oxygen in the channel of a shock tube. The results obtained from the first technique have been published in considerable detail in WADC TN 57-426, and thus will only be briefly discussed here. The investigations using the shock tube will be covered in detail.

QUARTZ FIBRE STUDIES

Experimental Techniques

The burning of a quartz cylinder wetted with liquid methanol in a gaseous oxygen atmosphere was investigated for conditions of natural convection, steady transverse oxygen flows of 200, 600, and 1,000 cm/sec, and oscillating flows associated with resonant acoustic pressure oscillations in the test chamber ranging up to thirty percent of the average gage chamber pressure. Observations were made at chamber pressures ranging from 1.0 to 10.2 atmospheres.

A photograph of the test apparatus used in the experimental studies of heterogeneous burning is shown in Fig. 1.

Figure 2 is a schematic diagram of the test chamber and associated equipment. The effects of static pressure on propellant consumption (with no through flow of gas) are obtained with a steady bleed of gas through the exhaust port. Steady gas flows through the chamber are obtained by capping off the exhaust port and placing orifice plates in the pressure transducer boss. High-amplitude acoustic standing waves are obtained by interrupting the flow of pressurizing gas through the exhaust port with a perforated wheel driven by an electric motor (pulsing siren).

Figure 3 is a more detailed schematic of the fuel injection and ignition system.

As initially envisioned, the test procedure was to burn the test fuel as a drop suspended at the end of a quartz fibre so that there would be as close simulation as possible to a free burning droplet. It was found during preliminary testing that it was impossible to retain a drop on the fibre when the chamber was excited with the siren. The method of using the cylindrical burning surface was then developed and has proved to be moderately satisfactory. Even with this method there are tests in which the burning propellants are blown off the fibre.

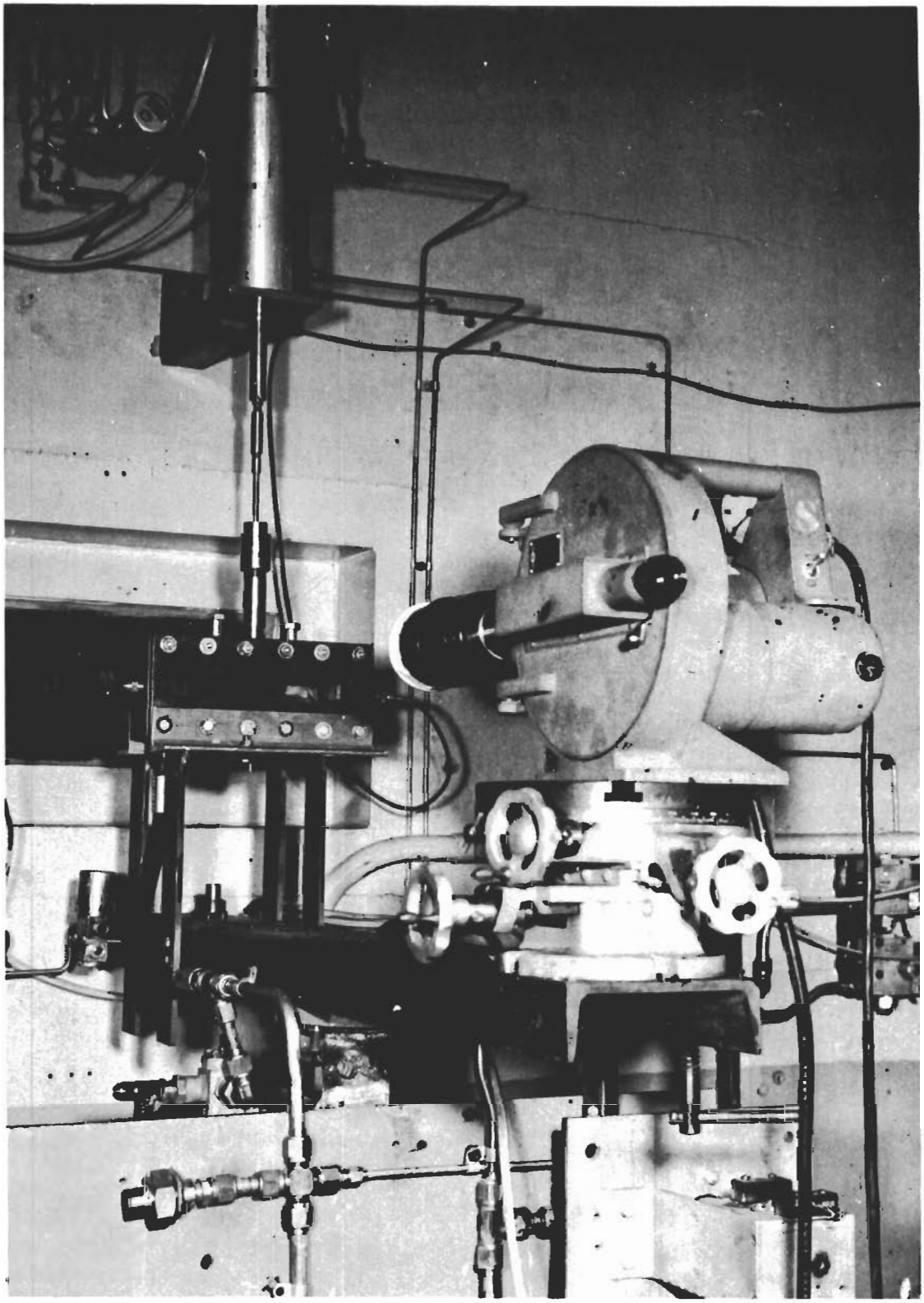

1254-7/9/7-S1A

Figure 1. Test Apparatus

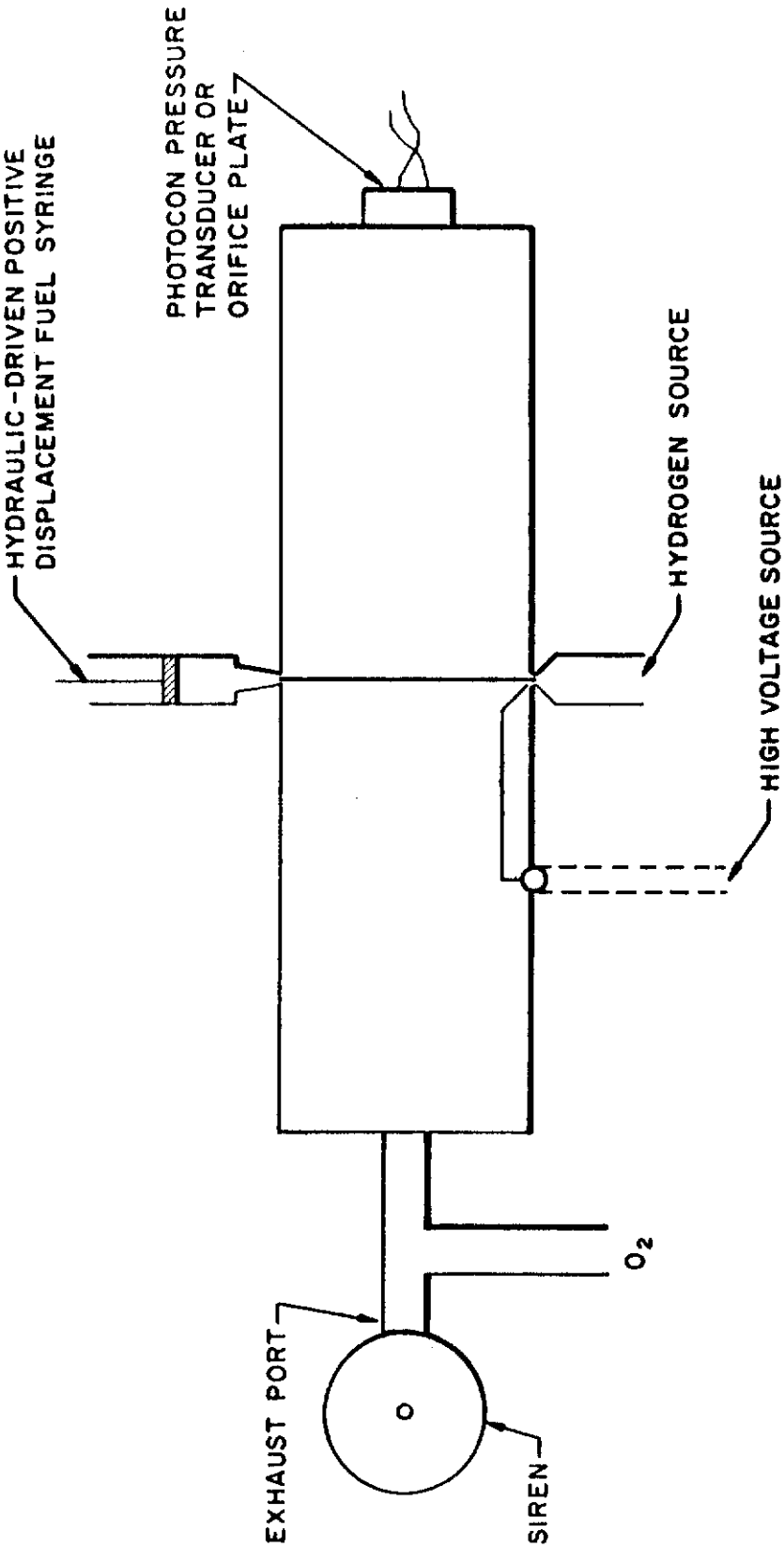

Figure 2. Schematic Drawing of the Heterogeneous Burning Apparatus

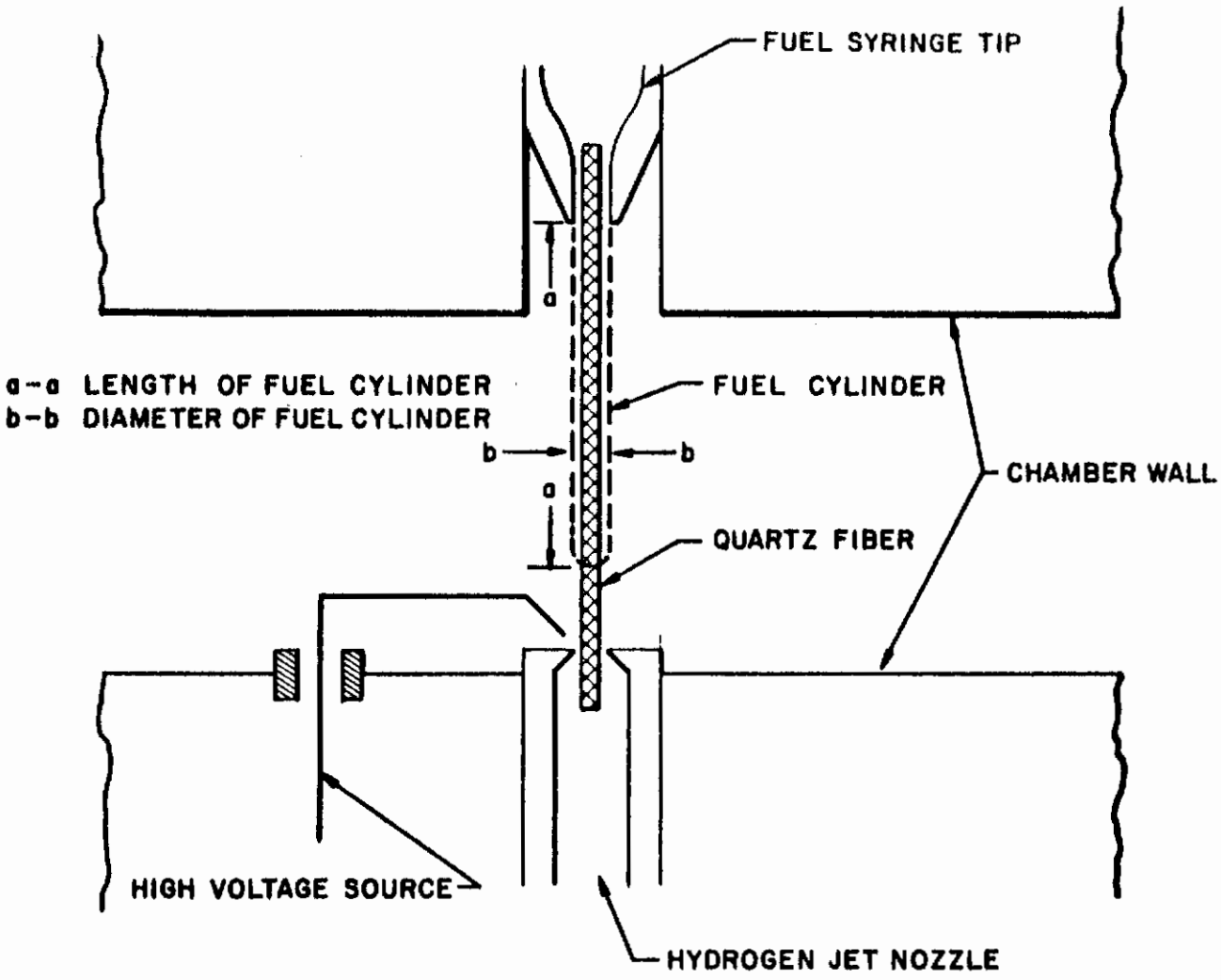

Figure 3. Details of Injection and Ignition System

The fibres used in the testing ranged from 350 to 500 microns in diameter and the fuel flowing down the fibre formed a cylinder having a total diameter of from 500 to 700 microns. The length and diameter of the fuel cylinder were determined from visual observation using a telescope mounted on a cathetometer. It was found necessary to assume that the diameter of the fuel cylinder would be the same for burning and nonburning conditions as there was not a sufficient usable test duration to permit accurate measurement of both length and diameter of the fuel cylinder before the fibre became grossly distorted. The fuel combustion rate was computed from the measured length and diameter of the fuel cylinder and the predetermined discharge rate of the fuel injection syringe.

Methanol was selected as the test fuel for these investigations because of its ability to wet the fibre, its ignitibility, and because its vapor pressure was sufficiently low to permit it to be retained in the syringe.

TEST RESULTS

In order to compare the experimentally observed consumption rates with analytically predicted rates, a conventional model of the combustion process was assumed as shown in Fig. 4 . There are several transport operations which are related to the consumption of fuel. Heat is generated at the flame front, a portion of which flows inward, evaporating the liquid fuel and heating the fuel vapor that is diffusing outward. Heat flows outward from the flame front while oxidizer diffuses inward to the flame front counter-current to the products of combustion which are diffusing outward.

Under stagnant conditions the equilibrium temperature and position of the flame surface and the various transport rates are all fixed by the geometrical transport relationships, the product transport properties, the flow, pressure, and the chemical composition of the fuel and gaseous oxidizer surrounding the burning fuel element. Under flow conditions the situation becomes hopelessly complicated; however, the average Nusselt and Sherwood numbers associated with the heat and mass transfer phenomenon may be expected to increase with almost identical functional relations to Reynolds number or Grashof number. Thus, it should be possible to relate overall mass consumption rate to Reynolds or Grashof numbers even without knowing the detailed intricacies of the individual combustion processes.

Combustion with Natural Convection

Under conditions where there was no externally forced flow in the vessel the hot gases generated by combustion tended to rise and ventilate the fuel element. These conditions are very similar to natural convection around a vertical heated cylinder (Ref. 1).

From standard correlations of heat transfer with Grashof number it follows for the combustion of methanol in oxygen (Ref. 2), limited in rate by the flow of heat necessary to evaporate the fuel, that the consumption rate per unit area of fuel surface should increase as the square root of pressure. Thus, for our apparatus, $N_f = 2.91 \times 10^{-4} P^{0.50}$ moles/cm^2 sec where N_f is the number of moles of fuel evaporated or burned per second per square centimeter of fuel surface area. Experimentally it was found that $N_f = 1.73 \times 10^{-4} P^{0.52 \pm 0.04}$ moles/cm^2 sec. The small

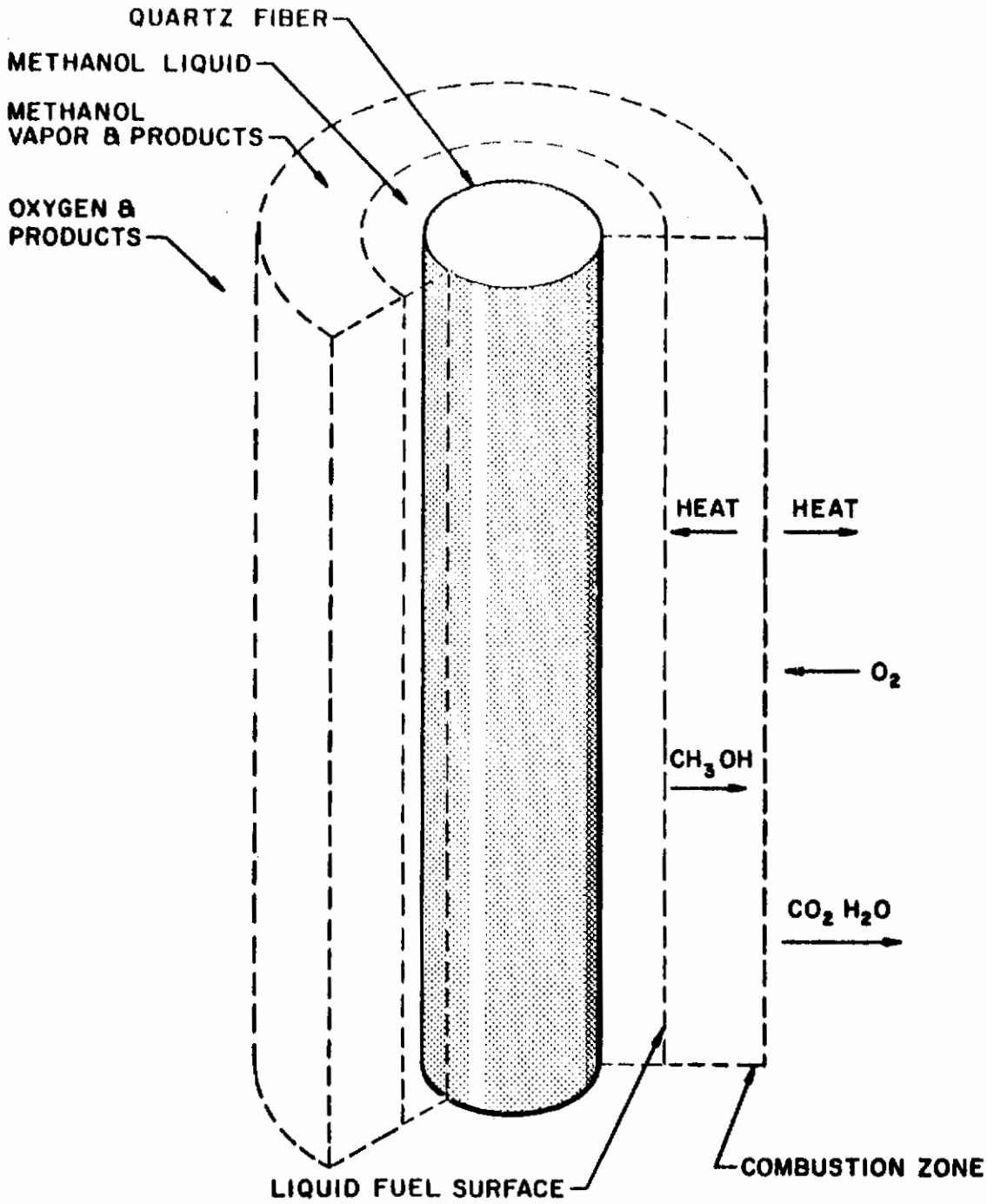

Figure 4. Combustion Model

difference in coefficients is understandable in view of the differences between combustion and nonreactive heat transfer (Fig. 5).

Combustion with Steady Forced Convection

The mass consumption rate of an evaporating or burning fuel element is related to several simultaneous mass and heat transfer operations, any one of which may be used to describe the consumption rate. The choice of defining parameters is generally governed by the necessity of estimating or measuring the required boundary conditions. For the no-flow conditions in the preceding section where the flame surface may be presumed to be relatively far from the fuel surface, a heat transfer model seems most appropriate. For the case of forced convection where the flame surface may be presumed to lie very close to the fuel surface, an oxidizer diffusion model appeared to be more suitable.

Two different correlations were taken from the published literature for transfer processes for a cylinder with forced transverse flow (Refs. 1 and 3). These yielded the theoretical consumption rate correlations (for methanol in oxygen):

$$N_f = 0.26 \times 10^{-4} (Re)^{0.58}$$

and

$$N_f = 0.45 \times 10^{-4} (Re)^{0.50}$$

The consumption rate was experimentally determined at three pressures and three gas velocities. The experimental values were correlated by the expression:

$$N_f = 0.23 \times 10^{-4} (Re)^{0.60 \pm 0.15}$$

Thus, theory and experiment are in agreement within the range of experimental error. These three curves are shown on Fig. 6.

Combustion in a Standing Acoustic Wave

Combustion rates were measured while the pressure vessel was strongly excited in its first longitudinal mode (1000 cps). Very high-amplitude pressure amplitudes were measured at the chamber end. Maximum attainable peak-to-peak amplitudes ranged from 21 percent to 25 percent of the mean absolute pressure in the vessel. According to classical acoustic theory the center of the chamber should be a position of no-pressure oscillation and maximum velocity oscillation; however, there is considerable doubt as to the applicability of classical acoustic theory at these high amplitudes.

If, as a first approximation, the classical acoustic expressions are used for the chamber, it is possible to compute a Reynolds number based upon the time-average

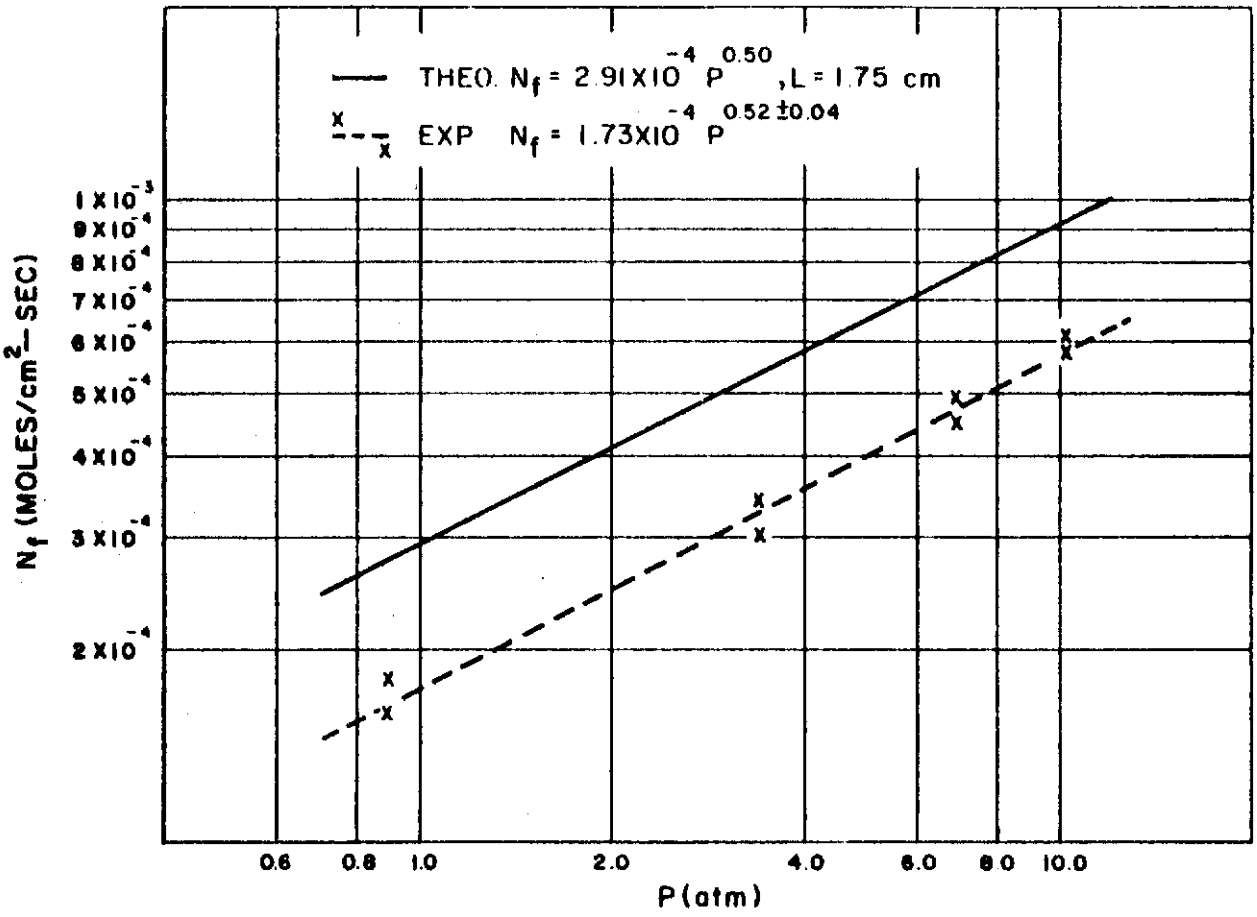

Figure 5. Consumption Rate for Cylinder of Methanol Burning in Oxygen With No Through Flow

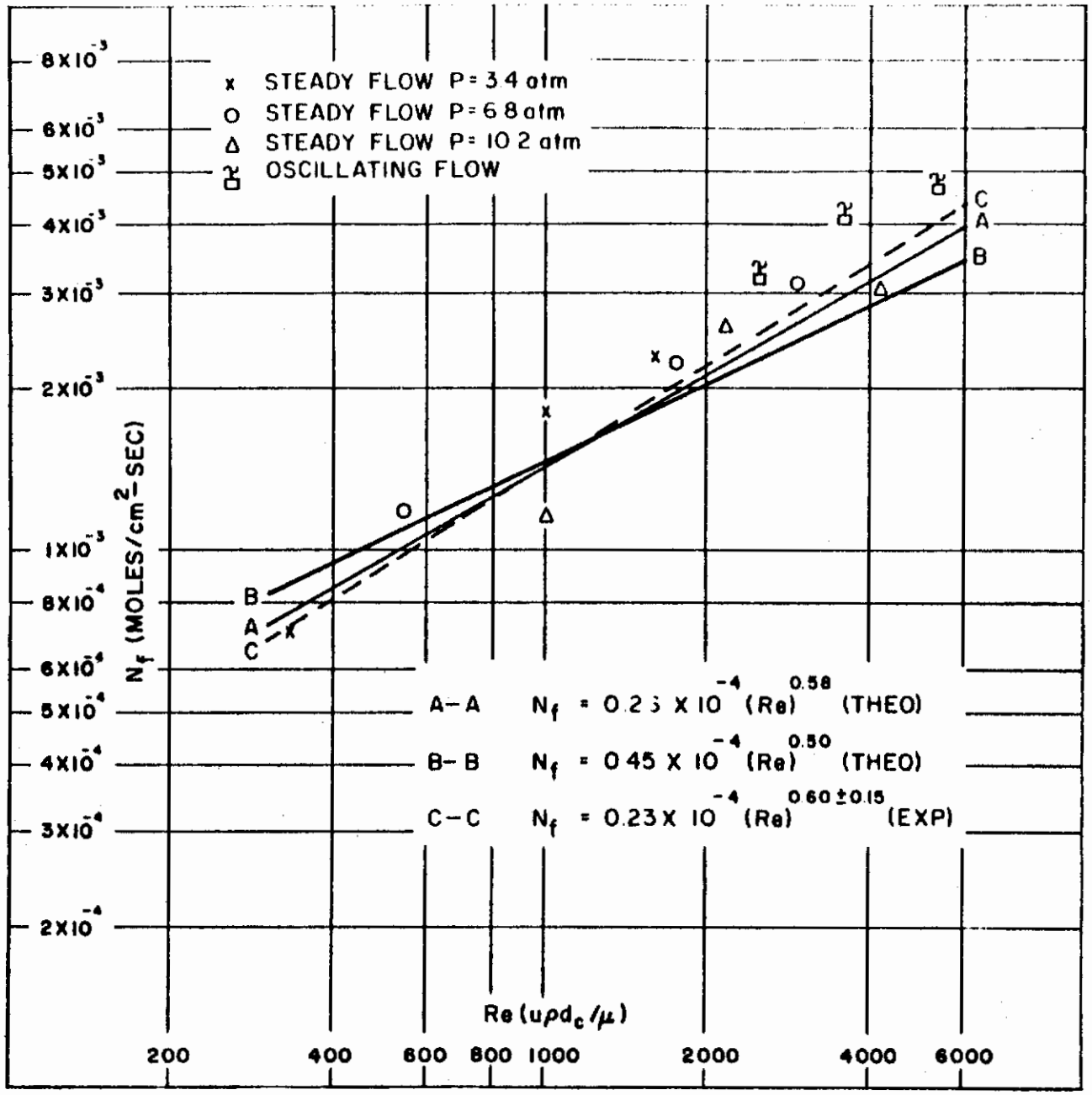

Figure 6. Consumption Rates for Methanol Cylinder With Steady and Oscillating Flows

gas particle speed. Thus, $\bar{u}$ the average particle speed at a velocity loop for a sinusoidal wave is

$$\bar{u} = \frac{P_{max}}{\pi \rho c}$$

where

P_{max} = peak-to-peak pressure amplitude measured at a pressure loop

ρ = gas density

c = local velocity of sound

Then Reynolds number is

$$Re = \frac{P_{max}\, dc}{\pi \mu c}$$

where

dc = cylinder diameter

μ = gas viscosity

A more general form is

$$Re = \frac{k\, P_{max}\, dc}{\mu c}$$

where k depends on the waveform, and is $1/\pi$ for a sinusoid, $1/4$ for a triangular wave and $1/2$ for a square wave.

When combustion rates experimentally measured in the acoustic field are correlated with this Reynolds number the relation is obtained:

$$N_f = 1.4 \times 10^{-4} (Re)^{0.41 \pm 0.30}$$

Statistical analysis of the data shows a large possible variation in the exponent. This is due primarily to the small amount of data and can be expected to be much smaller as additional points are obtained. These data points are plotted on Fig. 6 where it is interesting to note that they lie fairly close to the combustion rates obtained with steady flows at the same Reynolds numbers.

SHOCK TUBE STUDIES

Sprays of RP-1 (a kerosene-type fuel), heavy mineral oil, and several other hydrocarbons and alcohols were burned in an oxygen atmosphere in a 2-inch diameter shock tube 8 feet long. Except for the difficulty of obtaining nondetonative

ignition with fuels which are too volatile, and except for erratic behavior with fuels whose viscosity changes appreciably with ambient temperature variations, all the fuels behaved about the same.

Igniting the spray of fuel in oxygen at a closed end of the tube or at the center of an open-ended tube causes spontaneous detonation.

Sprays of fine droplets were more readily detonated than sprays of coarse droplets; i.e., a pulsing amplitude corresponding to approximately a 10-psi driver pressure is required to induce detonation of a spray of relatively large droplets produced with 3/32-inch non-impinging orifices while sprays of smaller droplets detonate spontaneously with no initiating pulse whatsoever. If very viscous fuels are sprayed into the tube under the same conditions as less viscous fuels, poorer atomization is attained and higher pulse levels may be sustained without initiating detonation. If the gas used to force the liquid through the injector is allowed to flow appreciably after the injectors have been emptied, causing fine gas-atomization, the detonation occurs spontaneously upon ignition.

Allowing an appreciable portion of the injected fuel to burn smoothly before pulsing the tube reduces the amplitude of the detonation produced, and a higher pulse amplitude is required to initiate detonation. In these last two respects the shock tube is similar in behavior to large liquid fueled rocket engines. When experimental liquid fueled rocket engines are pulsed to initiate a transverse mode of combustion instability, a larger pulse is required if it is applied at a downstream location where combustion is partially accomplished than if the pulse is applied near the injector where there is more unburned propellant. Similarly rocket motor injectors which produce coarsely atomized propellant are less conducive to transverse acoustic modes of combustion instability than those which produce finely atomized propellant.

The duration of the gas flow following the shock front (varied by changing the length of shock tube driver section) was found to have only a very slight effect on the amplitude of pulse required to initiate detonation.

Tests in which coarse, nonburning sprays of kerosene in oxygen are detonated by initiation with an exploding portion of hydrogen-oxygen mixture, demonstrate that it is not necessary to have vaporized or partially combusted intermediate material present in order to support detonation.

The effects of the wave perturbation upon combustion rate may be inferred by examining wave histories analytically or by comparing experimental pressure profiles with profiles computed using a numerical technique to approximate the wave action in the gas.

At Reynolds numbers per centimeter between 150,000 and 450,000, specific combustion rates measured in the shock tube appear to increase with Reynolds number with about the same relationship as the classical correlations for heat and mass transfer. At Reynolds numbers per centimeter above 450,000, specific combustion rate appears to increase very rapidly, being proportional to Reynolds number raised to the 1.46 power. This rapid increase in combustion rate may be due to a rapid increase in the rate at which the droplets are being shattered in the high-velocity gas stream.

It has been found possible to construct a numerical model of the wave and combustion interaction found in the shock tube which is soluble on an electronic data processing machine. This model may include the effects of nonlinear pressure-volume relationships for the gas, mass addition following any of several functional relations, attenuation due to shear at the walls, etc.

The numerical technique is simply to regard the gas as a series of adjacent free bodies, and compute the sequential positions and velocities by numerical double integration of the accelerations due to the pressure gradients, drag, and other forces. The gas state and mass addition may be any desired mathematical function of the chosen parameters. This model may eventually be varied so as to fit the experimentally measured pressure profiles. The preliminary computations performed so far have been for a tube of constant cross-section divided into 20 to 100 axial segments. Computational time intervals as small as one-hundredth of a millisecond have been found necessary to avoid undesirable arithmetical instability. The computations are performed on an IBM 704 Electronic Data Processing Machine. The data presentation is by printer and by photographing a cathode ray tube upon which the data are plotted in an analog presentation.

II

INTRODUCTION

"Acoustic" modes of combustion instability have been shown by many investigators to be most troublesome in the development of large-thrust rocket engines. Thus, the studies under the subject contract were focused on the further elucidation of the basic physical processes capable of initiating or sustaining the "acoustic" resonances of rocket thrust chambers assuming that the combustion could be considered as a system of fuel droplets burning in a gaseous oxidizer. The assumed model of individual fuel droplets burning in gaseous oxidizer was shown to be reasonable in the Summary Report describing the first phase of the current studies (Ref. 2).

Present knowledge of the phenomena which occur in the liquid fueled rocket combustion chamber indicates that the steps which act to limit and determine the combustion rates are the mass and heat transfer processes which are associated with the individual liquid propellant droplets. Several attempts have been made with fair success to model the steady-state combustion of liquid propellant rocket engines using the classic knowledge of these processes (i.e., Refs. 4, 5, 6, 7, 8, 9, and 10). The low-frequency instability of a rocket engine has also been modeled in a somewhat similar manner (Ref. 11). These computations use known or assumed values for drag coefficients, relation of Nusselt Number to Reynolds Number, initial droplet size, evaporation coefficients, gas state equations, momentum and energy-relations, etc. Similar computations have not as yet been attempted for the oscillatory wave action which can also occur in the thrust chamber; however, here also, the phenomena must follow many of the same physical relationships. The relation between combustion rate of a homogeneous combustible material and a traveling pressure wave, however, has been investigated for the purpose of modeling the initiation of detonation in a solid propellant (Ref. 12), and the ignition process in the chamber of a gun (Ref. 13).

The passage of a strong pressure wave through the material in the combustion chamber of a liquid propellant rocket engine produces certain changes in conditions which may influence the combustion rate. If this alteration in the combustion rate is of sufficient magnitude and is properly timed with respect to the pressure perturbation, then the wave can be sustained or enhanced. Processes which could conceivably affect the rate of heterogeneous combustion are:

(1) A pressure-sensitive propellant burning rate;

(2) A velocity-sensitive burning rate, where the heat and mass transfer processes are hastened by gas motion past droplets of propellant;

(3) Velocity-sensitive shattering of propellant droplets giving increased burning surface;

(4) Changes in local propellant distribution and mixing due to the relative displacement of

different size propellant droplets or vapor in the acoustic field; and

(5) Temperature-sensitive burning rate where combustible material reacts rapidly following the temperature rise behind a shock wave.

The program of study under the current contract has cast light on the first three of the above items. Item 4, which has been shown to be important in determining the sensitivity of a system to initiation of instability and the final amplitude of the oscillations cannot be properly evaluated except in actual model thrust chambers. Item 5 is probably a small effect when compared to the first three for the case of heterogeneous combustion at least for the pressure ratios of 2 to 3 (ratio of maximum to minimum pressure attained in a cycle) which are observed in unstable rocket combustion.

III

SHOCK TUBE

TEST APPARATUS AND TECHNIQUES

The shock tube shown in Figs. 7 and 8 was designed to facilitate the study of the interaction of pressure waves and heterogeneous combustion.

The tube is a two-inch-diameter cylinder, eight feet long, with bosses to accommodate high-speed instrumentation at intervals (1/4, 1/2, 1, 2, 4, 6, and 8 feet from diaphragm) along the length of the tube. Also, along the tube are four injectors for introducing liquid sprays. One set of injectors has single 3/32 (0.938)-inch-diameter holes. Another set of injectors has two 0.0664-inch holes each, while a third set has four 3/64 (0.0469)-inch holes (Fig. 9), thus each of the injectors has the same total hole area.

The measured amount of liquid to be injected (2 ml per injector in most of the tests) is placed in the axial passage and then blown into the tube by opening the solenoid-and pilot-actuated valve leading to the small (80 cc) pressurized nitrogen reservoir. After the experimental work was well-advanced it was discovered that this valve introduced considerable variation into the injection process. The valve was temperature-sensitive, allowing larger or smaller quantities of nitrogen to escape through a third port which was presumably always closed. This port was eventually capped off. The worst variation in the injection process was associated with "gas-atomization." As initially adjusted, the atomizing gas pressure decayed to insignificance just as the last of the liquid left the injectors. When this was not the case, a blast of gas could follow the injected liquid causing very fine atomization of the last of the liquid injected.

Such irreproducible "gas-atomization" generally caused spontaneous detonation of the tube contents upon ignition, and in any case, was probably responsible for the occasional fits of irreproducibility of the tube. The use of an injector having a floating piston separating the injection gas from the fuel (Fig. 10) would obviate such problems.

Early high-speed motion pictures taken of the injection process through the single-hole injectors showed that adequate atomization, without appreciable "gas-atomization," was obtained with 100 to 110 psi pressure of nitrogen in the 80.0 cc injection gas reservoir (Fig. 11). Under these conditions almost all of the liquid in the injector was injected in a time interval of approximately 30 milliseconds. Figure 12 shows the condition of the spray at a time approximately 70 milliseconds after the electrical signal is sent to the solenoid valve. It is clear that there is a clump of poorly atomized fuel at the head of the stream, followed by better atomized material. This is more apparent in Figs. 12B and 12C which are photographs of the liquid spray as it passes a fiducial mark about one foot from the injector using RP-1 injected from the single-hole injector with 100 to 110 psi injection gas pressure. The reference mark is 1/16 inch (1520.0 microns) in diameter. Figure 13 illustrates the effects of hole size and liquid

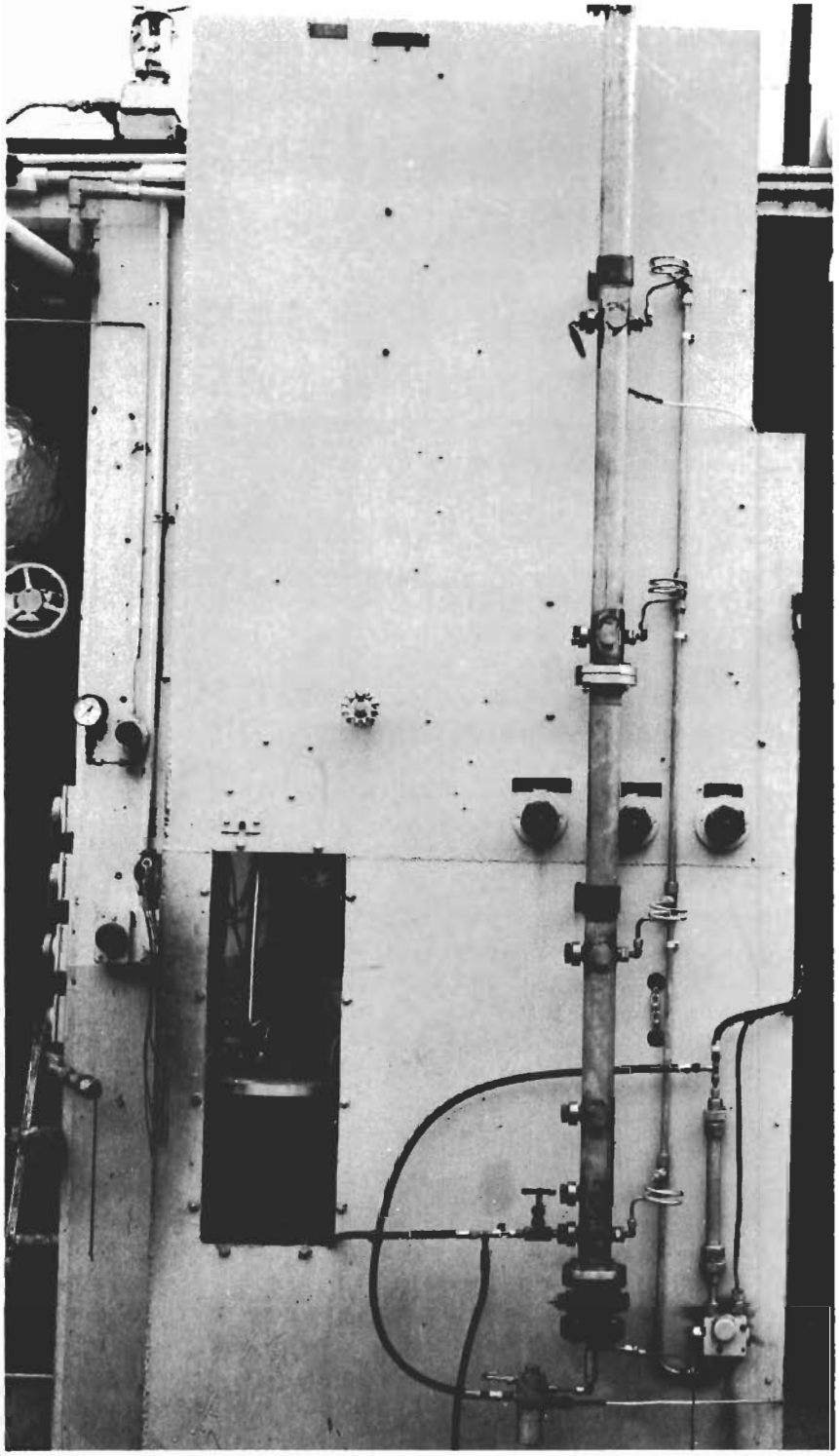

1254-11/24/8-S1

Figure 7. Shock Tube Installation

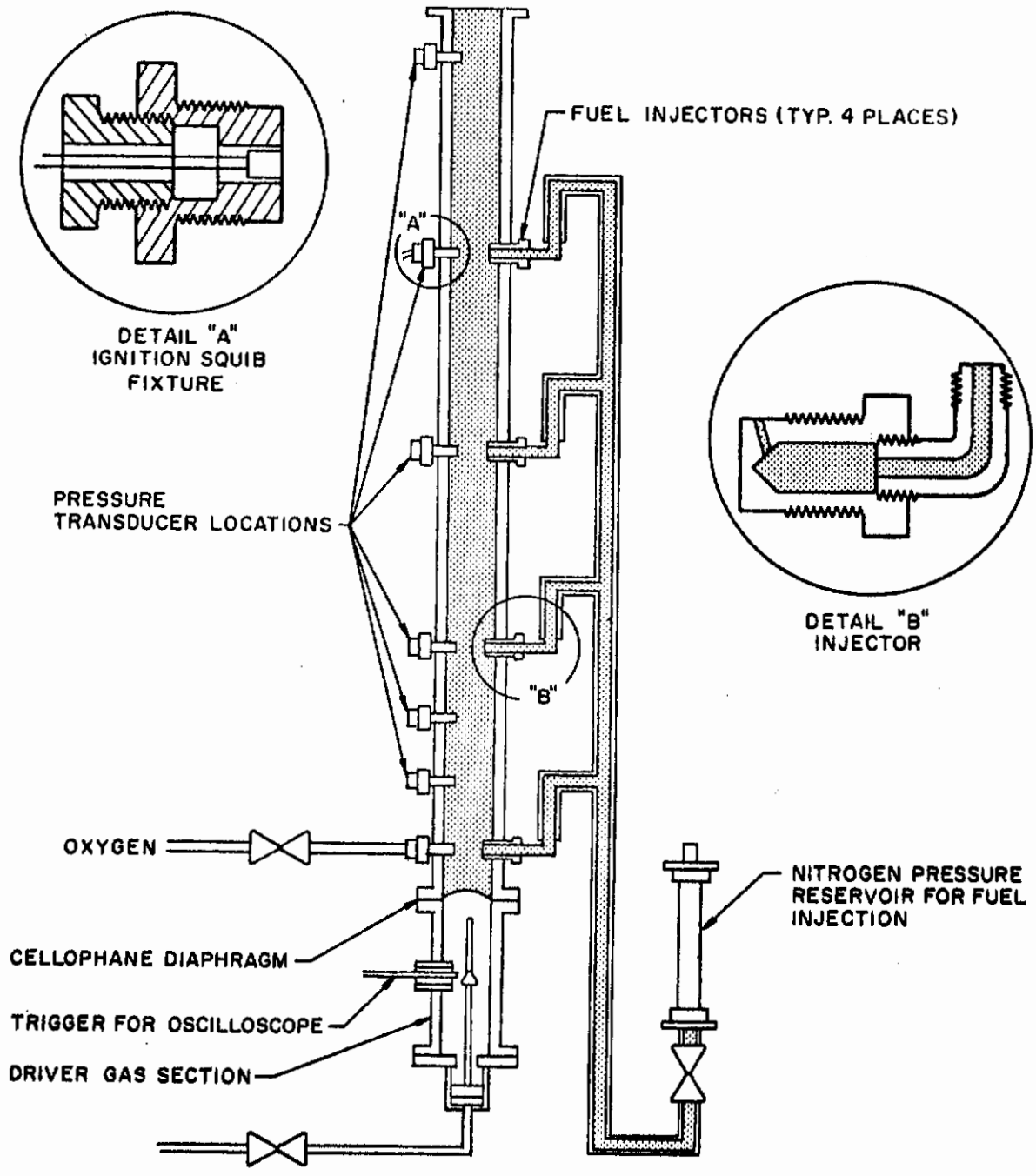

Figure 8. Schematic of Shock Tube Installation

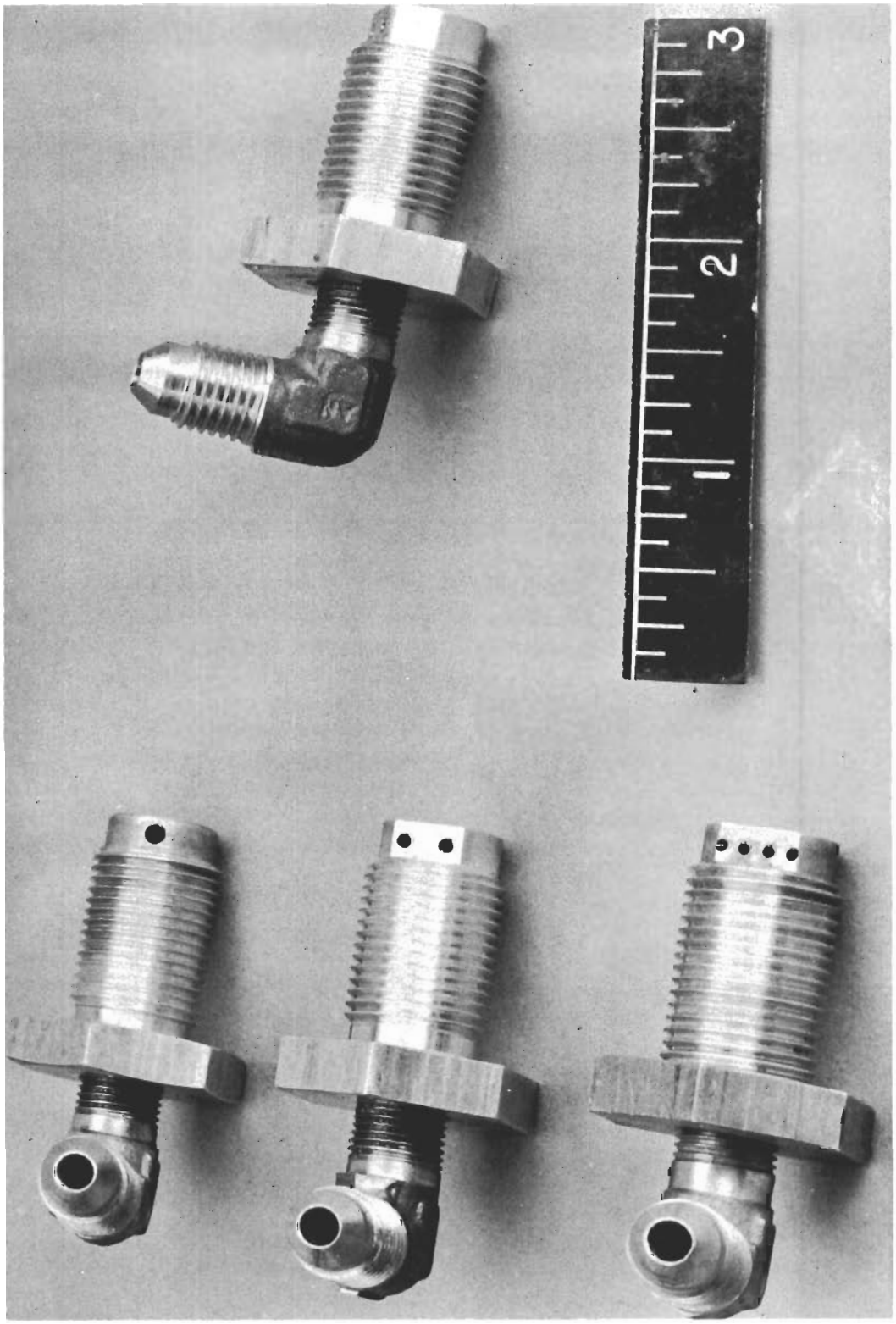

1254-11/24/8-S2C

Figure 9. Liquid Spray Injectors

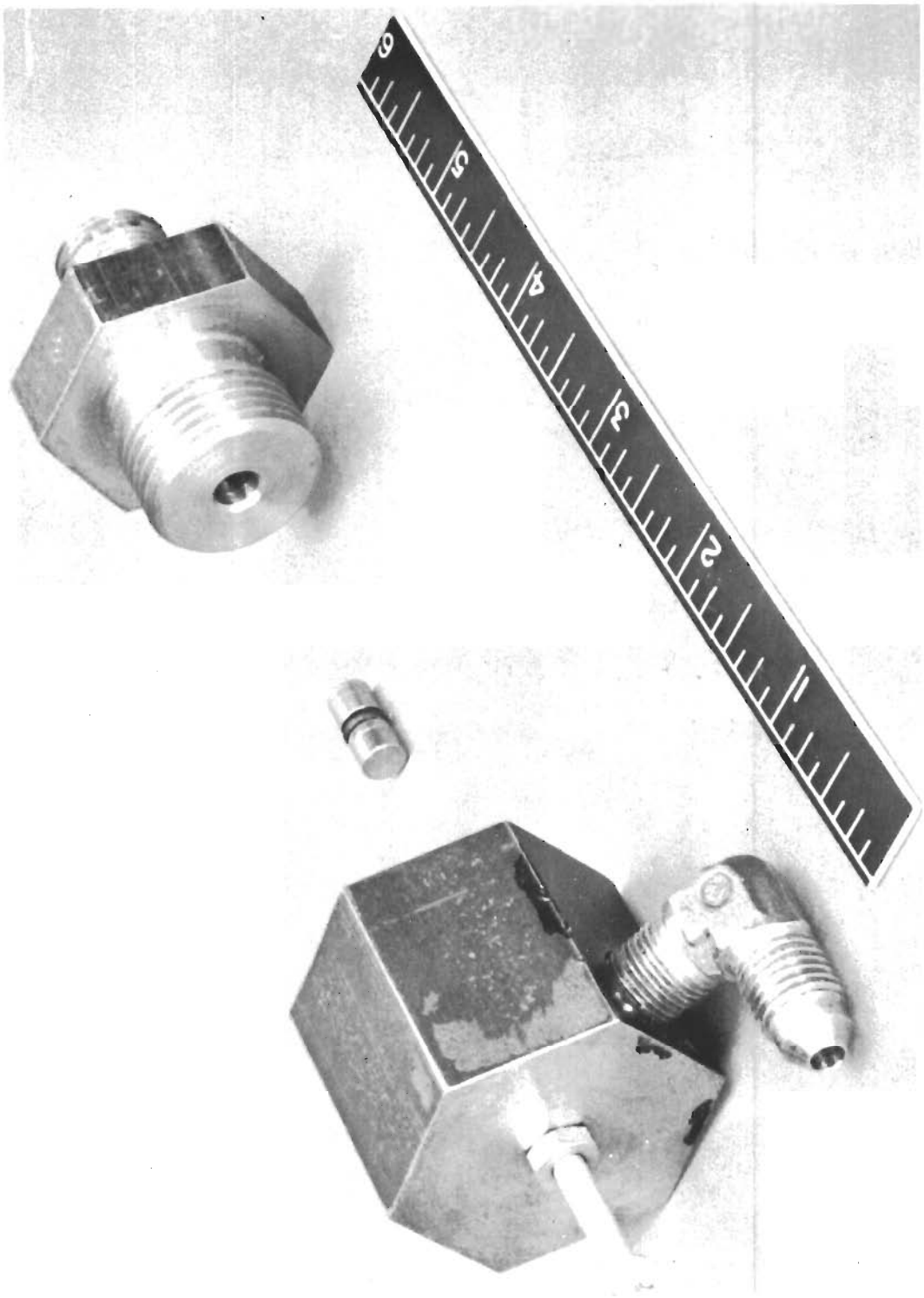

Figure 10. Floating Piston Fuel Injector Assembly

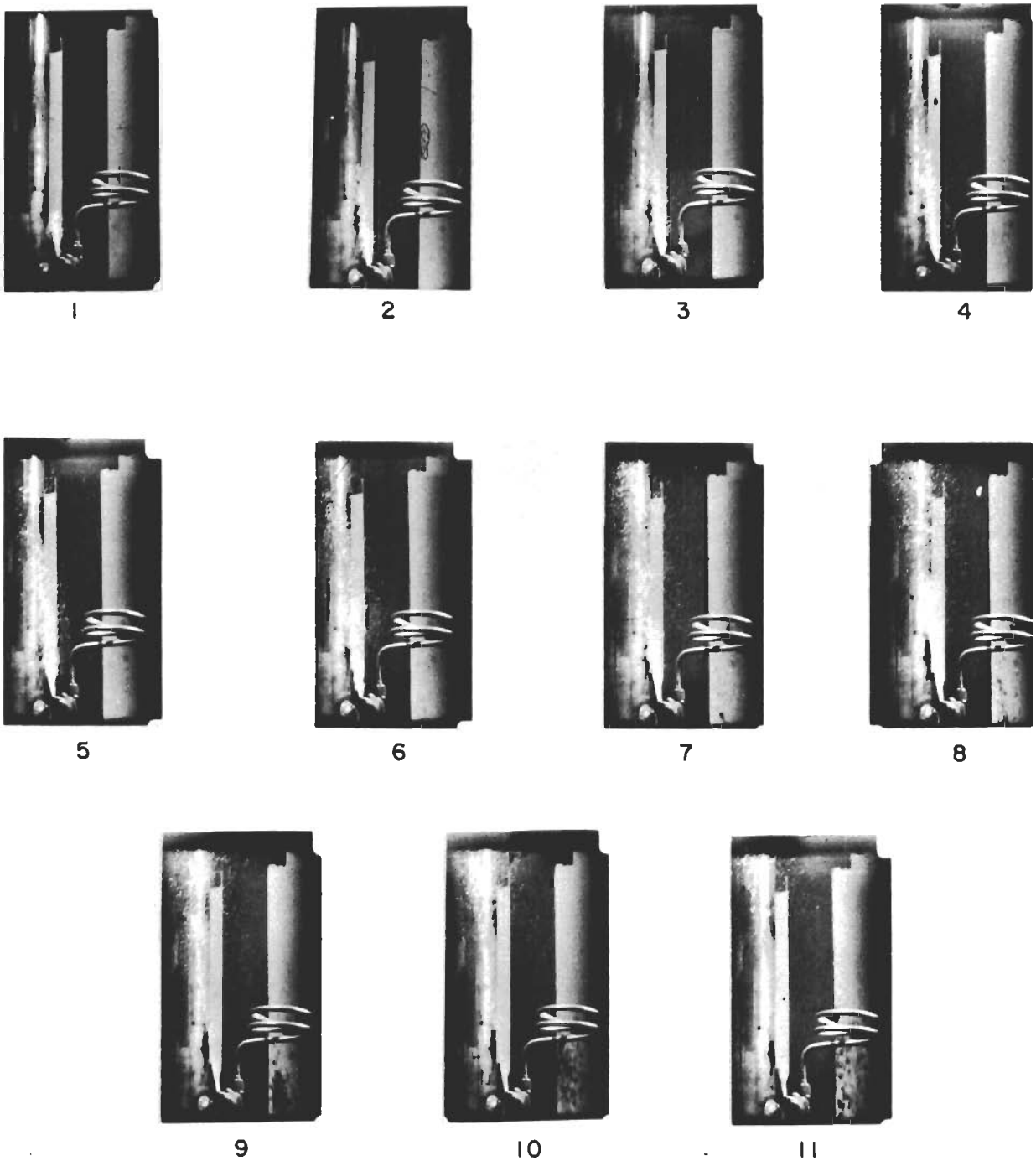

Figure 11. Spray Formation by Fuel Injector (one-hole injector; water, 100 psi; injection pressure, 4.3-ms interval between frames)

A. OVERALL VIEW OF RP-1 SPRAY FROM 1-HOLE INJECTOR — 70 MILLISECONDS AFTER START OF INJECTION, 100-110 PSI INJECTION PRESSURE.

B. RP-1 SPRAY FROM 1-HOLE INJECTOR. 100-110 PSI INJECTION PRESSURE — HEAD OF STREAM.

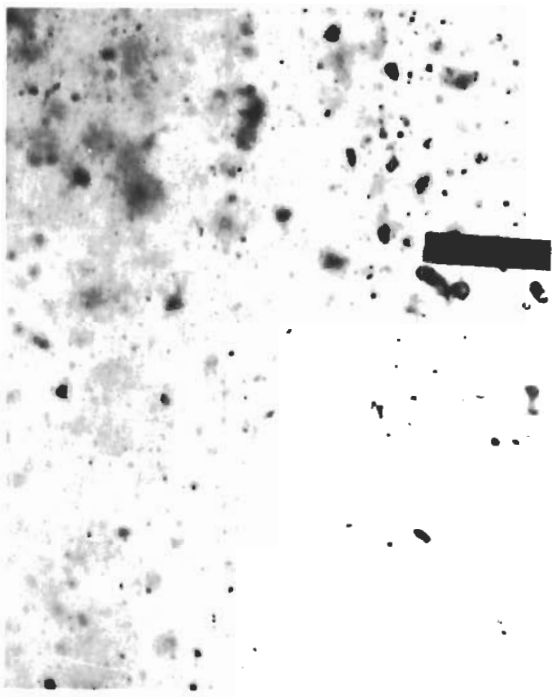

C. RP-1 SPRAY FROM 1-HOLE INJECTOR. 100-110 PSI INJECTION PRESSURE — FURTHER DOWN IN STREAM.

(The Reference Mark is 1/16 in. (1520 Micron) in Diameter)

Figure 12. Spray from Injectors

A. RP-1 SPRAY FROM 2-HOLE INJECTOR. 100–110 PSI INJECTION PRESSURE.

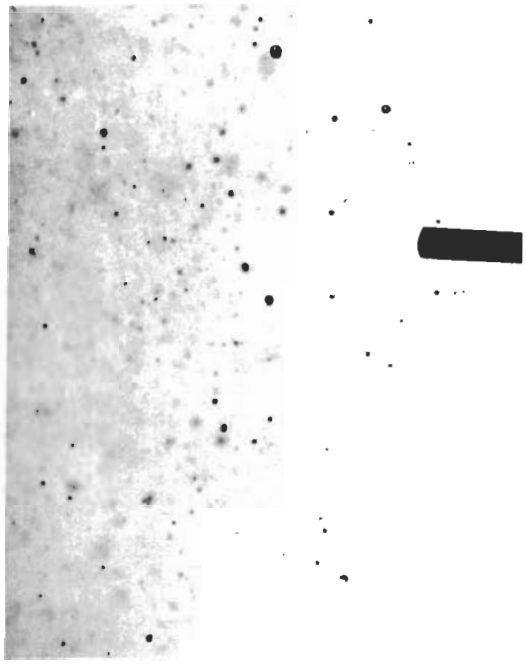

B. RP-1 SPRAY FROM 4-HOLE INJECTOR. 100–110 PSI INJECTION PRESSURE.

C. MINERAL OIL SPRAY FROM 1-HOLE INJECTOR. 100–110 PSI INJECTION PRESSURE.

D. MINERAL OIL SPRAY FROM 1-HOLE INJECTOR. 100–110 PSI INJECTION PRESSURE.

Reference Mark is 1/16 in. (1520 micron) in diameter

Figure 13. Spray from Injectors

viscosity upon droplet atomization. A "mean droplet diameter" is rather difficult to define for such a transient injection process where many of the fuel particles are nonspherical and where extent of subdivision seems to depend upon both distance from the injector and elapsed time after initiation of injection. A better method of fuel atomization, which would evenly distribute droplets of a known size distribution would make analysis of the ensuing processes much easier. In fact, if the shock tube were once calibrated with droplets of known size it could then be used to determine effective mean sizes of unknown sprays in terms of their combustion rates. If the transient flow atomization process used here resembles the more commonly described steady-state atomization process, then the final mean droplet diameters should be proportional to the orifice diameter of the injection elements, and the mean droplet diameters produced by the 1-, 2-, and 4-hole injectors should stand in the ratios of 2, $\sqrt{2}$, and 1. The 2- and 4-hole injectors, however, appeared to suffer from considerable re-agglomeration of atomized material.

If the combustion in the tube is to take place in an oxidizing atmosphere other than air, then the desired gas is passed through the tube for a few minutes previous to injection of the fuel. In almost all cases the gas used was pure oxygen.

The spray of fuel droplets is ignited with a small pyrotechnic squib which is electrically fired at the same time the fuel is injected. The squib, and the fixture which holds it, are illustrated in Fig. 14. Two types of ignition squibs were used during the course of this investigation. The E-32 or EB-2 have a burning time of only 20 or 30 milliseconds and throw a shower of hot sparks into the tube. The PA-1 burns quietly with a candle-like flame for 2 or 3 seconds without the ejection of any particulate matter.

At a timed interval after injection and ignition, a pressure pulse or shock wave may be passed through the burning mixture from one of several available driver sections (Fig. 15).

Two general types of driver sections are used with the shock tube. One is merely a one-inch extension to the tube which may be sealed off from the remainder of the tube with a cellophane diaphragm. The one-inch-long cavity is filled with an explosive mixture of oxygen and hydrogen gases which is initiated with a spark plug and ignition coil. This means of initiation of detonation may be used without previous ignition of the fuel-oxygen mixture if desired, as it furnishes ignition as well as a pressure pulse.

The other type of driver section used is assembled from a series of various length extensions (to vary shock duration) which may be fitted to the end of the detonation tube and separated from it with a sheet of cellophane or other suitable diaphragm material. The driver section is pressurized to the desired level and at the desired time the diaphragm is punctured by a pneumatically actuated rod (Fig. 15). As the resulting pressure wave passes up the tube, a suitable triggering device may be used to initiate the sweep of an oscilloscope which is photographed to record the pressure history measured by a photocon pressure pickup mounted at one of the several downstream stations. The electrical outputs of the pressure pickups are compensated with an on-line analog computer (the DADEE) to remove the effects of the mass and friction of the moving elements in the pickup and thus to yield a true picture of the driving function. This effect is illustrated in Fig. 16.

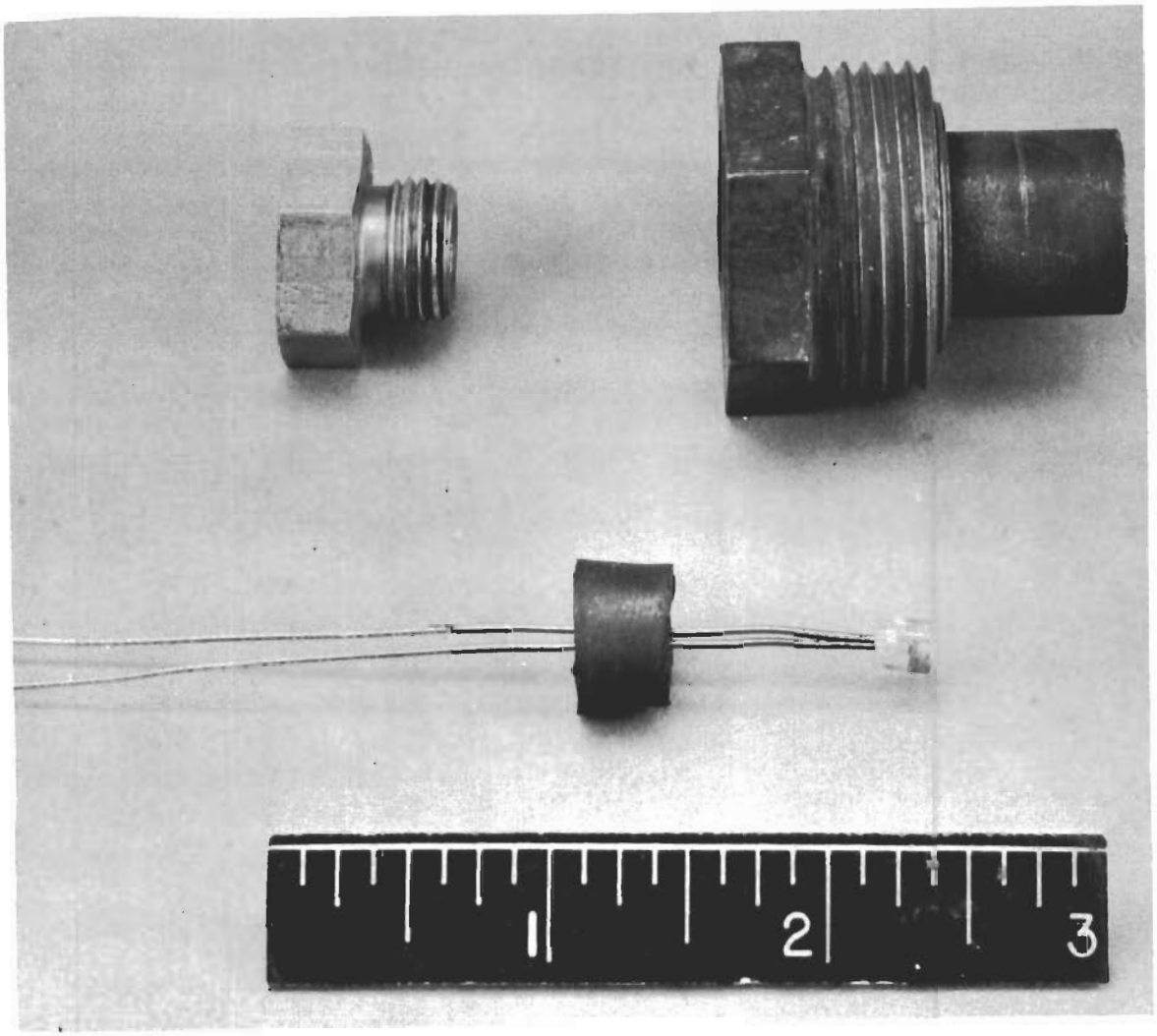

1254-11/24/8-S2B

Figure 14. Squib and Fixture

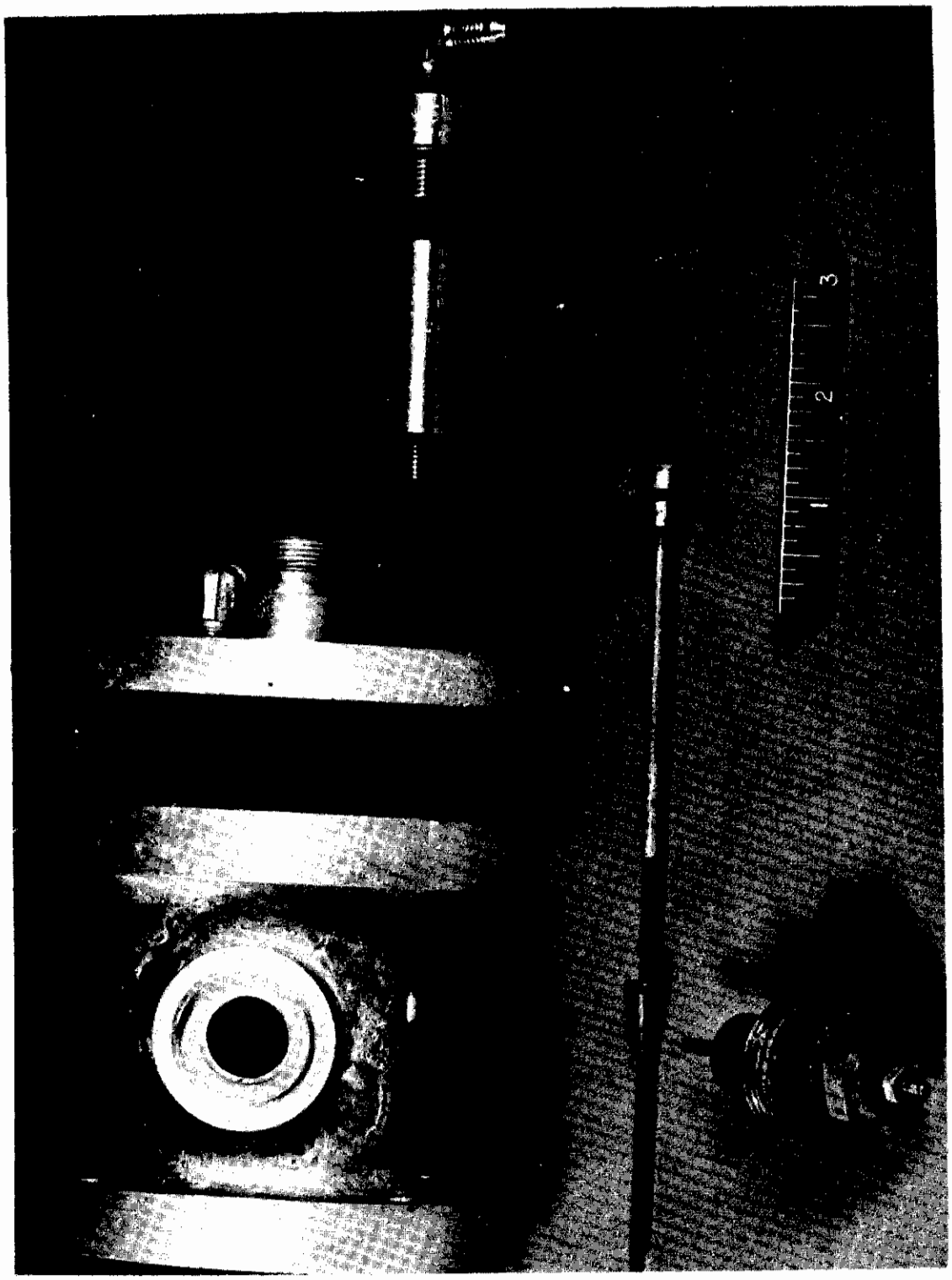

1254-11/24/8-S2A

Figure 15. Exploded View of Driver Section

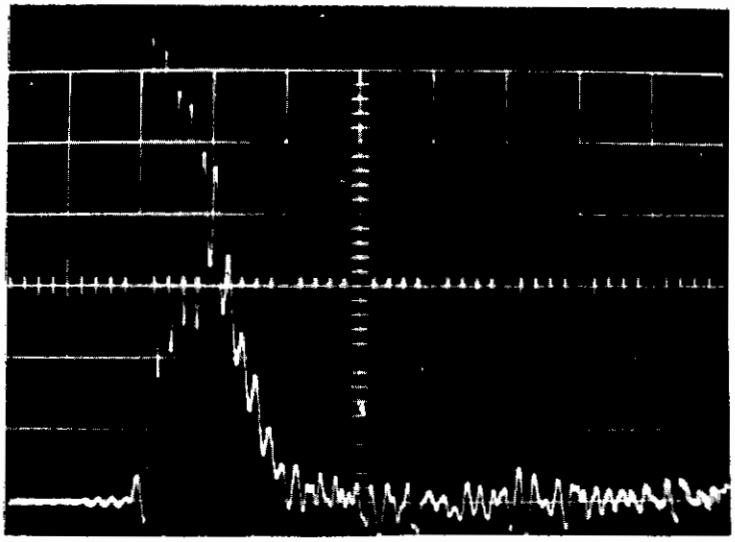

UNCOMPENSATED OUTPUT OF PRESSURE PICKUP EXPOSED TO SHOCK ONE FOOT DOWNSTREAM OF DIAPHRAGM. 13 PSIA INITIAL AIR PRESSURE BEFORE PASSAGE OF SHOCK WAVE. 23. PSIA AIR PRESSURE IN 4.0" LONG DRIVER SECTION.

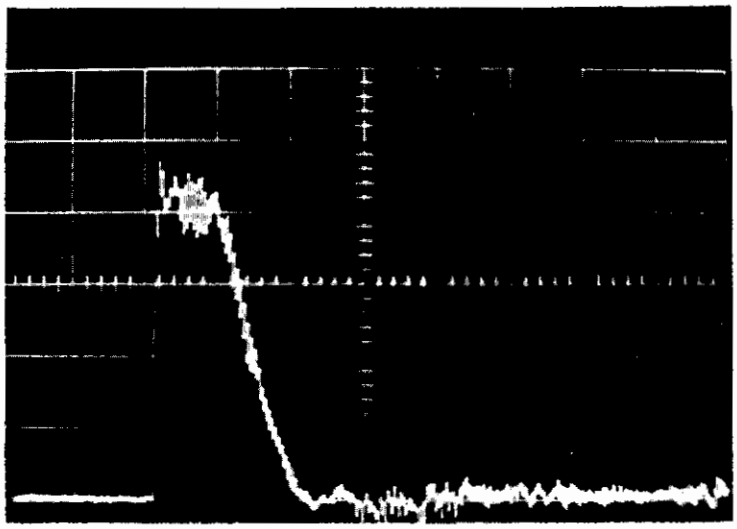

SAME CONDITIONS AS ABOVE EXCEPT FOR COMPENSATION OF PICKUP OUTPUT BY DADEE. SCALE: ONE PSI PER VERTICAL DIVISION. 1/2 MILLISECOND PER HORIZONTAL DIVISION.

Figure 16. Effect of Compensation Upon Pressure Pickup Output

Placing the pickup at different locations along the tube during successive tests permits the velocity and the growth or decay of the wave to be measured. The recordsobtained for the passage of pressure pulses (initiated by detonation of a stoichiometric hydrogen-oxygen mixture in a driver section one-inch long) through dry air, a spray of water in air, and a spray of RP-1 (a kerosene-type fuel) in oxygen are illustrated in Figs. 17and 18. The pulse history at stations one, two, four, six, and eight feet from the diaphragm are shown. It is observed that the pulse attenuates in passing through dry air or a spray of water in air, but is considerably enhanced in passing through the spray of RP-1 in oxygen. This enhancement would be expected if the action of the wave were to markedly accelerate combustion at the position of, and in the wake of the pressure-velocity-displacement-temperature perturbations which constitute the wave. The distance-time relations of these waves are plotted in Figs. 19, 20, and 21. The scatter in the time-distance plots would probably be decreased if all the points were taken in a single firing instead of in successive firings of the tube since the oscilloscope trigger was not precisely reproducible.

OBSERVED PHENOMENA

When a spray of liquid fuel is burned in oxygen in the detonation tube, one of two rather clearly defined phenomena occurs. Either the fuel burns quietly at about the normal rate for single stagnant droplets or else it detonates with a loud report producing pressures as high as 500 psi with the steep-fronted wave moving at velocities in excess of Mach 1.0.

Detonation may be induced by igniting any spray of fuel in oxygen at the closed end of the tube. Having the end completely closed produces detonation as does a partial closure having an opening area about 10 percent of that of the tube. Igniting at a closure consisting of a sheet of cellophane with a burst pressure of ten to fifteen psi also causes detonation. By reasons of symmetry, igniting at the center of the eight-foot tube with both ends open should produce the same effect as igniting a closed-end four-foot tube at the closed end, i.e., if initial fuel distribution, flame spreading, and inertial resistance to flow are symmetrical about the ignition point, then pressure rise will also be symmetrical, giving a zero pressure gradient across the ignition point. When such ignition is provided, a detonation is produced.

If coarse spray from the one-hole injector is ignited at or near the open end of the tube, however, smooth combustion results as long as a relatively nonvolatile fuel such as kerosene or mineral oil is used. The time required to complete the combustion in this case appears to be slightly less than a second. If the burning time for the droplet is computed using the equation:

$$\tau = \frac{D_0^2}{k'}$$

where D_0 is assigned a value of 1000.0 microns or .10 cm, and where .025 cm^2/sec is used for k' (the value reported for n-heptane burning in pure oxygen) then

$$\tau = \frac{(.10)^2}{.025} = .40 \text{ sec}$$

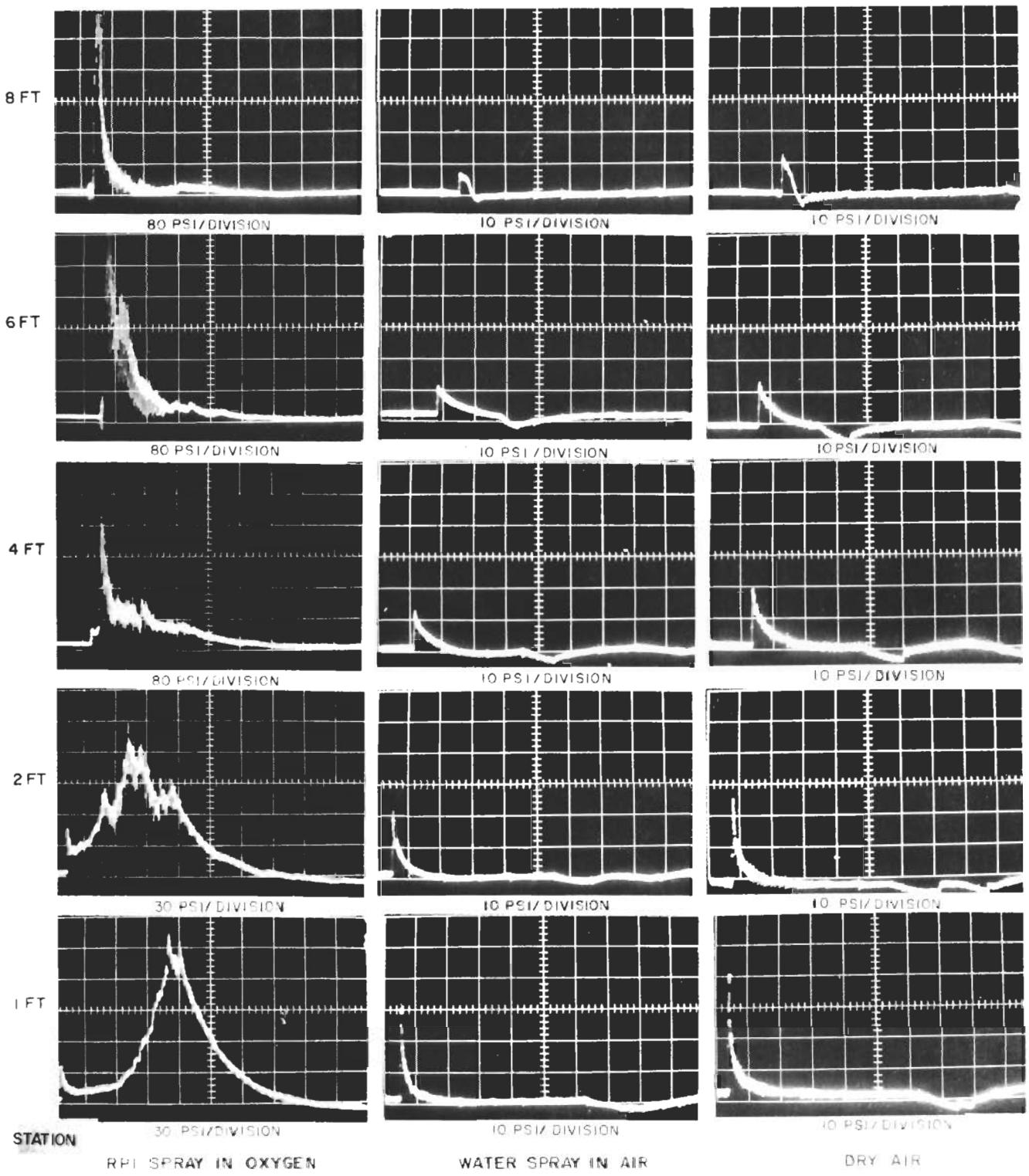

Figure 17. Pressure Pulse Amplitude vs Position in Detonation Tube (Horizontal scale is time, 2 millisec/div Vertical scale is pressure as indicated)

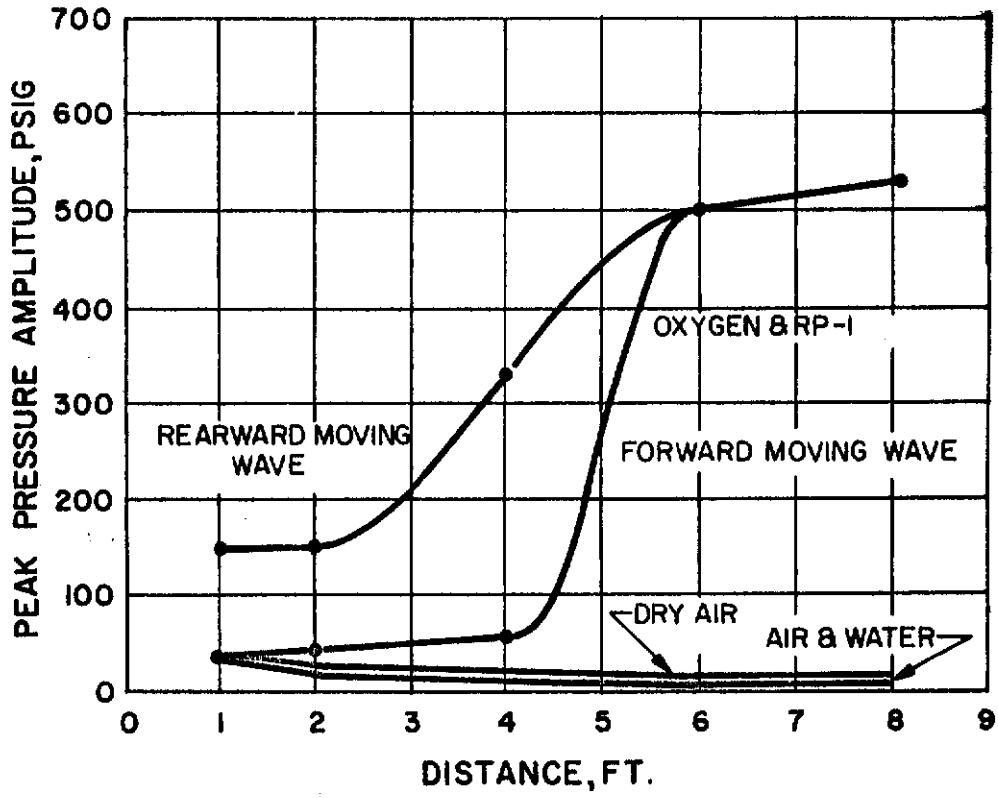

Figure 18. Peak Pressure vs Position in Shock Tube for Dry Air, Water Spray in Air, and RP-1 Spray in Oxygen

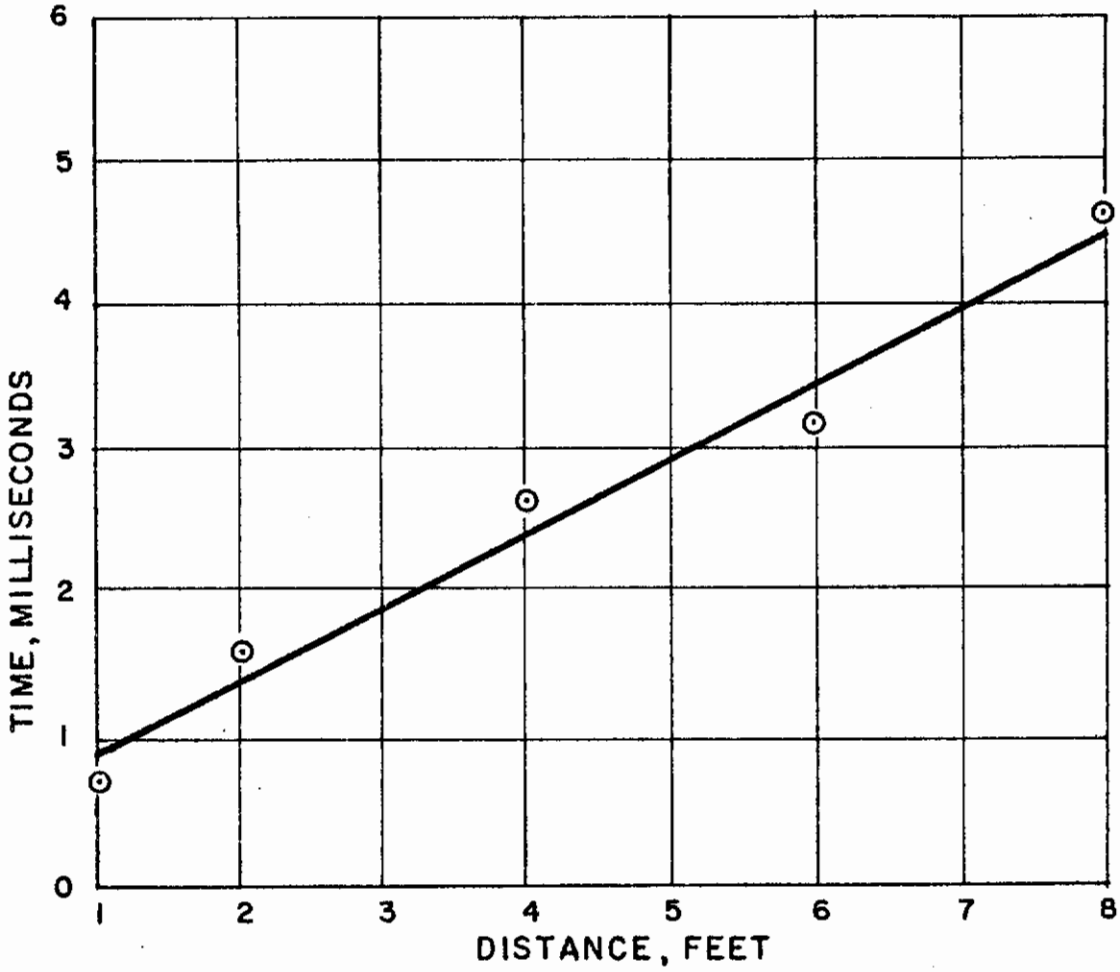

Figure 19. Shock Wave in Dry Air (Velocity ≅2000 ft/sec)

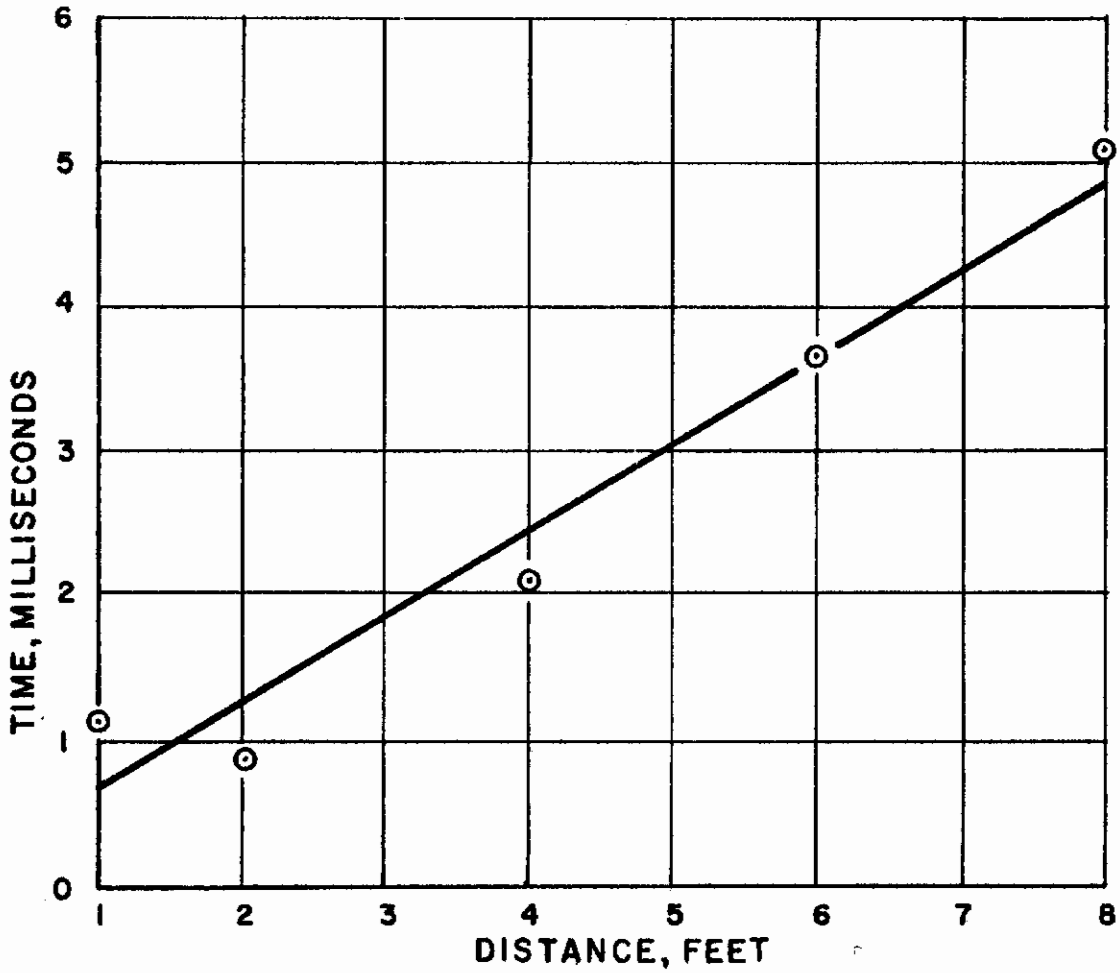

Figure 20. Shock Wave in Air Containing Water Spray
(Velocity ≅ 1650 ft/sec)

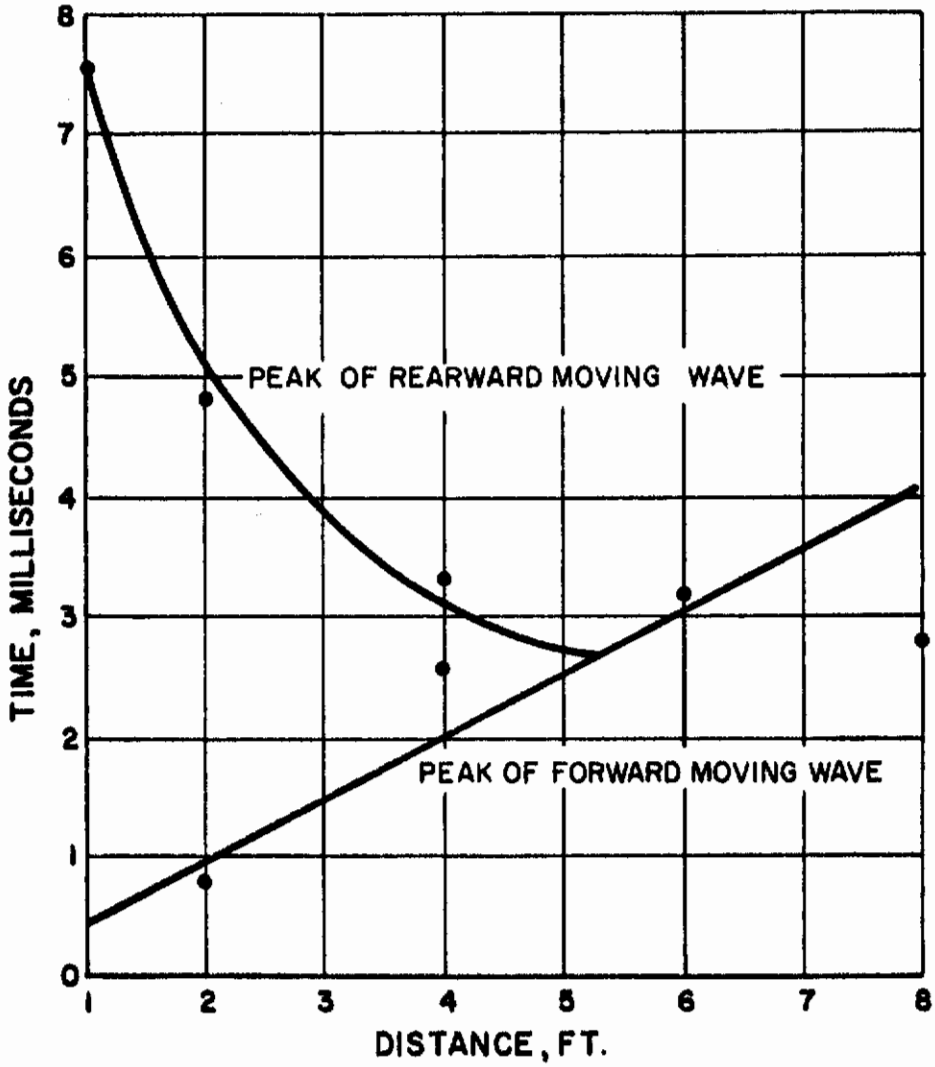

Figure 21. Experimental Time-Distance Plot for Shock Propagating Through Tube Initially Containing an RP-1 Spray in Oxygen (Velocity = 1900 ft/sec)

Thus, the experimentally observed combustion time is the proper order of magnitude for stagnant drops burning in oxygen-rich gas.

In the first series of tests in which fuels of lower molecular weight such as methanol, toluene, and iso-octene were used in the tube, spontaneous detonation occurred in all cases regardless of method of ignition or injector used. This was presumably due to vaporization of enough fuel to make a combustible vapor phase; however, the low viscosity of these fuels and their consequent good atomization might have been causing the effect, as could the erratic operation of the injection gas valve. This spontaneous detonation was absent when the tube was fired on a colder day.

When the 4-hole injector having small diameter (3/64 inch) holes, and thus producing fine drops was fired, spontaneous detonation was produced at the time of ignition with both kerosene and heavy mineral oil, even though ignited near the open end of the tube. Conversely, if jellied kerosene or very viscous, cold, mineral oil is used with the 3/32-inch, one-hole injector, very poor atomization results, and detonations could not be produced even with strong initiating shocks.

If fuel is injected and then pulsed without previous ignition by the explosion of a stoichiometric mixture of oxygen and hydrogen gas, a detonation is produced. The fact that a coarse spray of nonvolatile fuel can be detonated without combustion being established prior to the arrival of the pressure pulse, seems to indicate that the combustion of the pristine liquid fuel is sufficiently rapid following the passage of the pressure pulse to support the detonation wave, and that it is not required that either prevaporized or partially combusted material be present before the arrival of the pulse.

If a spray of fuel is injected into the oxygen-filled tube, ignited, and then pulsed with a shock wave from a pressurized, oxygen-filled driver section shortly after the establishment of stable combustion, a detonation can be produced. Whether or not a detonation is produced depends upon the pressure used in the driver section, and thus upon the strength of the shock wave produced. Since this threshold value is sensitive to ambient temperature, ignition squib condition, alignment of injectors, etc., it is best to compare fuels or conditions in a short period of time without changing these factors.

For the conditions of a four-inch-long driver section, a delay between ignition and pulsing of 200 milliseconds, an eight-milliliter total amount of fuel injected into the tube (about three times the stoichiometric amount), the single-hole injectors and 100-psi injection pressure, a driver pressure of 11 or 12 psi will generally produce detonation, while 10 psi or below generally will not. This same threshold value is found for both kerosene (RP-1) and heavy mineral oil (N.F., 150 centipoise) as long as the experiment is performed at temperatures where the mineral oil is reasonably fluid.

If the initial shock properties are computed for this threshold driver pressure assuming that the gaseous contents of the shock tube still retain the properties of the initial charge of oxygen, it is found that the Mach number of the wave should be 1.15 which is 1313 feet per second. The particle velocity of the gas behind the shock should be 252 feet per second, while the pulse over-pressure should be 4.15 psi above the local ambient pressure of 13 psi. Such a pulse is illustrated in Fig. 16. Under these conditions the droplet combustion should be accelerated to about thirty times the rate in still gas due to the gas velocity past the droplets.

In addition, the gas forces acting upon the larger droplets are greatly in excess of the minimum value necessary to cause them to break up. It is probably best to view this threshold shock value only as a boundary condition, and one which would differ if tube length, fuel amount, and other variables were changed. This "threshold value" shock is the minimum perturbation which causes the pulse to attain a high strength before leaving a tube 8 feet long containing fuel and oxidizer introduced in a particular manner and amount.

If the delay between ignition and pulsing of the contents of the detonation tube is varied, the threshold driver pressure required to initiate detonation varies also (Fig. 22). As would be expected, when the delay between ignition and pulsing is long enough to permit most of the fuel or oxygen to be consumed, a higher-strength pulse is required to initiate detonation. Under such conditions the detonation which is produced is not as strong as when a fresh charge is initiated.

If the length of the driver section is varied, the duration of the shock plateau generated is varied accordingly. Surprisingly, varying the length of the driver section eight-fold changes the threshold driver pressure required for detonation only slightly (Fig. 23). This was unexpected because droplet shattering was thought to be important in enhancing combustion rates, and previous investigations in which single droplets are shattered in a shock tube have shown that considerably higher-strength shock waves are required to shatter droplets when the shock duration becomes short. It would also be expected that a shock wave of long duration would give a longer period for the combustion processes to respond to the effects of the wave.

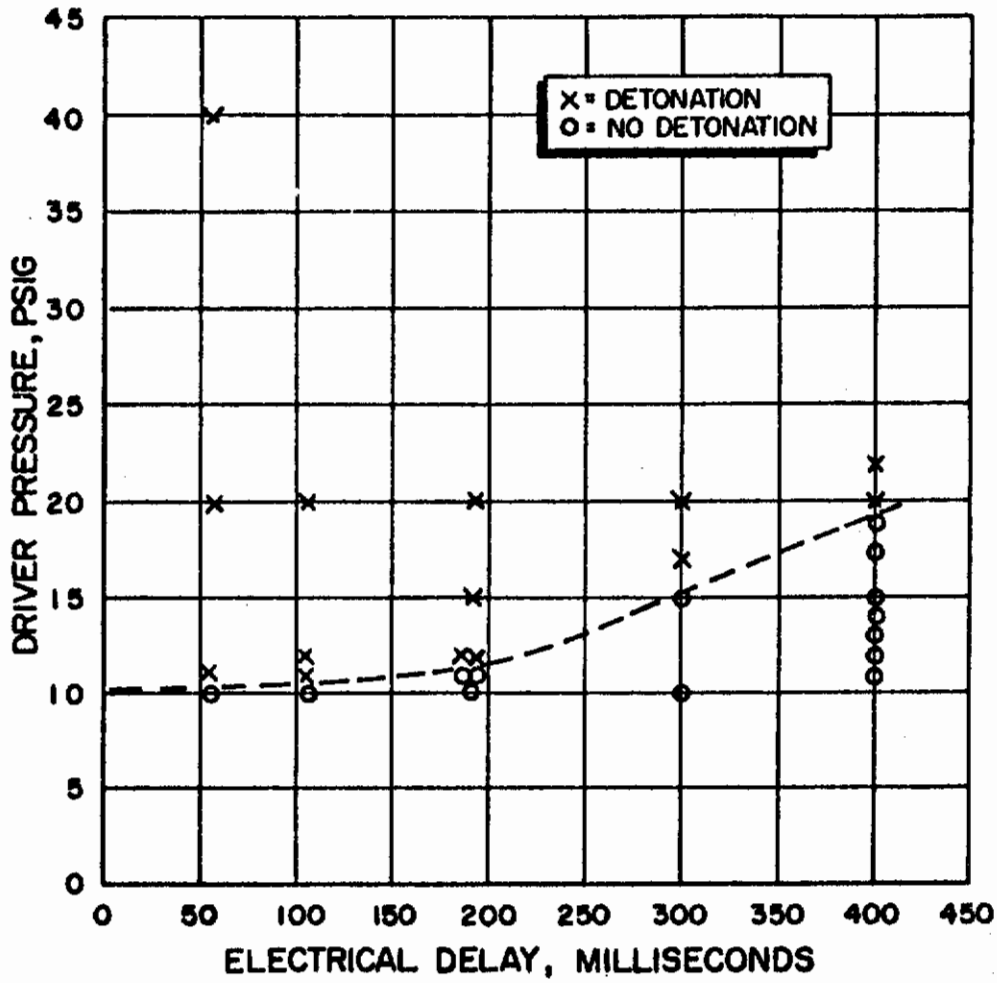

Figure 22. Effect of Delay on Pulse Strength Required to Trigger Detonation (8-inch Driver Section)

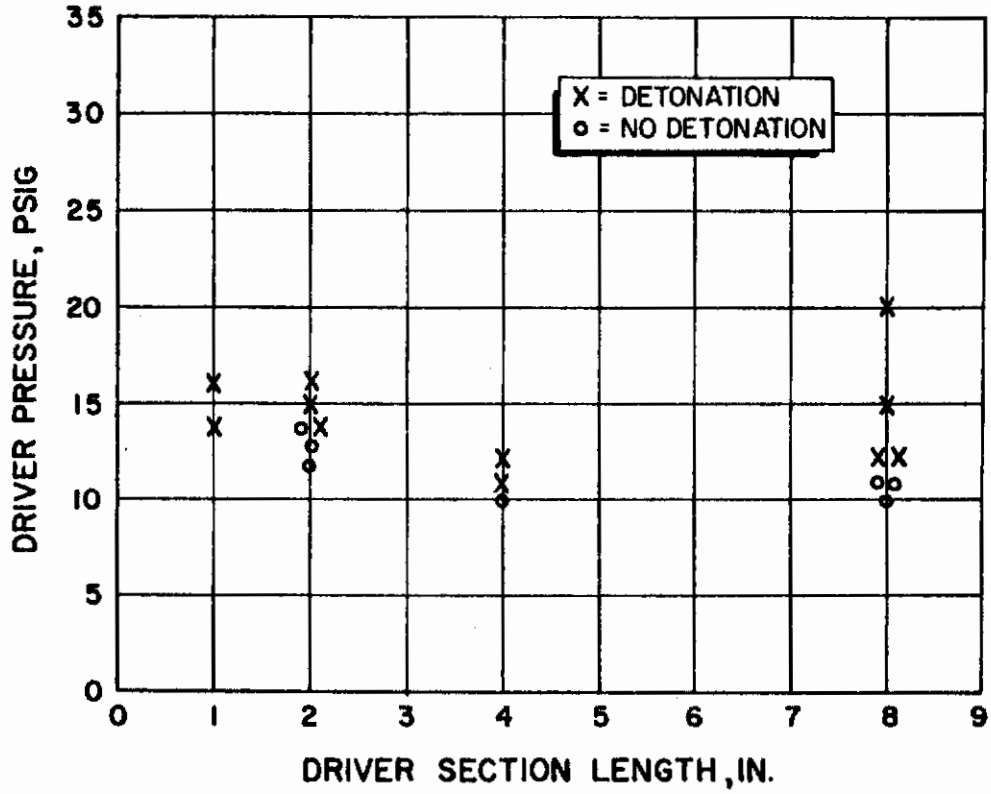

Figure 23. Effect of Driver Section Length on Pulse Strength Required to Trigger Detonation (190 ms Electrical Delay Between Ignition and Introduction of Shock Wave)

IV

DISCUSSION OF TEST RESULTS

When a droplet of fuel burns at steady-state in a stagnant oxidizing atmosphere the diameter is found to vary with time (Refs. 14, 15, and 16):

$$D^2 = D_0^2 - k' t \tag{1}$$

or

$$\frac{d D^2}{dt} = - k'$$

The evaporation constant, k', in this equation may be estimated from the latent heat, thermal conductivity, flame temperature, boiling temperature, and other properties of the appropriate materials (Refs. 14, 17, and 18). The value k' is determined by the rate at which heat is transferred from the hot combustion gases, to the evaporating drop, and by the rate at which oxidizer gas can diffuse to the flame. For a fuel droplet burning steadily in stagnant pure oxygen, a reasonably good approximation for k' based on heat transfer alone is:

$$k' = \left[\frac{8 \, k_g \, \Delta t}{\rho \, L} \right] \left[\frac{L}{c_p \, \Delta t} \ln \left(1 + \frac{c_p \, \Delta t}{L} \right) \right] \tag{2}$$

where k_g is thermal conductivity of the vapors surrounding the droplet, Δt is the difference in temperature between the combustion products and the surface of the boiling droplet, ρ is the density of the liquid fuel, L is the latent heat of the fuel, and c_p is the mean specific heat of the fuel vapors. The bracketed term involving fuel vapor specific heat takes into account the counter-current flow of heat toward the droplet and fuel vapor absorbing heat flowing away from it. When the oxidizer is flowed past the droplet, the heat and mass transfer processes, and consequently the combustion rate, are speeded up. Since the combustion process bears the same relation to Reynolds number as the heat transfer or mass transfer processes, the classical correlations of Nusselt or Sherwood numbers to Reynolds number can be used to compute combustion rate. Here Reynolds number is defined:

$$Re = \frac{\rho \, V \, D}{\mu}$$

where ρ is gas density, V is the relative velocity between gas and droplet, D is droplet diameter, and μ is gas viscosity. This numerical group describes the nature of the flow in the neighborhood of the droplet.

The Nusselt number determines the rate of heat transfer in a system with flowing fluids. The Nusselt number is defined:

$$Nu = \frac{h\ D}{kg}$$

where D is droplet diameter, kg is gas thermal conductivity, and h is the heat transfer coefficient, which is the variable sought. The heat transfer coefficient is used in the equation for heat transfer:

$$Q = A \times h \times \Delta t$$

where Q is the heat transfer rate, A is the surface area of the object, such as a droplet, to which the heat is being transferred, and Δt is the total temperature difference between the surface of the object and the bulk temperature of the gas.

Sherwood number is defined:

$$Sh = \frac{R\ T\ kg'\ D}{D_{AB}}$$

where R is the gas constant, T is the gas temperature, D is the droplet diameter, while D_{AB} is the diffusivity for a material "A" diffusing through the material "B." The value kg' is the mass transfer coefficient used in the equation for mass transfer (where P_i is not too large compared to total pressure):

$$W_i = A \times kg' \times \Delta P_i$$

W_i is moles per second of material i diffused from the droplet, A is the surface area, and ΔP_i is the difference in partial pressure of the material i being diffused between the droplet surface and the main stream of gas.

Since the mass consumption rate of a droplet burning in a flowing gas stream may reasonably be expected to be proportional to Nusselt (or Sherwood) number, and since the value for Nusselt number is 2.0 for a sphere in an infinite stagnant medium, it follows that for a droplet burning in a flowing gas stream:

$$\frac{d\ D^2}{dt} = \frac{k'\ Nu}{2} \qquad (3)$$

One commonly used analytic approximation of the correlation of Reynolds, Prandtl, and Nusselt numbers for a sphere is (Ref. 19):

$$Nu = 2 + .6(Pr)^{1/3}\ (Re)^{1/2} \qquad (4)$$

For the special case of a sphere surrounded by a gas having a Prandtl number of .7 (representative of the rocket conditions of interest):

$$Nu = 2 + .53\ (Re)^{1/2} \qquad (5)$$

A slightly different correlation of the data and some estimate of the spread in data may be found by comparison with Ref. 1. For spheres immersed in near-ideal gases, the Nusselt number and Sherwood numbers are essentially equal and bear very closely the same relationship to Reynolds number; therefore, it is not necessary to decide which of these should be used to estimate the combustion of a droplet.

If each droplet in a group behaves according to Eq. (3) it follows from substitution for D in terms of M that for the group:

$$\dot{M} = 3/4\ M \frac{k'\ Nu}{D^2} \qquad (6)$$

where M is the mass of fuel in the assemblage of droplets and where D is the diameter of monodisperse droplets or a suitable mean diameter for a group of droplets having distributed sizes. Here $\dot{M}$ is the mass combustion rate for the fuel.

It is the enhancement of this parameter at the proper time which can act to sustain or enhance the amplitude of a pressure wave passing through the burning media. This enhancement in turn must come from the effect of the wave upon one of the parameters k', Nu, or D. The perturbation in the values for k' and Nu are related to the perturbations of pressure, temperature, velocity, etc., which constitute the wave, while a rapid change in D, the mean droplet diameter, can arise from shattering of the droplets, a process which also depends upon the action of the wave.

EFFECTS OF A SHOCK WAVE UPON COMBUSTION RATE

The increase in pressure following a shock wave increases boiling temperature of the fuel and decreases the latent heat of evaporation of the liquid propellant. The 4-psi over-pressure following the threshold value shock wave needed to cause detonation in many of our experiments would increase the boiling temperature of kerosene at most, 20 or 30 C, and would reduce the latent heat by a few percent. There would thus be two effects from increased pressure, i.e., increase of boiling temperature, with increased heat requirement for heating the droplet to the new higher boiling point and lower latent heat of evaporation, which would increase k' by a few percent. These two effects, being in opposite directions, would tend to cancel each other out, and the resultant effect would be inappreciable.

The temperature of the gas flowing behind a shock wave is raised, owing to the energy of compression added to it, in passing through the front. For the low pressure ratio of the threshold value shock wave, the pressure-temperature relationship will not differ greatly from that for low-amplitude acoustic waves where the temperature ratio is equal to the pressure ratio raised to the (gamma minus one/gamma) power, where gamma is the ratio of specific heats for the gas, about 1.3 or 1.4. If this relation holds, the temperature would increase about five or ten percent; and if the gas surrounding the droplet was initially quite hot compared to the surface temperature of the droplet, the k' and combustion rate could be increased by the same five or ten percent. The relation of temperature to pressure ratio for higher strength waves may be obtained from classical shock wave equations (see Fig. 29).

The particle displacement of the gas is important in enhancing mixing in a rocket engine running unstably as k' is approximately proportional to the oxygen concentration in the gas surrounding the droplet, and this concentration may be

varied considerably as the gas is swept past the propellant streams. This is a rather complex effect, however, and probably cannot readily be determined with the detonation tube.

EFFECT OF REYNOLDS NUMBER

Reynolds number, and thus the Nusselt number, may be derived from knowledge of velocity, density, etc., of the gas flowing behind the shock front. If the droplets are large, and can be presumed to accelerate slowly, the relative velocity is just equal to the gas particle velocity, and Eq. (5) and (6) can be readily evaluated. For a 1000 micron diameter droplet standing still in the 252 foot per second flow velocity following the threshold value shock, the Reynolds number is 5100. This yields a Nusselt number of 66. Thus, the effects of Reynolds number in the gas behind the threshold value shock wave is to increase the value of the heat and mass transport processes, and consequently the combustion rate thirty-three fold compared to the stagnant values. This is a very considerable effect. If the droplets are small enough to accelerate rapidly in the flowing gas stream, then the values for relative velocity must be obtained by evaluating the droplet accelerations from appropriate drag coefficients, and by integrating these accelerations with time in order to get droplet velocity. This technique has been discussed at some length in the literature (Refs. 4, 20, 21, and 22). The relative velocities will, of course, never be larger than for the case where the drops remain at rest, so the maximum possible Reynolds number is readily computed.

EFFECT OF WEBER NUMBER

Several investigators have studied the effects of high-velocity gas flow upon droplets. Most of these investigators have found that for gas flows of long duration, droplet breakup occurs when the Weber number for the droplet is equal to about 10 or greater (Refs. 23, 24, and 25).

Weber number is defined:

$$We = \frac{\rho V^2 R}{\sigma}$$

where ρ is gas density, V is relative velocity between gas and drop, R is drop radius, and σ is droplet surface tension. The Weber number is proportional to the ratio of aerodynamic forces acting on the drop to cohesive surface tension forces. If the duration of the gas flow is very short, i.e., less than the natural period of oscillation of the drop, then a correspondingly higher Weber number is required to cause droplet breakup (perhaps as high as 100) (Ref. 26). While this equation defines the conditions under which a droplet is likely to shatter, it does not, unfortunately, tell what will be the sizes of the droplets which are formed, nor does it tell the rate at which the droplet subdivision, and distribution of the small resultant droplets takes place. It is this information which is of utmost importance in defining combustion rates under the extreme conditions found in rocket engines having low contraction ratios, and in combustion instability.

If droplets shattering in a high-velocity gas stream are photographed, and examined, it is noted that at Weber numbers only slightly above the critical value for shattering, the droplet initially flattens, then forms a "parachute"-shaped bag with a thick toroidal rim. The next steps are for the central membrane of the bag to burst forming very small droplets, and then for the toroidal ring to pinch into perhaps a dozen or so fairly evenly sized drops which contain most of the mass of the initial droplet. This action may take an appreciable fraction of a millisecond or even several milliseconds to complete, the time depending upon the size of the droplet and the velocity of the gas stream. If, however, the Weber number is much higher than the critical value, there is no such bag formation, instead, very fine droplets are sheared off of the edges of the drop. This latter process apparently starts almost immediately and appears to be something which proceeds at a well-defined rate. In the case illustrated in Fig. 24 the start of the disintegration of the droplet is somewhat delayed and the droplets formed are quite coarse because of the very low pressure ratio employed. This low pressure ratio slows down the action and permits better photographs to be obtained.

It seems likely that it is this latter shear type of droplet breakup which is important in stimulating combustion of drops in the shock tube. One indication of this is that the conditions following the smallest shock capable of initiating detonation in RP-1 spray from the one-hole injectors would give a Weber number of 390 (based on a 1000 micron drop) which is very far above the critical value. The Weber number of a droplet behind the well-developed detonation wave is in turn still much larger. Another reason to believe that it is the rate of breakup which is important rather than the breakup threshold is that a spray of large droplets requires a higher [illegible] shock for initiation than a spray of small droplets, whereas the large droplets can be made to break up, given sufficient time, at a lower shock strength than the smaller droplets.

Figure 24. Shear Type Breakup of a Drop Behind a Shock Wave Initial Drop Diameter 1460 Micron. Gas Velocity 53.9 ft/sec, .164 ms Int., Re=8550, We=55.5, P/P_o=1.06

V

ANALYTIC TECHNIQUES

STEADY-STATE PHENOMENA

Although the steady-state processes in the tube are of relatively little interest compared to those associated with wave action, it is still instructive to make some steady-state computations, both for the sake of illustrating some of the ways in which the interaction of flow and combustion can be represented, and because some situations are found in which it appears that the generation of wave action would be almost inevitable.

Consider the case where the detonation tube contains a spray of fuel droplets in oxygen and is closed at one end. If its contents are now ignited and if combustion is sufficiently prolonged to reach a steady state, then at any station a distance x from the closed end, the combustion gas which flows past, is equal in amount to that generated by all the burning material between the closed end where x = 0 and the position x itself. From Eq. (5) and (6) it follows that if Y is the mass velocity (ρV) of gas at station x,

$$\frac{dY}{dx} = \frac{3\,k' \left[2 + .53 \left(\frac{D\,Y}{\mu}\right)^{1/2}\right] \left[\frac{\text{mass of fuel}}{\text{unit length of tube}}\right]}{4\,D^2}$$

If the Reynolds number $\frac{D\,Y}{\mu}$ is assumed to be large compared to 2, then it is posibe to make the approximation:

$$\frac{d\,Y}{d\,x} = \frac{3/4 \times .53\,k' \left(\frac{\text{mass of fuel}}{\text{unit length of tube}}\right) Y^{1/2}}{D^{3/2}\ \mu^{1/2}}$$

If $\frac{\text{mass of fuel}}{\text{unit length of tube}}$, D, etc., are regarded as constant:

$$\frac{d\,Y}{d\,x} = K\,Y^{1/2}$$

This merely states that the rate of gas generation for a unit length of tube is proportional to the square root of the mass velocity (and therefore Reynolds number) at that position in the tube. The assumption that mass of fuel per unit length of pipe remains constant is approximately true for the early stages of combustion.

If this equation is separated and integrated it appears that

$$Y = (1/4)\ K^2X^2$$

In other words, the mass flow of combustion gas increases with the square of the distance downstream from the closed end. This is a very rapid rate of increase considering that the combustion rate only increased with the square root of mass velocity.

If the combustion rate were to increase faster than linearly with gas mass velocity, then the mass velocity Y becomes infinite at a prescribed distance from the closed end, with the mass flow showing a more or less hyperbolic relation to distance. Whether the "explosive" hyperbolic form applies strictly or not, it seems obvious that the combustion in any such case cannot remain "steady state," but will tend to form a shock wave or pressure wave as soon as a sufficiently large value of mass velocity is attained in the tube. This high mass velocity may be obtained simply from a long tube with rapidly burning propellant, or possibly by the occurrence of some phenomena, such as droplet shattering, which causes combustion rate to increase as a rapidly increasing function of mass velocity, or by artificially increasing mass velocity at some upstream point by use of a shock tube driver section or some similar device.

WAVE PHENOMENA

While such a "steady-state" analysis of the shock tube is instructive in illustrating the relationships which can lead to initiation of explosive combustion rates, it is not at all adequate to analyze the experimental data obtained in which wave action is all-important. To analyze such data the wave action must be considered. Unfortunately, attempts to analytically manipulate wave equations which consider the effects of mass and heat addition, viscous attenuation, and nonlinear pressure-volume relations become so difficult as to be completely out of the question.

Thus, one must either resort to drastically simplified analytical techniques or base the computations on numerical techniques suitable for machine computation.

Simplified Wave Analysis

The pressure in any short axial element of the tube may be represented:

$$P = \frac{R}{A}\ \frac{T}{W_m}\ \frac{M}{L} \qquad (7)$$

where

P	=	pressure
R	=	the gas constant
A	=	tube cross-section
T	=	temperature of the gas
W_m	=	molecular weight of the gas

M = the mass of the gas phase contained in the element
L = the length of the element

Now, if R, A, and L remain constant, the only way the pressure in the element can be altered is by changes in $\frac{T}{W_m}$ and M. This change can be occasioned by externally adding energy to the contents of the element, by chemical action within the element, or by material flowing into the element.

If a fairly low-amplitude sound pulse were traveling down the tube without either attenuation or augmentation, it would retain its initial wave form and amplitude and would simply move down the tube at some constant velocity C. Thus, as the wave passed each element of tube there would be enough net flow of material into that element of the tube to increase the pressure by the amount of the overpressure of the wave.

If there were combustion also taking place in the specified element of the tube the pressure could be increased still further by this means. In our simplified analysis we will assume that these two actions are separable and additive. Then

$$P = P_{wave} + P_{combustion} \tag{8}$$

then

$$P_{(1 + c\,\Delta t,\ t + \Delta t)} = P_{(1,t)} + (R/AL)\Delta \quad (TM/W_m)$$

where $P_{(1,t)}$ is pressure measured at axial location of the tube 1, and at a time t. Now if the chemical action is the combustion of a liquid hydrocarbon in an oxidizer that was initially pure oxygen, the temperature and mol wt of the gas are related to the amount of fuel that has been added to the oxygen. This relation is shown in Fig. 25 where the ratio of pressure to initial oxygen pressure is plotted for various weights of fuel added to the initial weight of oxygen.

The curves of Fig. 26 are pressure profiles in the shock tube at times 0 m.s., 1 m.s., 2 m.s., 3 m.s., and 4 m.s. after initiation. They are taken from the data of Fig. 17 by cross-plotting. To readily observe the growth due to chemical action in the 1 m.s. intervals, the curves may be superimposed as in Fig. 27, by moving each curve a distance $c\,\Delta t$, where c is presumed to have the constant value 1900 feet per second. The difference between each curve and the one vertically above it represents the extent of the combustion processes taking place in that time interval. One can readily obtain combustion rates by use of Fig. 25 and 27(Appendix II).

With knowledge of the initial fuel mass injected into the tube, and a little care in "bookkeeping," the mean values for $\dot{M}/M$ can be calculated for each one of these positions and times. In Fig. 28, the logs of these values are plotted vs log of the mean pressure ratios. The curved lines plotted in Fig. 28 correspond to the straight lines fitted through the plots involving Reynolds number. If the Reynolds numbers per centimeter $(\rho V/\mu)$ are computed for the average pressure ratio corresponding to each time and position (Fig. 29), then a plot of log $\dot{M}/M$ vs log Reynolds number per centimeter can be plotted (Fig. 30), or if the mean droplet

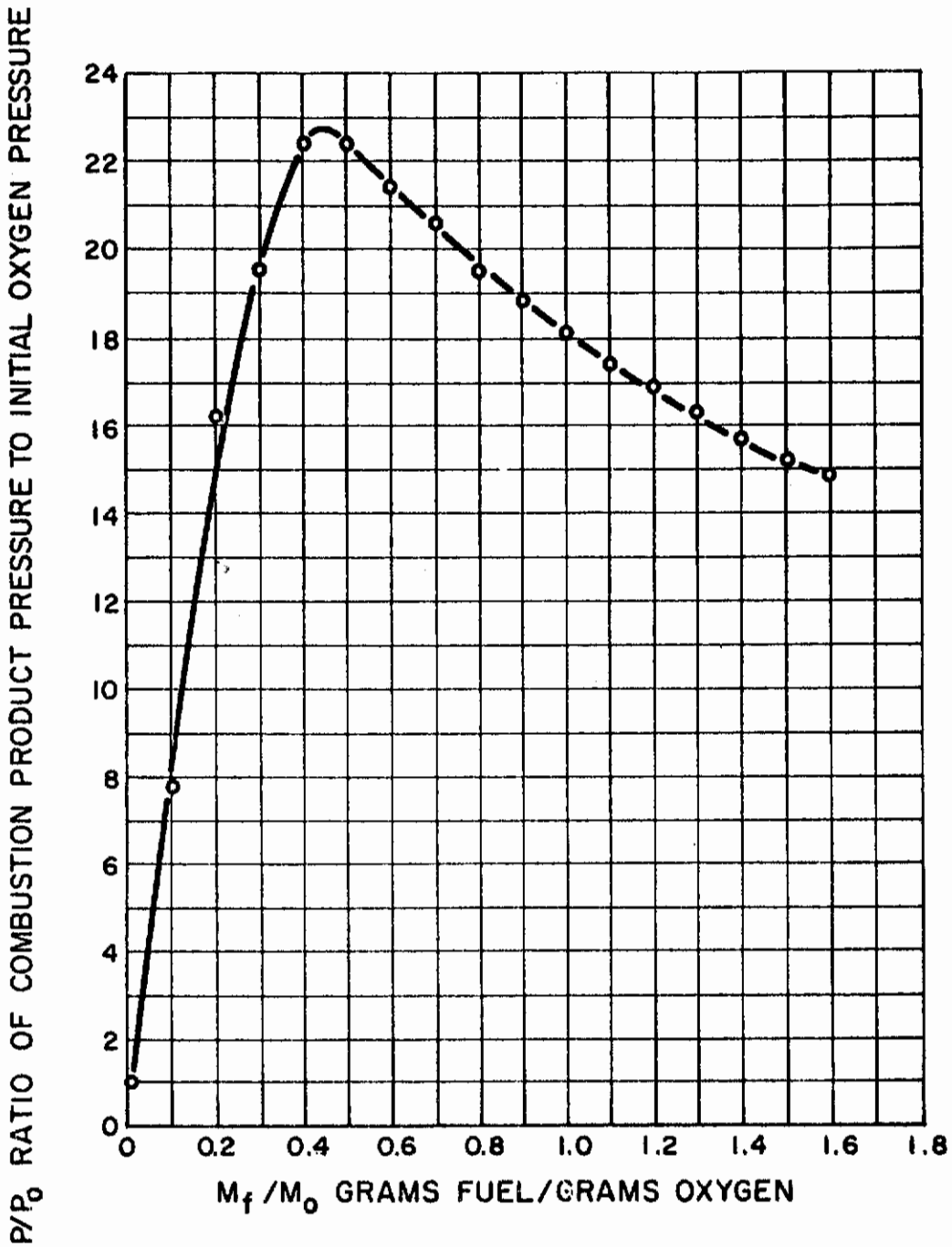

$$\frac{P}{P_0} = \frac{\left(\frac{T}{\text{mol wt}}\right)_{\text{COMBUSTION PRODUCTS}}}{\left(\frac{T}{\text{mol wt}}\right)_{\text{INITIAL OXYGEN}}} \times \frac{M_f + M_o}{M_o}$$

Figure 25. Pressure Generated by Isochoric, Adiabatic Combustion of RP-1 in Oxygen

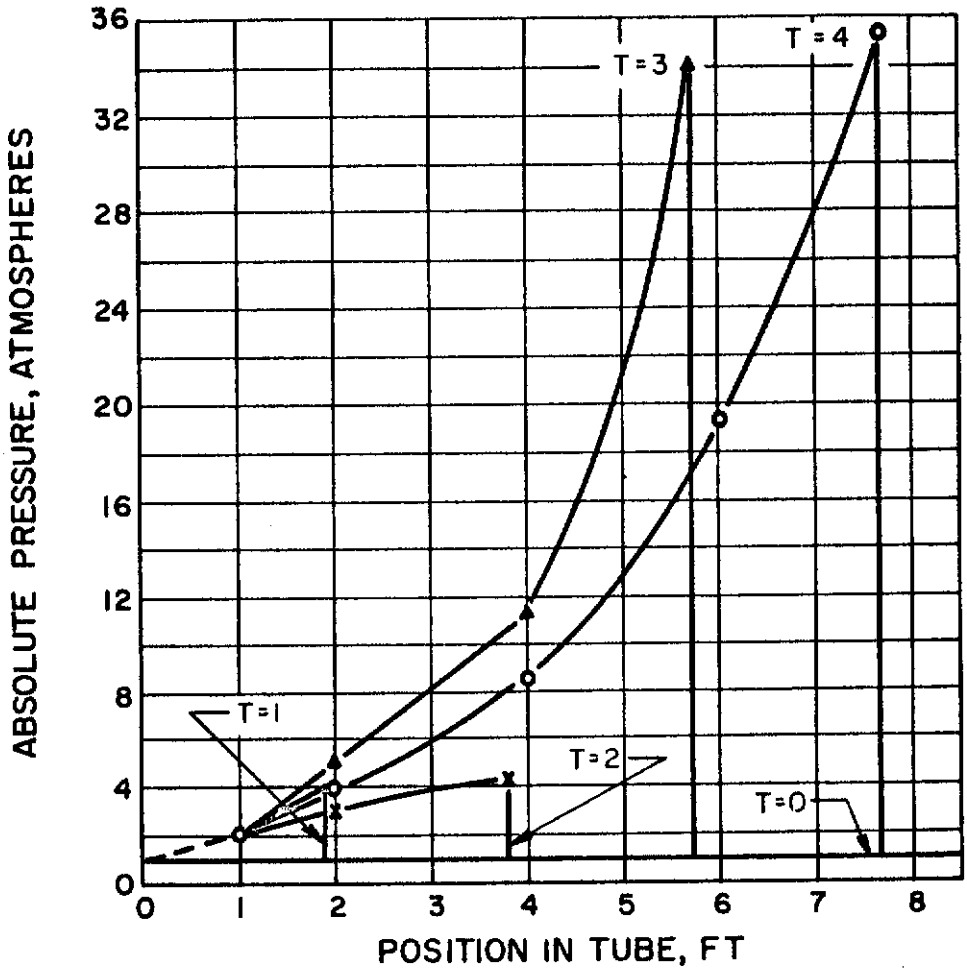

Figure 26. Pressure Profiles in the Shock Tube at Times 0, 1, 2, 3, and 4 Milliseconds After Start

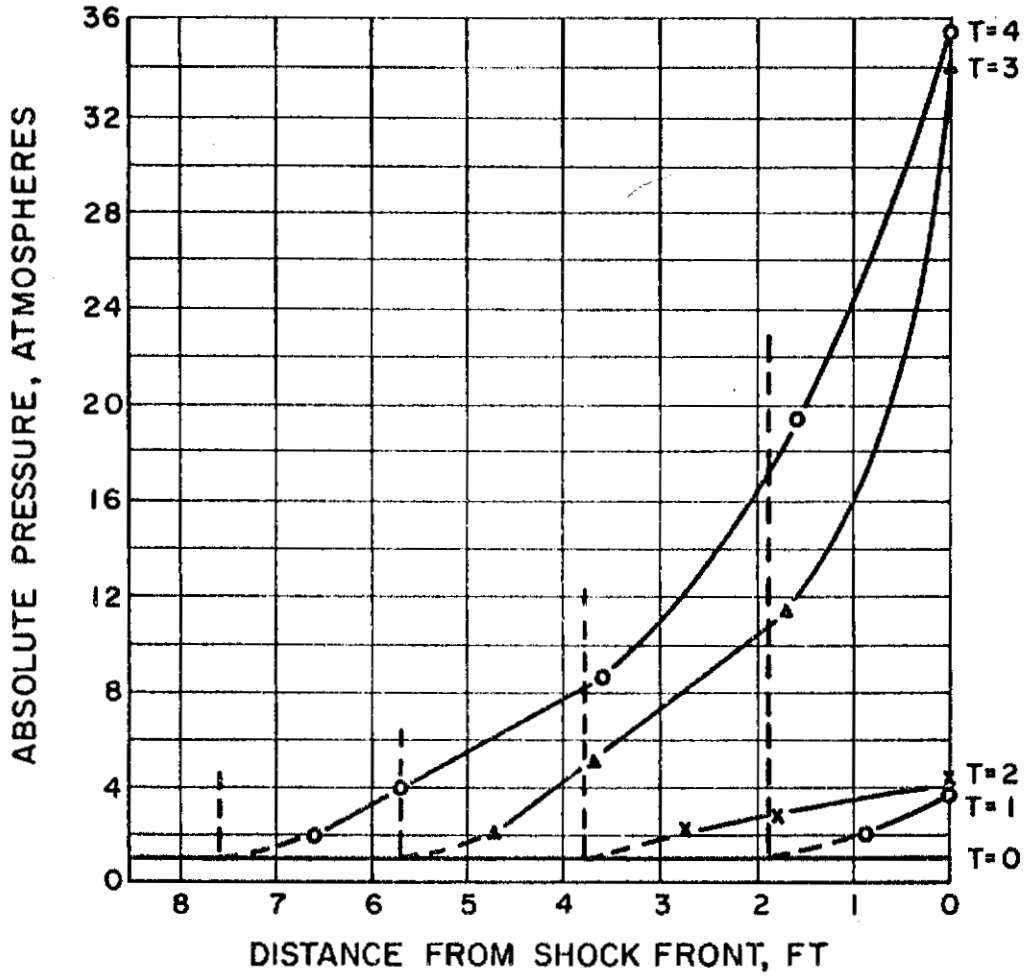

Figure 27. Pressure Profiles in the Shock Tube Superimposed so as to Show the Pressure Growth Due to Combustion at the Various Positions and Time Intervals

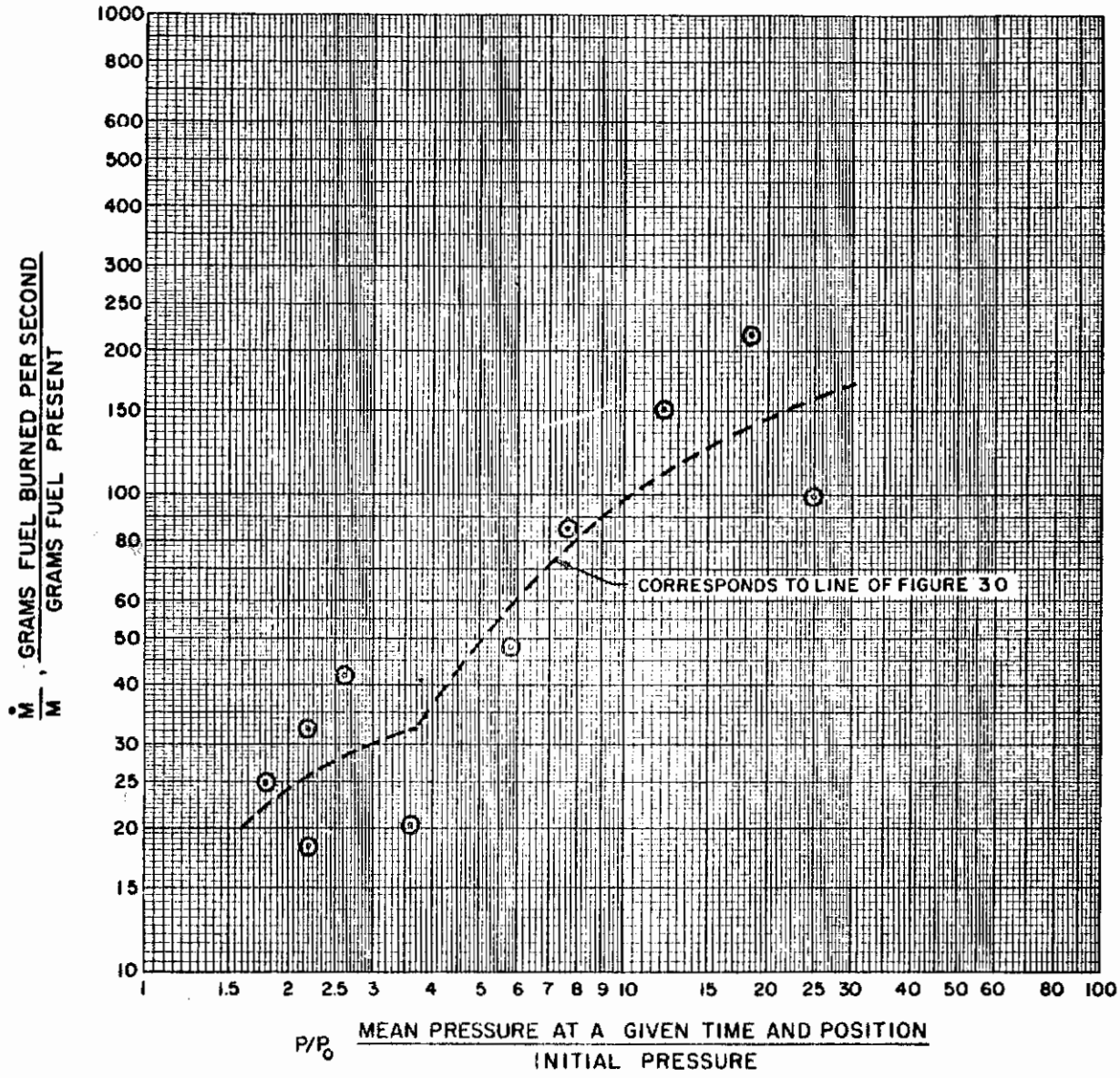

Figure 28. Specific Combustion Rate Plotted vs Local Pressure Ratio of Wave

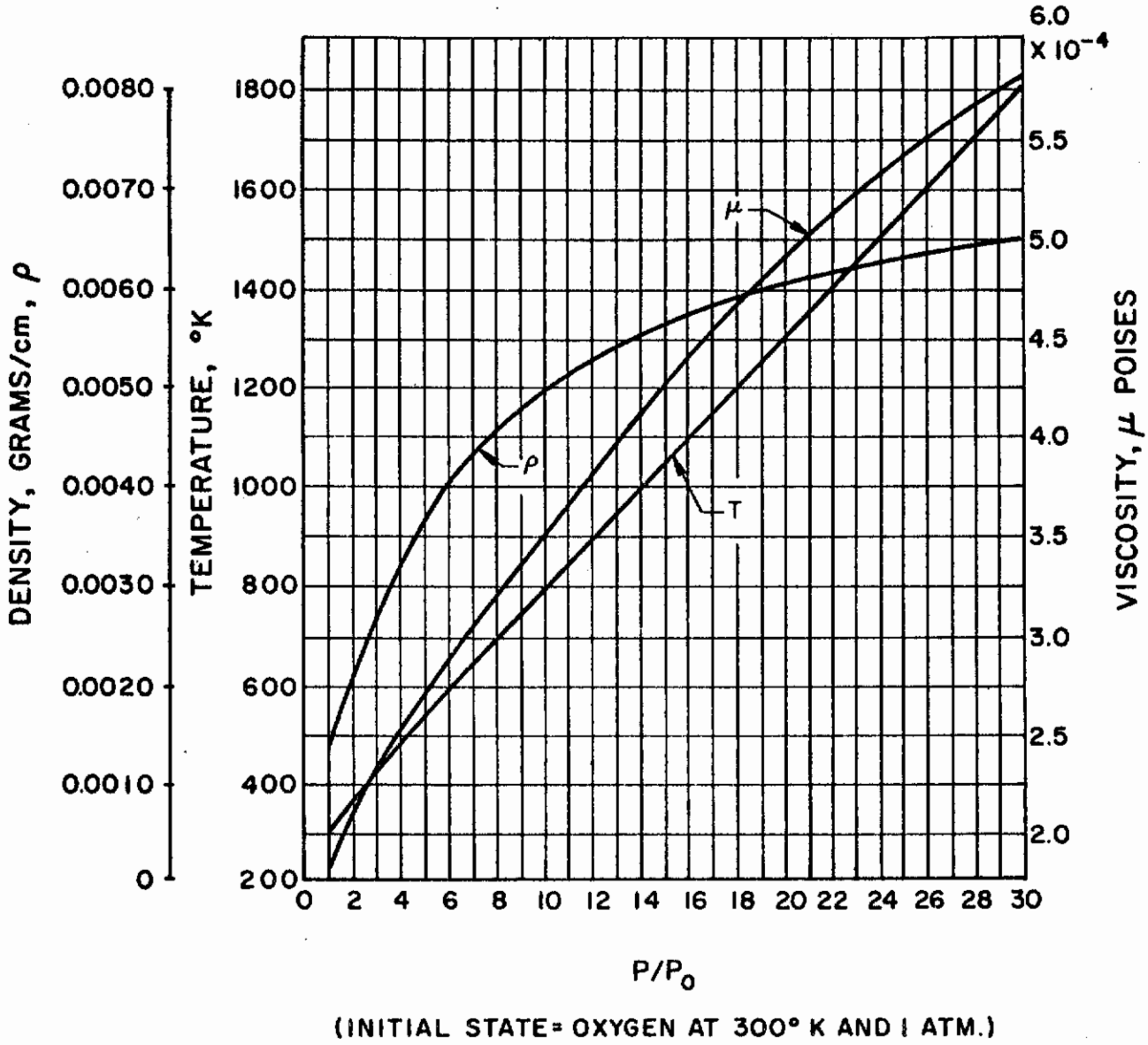

Figure 29. Theoretical Shock Wave Parameters Density, Temperature, Viscosity, Wave Velocity, Particle Velocity and Re/cm Behind Shock vs Pressure Ratio Across Shock

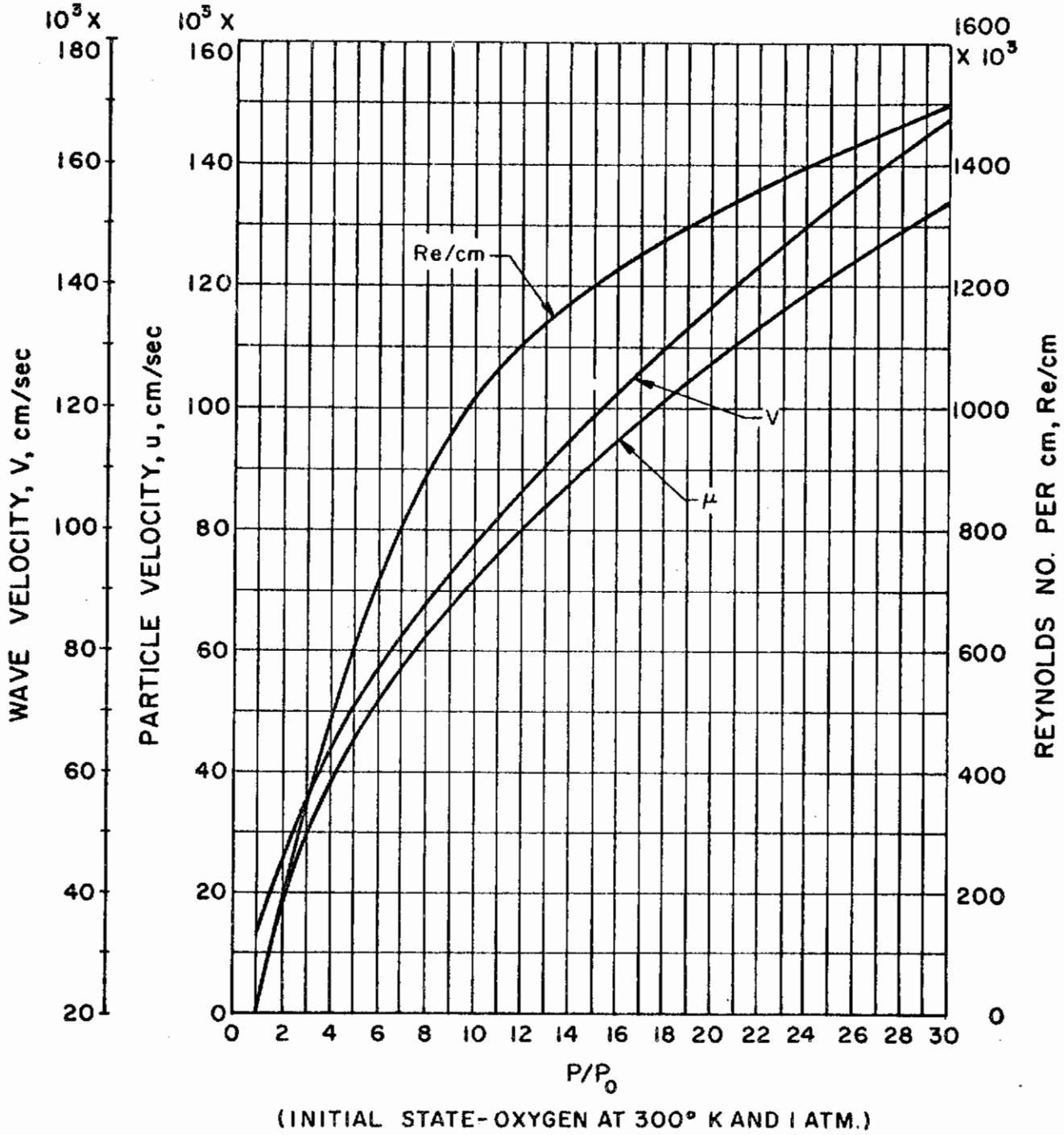

Figure 29 (Continued)

size is estimated to be 1000 microns specific combustion rate may be plotted vs Reynolds number (Fig. 30). Because of the functional relationship between pressure ratio and Reynolds number per centimeter it is inconsistent to fit straight lines through logarithmic plots of both $\dot{M}/M$ vs pressure ratio and $\dot{M}/M$ vs Reynolds number per centimeter. The present scattered data defines the functional relation rather poorly, and looking at these plotted data alone it is difficult to decide whether a single straight line or two lines on Fig. 30 or a single line on Fig. 28 would best fit the present data points. The accumulation of additional data should resolve this question. Reynolds number is taken from the classic shock wave equations relating pressure ratio, particle velocity, temperature, density, etc. The equations can only approximately relate pressure ratio and the various parameters for our shock tube, where mass addition, heat addition, etc., are important. Further work is necessary to accurately establish the Reynolds number values.

It is seen that the portion of the curve lying between Reynolds number values of 15,000 and 45,000 (Fig. 30) exhibits a slope of about .296 ±.48 which does not differ significantly from the behavior in the experimentally known combustion region and indicates that the increase in combustion rate behind the weaker shocks probably is due to enhanced heat and mass transfer due to the local velocities. At Reynolds numbers beyond 45,000, however, there appears to be a considerable increase in specific combustion rate. This may be inferred from the plotted points of Fig. 30 which are somewhat sketchy, or it could be inferred equally well directly from Fig. 18 which shows rapid wave amplitude growth after the wave attains an amplitude of 4 or 5 atmospheres. It is worthwhile to consider whether this is due to droplet shattering. Let us consider how droplet shatter might relate to the flow variables.

DROPLET SHATTERING RATE BASED UPON A MOMENTUM TRANSFER MODEL

At low Weber numbers when gas flows past a droplet, it remains intact, and momentum is transferred to it:

$$\frac{d\,(MV)}{dt} = \frac{C_D\ \rho\ V^2\ A}{2} = M\ \frac{D\ V}{dt} \tag{9}$$

but when Weber number is high, the shear forces are large relative to the forces holding the outer layers of the droplet to the center, and thus will be expected to strip off the outer layers.

$$\frac{d\,(MV)}{dt} = \frac{C_d\ \rho\ V^2\ A}{2} = M\ \frac{dV}{dt} + V_d\ \frac{dM}{dt} \tag{10}$$

where V_d is the velocity of the shed material relative to the drop.

The forces which still tend to accelerate the central portions of the droplet will come from the pressure forces and from the shear forces transmitted from the outer to the inner layers of droplet fluid. The shear forces (and some of the pressure forces) will tend to strip off layers of liquid. In a rigid, nonevaporating body $V_d\ \frac{dM}{dt}$ is zero; however, in a body which possesses small cohesive forces relative to the accelerating forces setting upon it (i.e., a high Weber number and

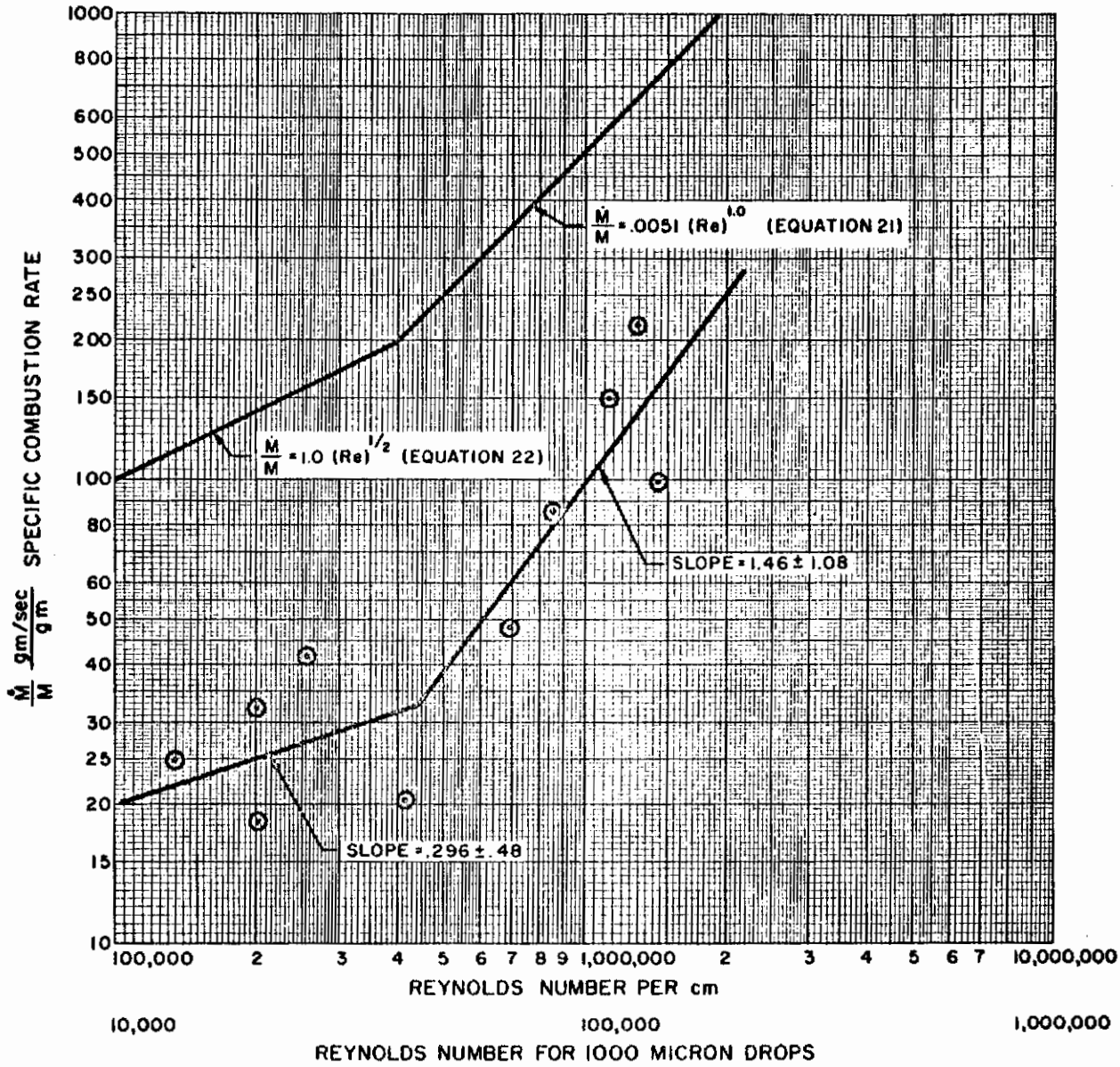

Figure 30. Specific Combustion Rate Plotted vs Reynolds Number per Centimeter and vs Reynolds Number Based on a 1000 Micron Diameter Fuel Drop

very nonviscous liquid). The value for $V_d \frac{dM}{dt}$ may represent an appreciable portion of the total momentum exchange. Let us set

$$V_d \frac{dM}{dt} = K_1 \frac{d(MV)}{dt}$$

where K_1 can range from 0.0 to 1.0. Then

$$V_d \frac{dM}{dt} = K_1 \frac{C_D \rho V^2 A}{2} \tag{11}$$

V_d may potentially range from 0.0 up to the full relative velocity between the drop and the gas stream. Thus, $V_d = K_2 V$, where again K_2 may vary from 0.0 to 1.0. The relation may now be written

$$\frac{dM}{dt} = \frac{K_1}{K_2} \frac{C_D \rho V A}{2} \tag{12}$$

$\frac{dM}{dt}$ is not defined until the value of the coefficient K_1/K_2 is known, and it may potentially vary from 0.0 to ∞ ; however, one would expect neither K_1, nor K_2 to differ very far from unity, and thus the value of their ratio should not differ from 1.0 by a very large factor. The value of this factor might very well be expected to vary with Reynolds number, Weber number, fuel viscosity, etc. The value for C_D has been examined for distorted liquid droplets in high-speed gas flows (where R_e varies from 300 to 4000)(Ref. 25) and has been found to remain approximately equal to 2.0 the drag coefficient is based upon the diameter of the initial spherical droplet. Thus:

$$\frac{dM}{dt} \cong \frac{K_1}{K_2} \rho VA \tag{13}$$

This is an interesting form as ρVA is just the mass rate of gas approaching the drop in the stream tube equal to its initial undisturbed cross-section.

If the initial frontal area of a group of spherical drops is expressed in terms of fuel density, droplet mass, and diameter:

$$A = \frac{3}{2} \frac{M}{\rho_1 D} \tag{14}$$

where ρ_1 is fuel density.

Now lump the unknown variables together:

$$\alpha = \frac{C_D K_1}{2 K_2} \tag{15}$$

Then, combining Equations 12, 14 and 15

$$\frac{dM}{dt} = \frac{3}{2} \frac{M \alpha \rho V}{\rho_1 D} \tag{16}$$

If ρV, the mass velocity, is expressed in terms of Reynolds number for the sake of comparison with other relations containing this parameter:

$$\rho V = Re \times \frac{\mu}{D} \tag{17}$$

Then $$\frac{dM}{dt} = \frac{3}{2} \frac{M \alpha \mu Re}{\rho_1 D^2} \tag{18}$$

(It should be cautioned that this expression does not predict any effect of gas viscosity upon $\frac{dM}{dt}$. It may appear to only because of the variables hidden in the Reynolds number.)

If the material which is shed from the droplet is very fine it might be expected to burn very rapidly following its formation. In Ref. 26 the relation between shock tube driver pressure and diameter of shattered droplets is given. According to this source, for the pressure ratios of interest, the material shed would have droplet diameters on the order of 15 microns. If this is the case the fuel would be expected to be consumed in about 1/10 of a millisecond after it is shed.

When the combustion of the shed material is so rapid, the mass rate of shedding is essentially equal to the mass combustion rate. Making this assumption, we can specify a theoretical value for the specific combustion rate associated with shedding of fuel from a shattering droplet (or group of droplets):

$$\frac{\dot{M}}{M} = \frac{3}{2} \frac{\alpha \mu Re}{\rho_1 D^2} \tag{19}$$

Comparing this with the specific combustion rate based upon the heat transfer and diffusion processes from Eq. (6)

$$\frac{\dot{M}}{M} = \frac{3}{4} \times \frac{k' \times 0.53 (Re)^{1/2}}{D^2} \tag{20}$$

inserting the reasonable values: $k' = 0.025$, $\mu = 1.8 \times 10^{-4}$, $\rho_l = 0.80$ for the process of droplet shedding:

$$\frac{\dot{M}}{M} = \frac{3.4 \times 10^{-4} \ \alpha \ Re}{D^2} \tag{21}$$

while for the process of heat and diffusional mass transfer:

$$\frac{\dot{M}}{M} = \frac{0.01 \ (Re)^{1/2}}{D^2} \tag{22}$$

It now is apparent that at low values of Re (and α) the droplet shedding process is a very much slower process than the normal burning process, even though the Weber number of the drop may be far above the values where the initiation of shattering is possible.

As the Reynolds number gets large the specific combustion rate due to droplet shedding increases faster than the specific combustion rate due to heat and diffusional mass transfer processes, and eventually the rate due to shedding will become the faster and more important process. If the two processes are equated, to determine the cross-over point:

$$Re_{(cross\text{-}over)} = \frac{870}{\alpha^2} \tag{23}$$

If it is presumed that the rapid acceleration in specific combustion rate shown in Fig.30 at a Reynolds number of about 45,000 is due to this change over in the mode of combustion, then a value for α may be computed

$$45{,}000 = 870/\alpha^2 \tag{24}$$

$$\alpha = 0.14$$

which seems reasonable. Thus, it is not unreasonable to assume that the increase in specific combustion rate at Reynolds numbers above 45,000 is due to droplet shattering.

Comparison of Simple Analysis and Experiment

On Fig. 30 the theoretical curves from Eq. 21 and 22 are drawn in for comparison with the experimental values. The slopes of the experimental and theoretical lines are similar, but the experimental lines are smaller by roughly a factor of five. Possible reasons for this discrepancy may be:

1. Incorrect estimate of the mean droplet diameter in the shock tube. If the droplets were assumed somewhat coarser than 1000 microns, this would lower the theoretical curve.

2. Too high value used for k'. The value used, .025 cm^2 per second, is for heptane burning in pure oxygen. If the oxidizer were less than 100 percent oxygen a correspondingly smaller value for k' should be used.

3. No allowance was made for warm-up for the droplets. It is interesting to note that the three experimental points which fall furthest below the line were all for the first millisecond after the passage of the shock front.

4. The spray of fuel droplets may have been unevenly distributed or unavailable for combustion. If large clumps of fuel were formed by the injection process, they would rapidly react with all the oxygen in the near vicinity and then contribute no more to the combustion. Any fuel sprayed onto the walls of the tube might not react as rapidly as droplets in the channel of the tube.

5. The effects of wave attenuation were not considered. Appreciable combustion must have been required just to overcome these attenuation effects.

6. The combustion process, in order for momentum to be conserved, must produce right and left moving wavelets of equal magnitude. Where these pass through each other their particle velocities cancel, and thus Reynolds number is lower than if all of the over-pressure were associated with a right-moving wave. This cancellation effect was ignored in the simple model.

NUMERICAL WAVE MODEL

The detailed model of the shock and detonation processes developed during the current studies is based upon numerical techniques. The contents of the shock tube are initially divided axially into a convenient number of segments. Each of these segments has a defined mass, a defined initial length (and volume), an initial pressure, and may have an initial velocity. In addition to the mass of gas present in each element there may be an initial amount of liquid fuel. The force acting to accelerate each gas element is the algebraic sum of the difference in pressure forces acting on its ends, the shear forces on the walls, and the momentum flux from mass addition from the liquid droplets (which are presumed to remain at rest). The mass addition rate may be any desired function of Reynolds number, Weber number, initial droplet size, etc. The change in velocity of each element during each interval of time is assumed to be just the acceleration multiplied by Δt. The motion of each element during each element of time is computed as velocity multiplied by Δt. The pressure in each element may be computed by any one of a number of possible state equations such as:

$$P V^{\gamma} = K M \qquad (25)$$

where M is the mass of gas in the element or $P V = (\gamma - 1) E$ where E is internal energy, or by any other desired analytic or tabular formulation. There are several simplifications involved in this model of wave action. These are not inherent in the method but merely are chosen to permit an answer to be obtained in

the computing time available. The present computing program contains several thousand instructions and is of the maximum size which can be fitted into the 8000 magnetic memory cores of the IBM 704 Electronic Data Processing Machine.

For a 24-segment model of an eight-foot shock tube, ten microseconds appears to be a reasonable time interval, if mathematical instability is to be avoided. Thus, if 100 computational operations are performed for each element per time interval, there would be 24 x 100 x 100,000 or 2.4×10^8 computations for each second of model time. Though fairly expensive, results are obtained which are completely beyond the capabilities of any known analytic technique.

The model may be operated for any desired initial distribution of pressures, masses, velocity, etc., along its length, and each end may be open or closed. In addition, the two ends may be connected to form a toroid for the purposes of computation, with material leaving one end and entering the other.

The computed resultant distributions of pressure, velocity, etc., may be recorded in digital form by a printer, or they may be presented in analog form by machine plotting the points on the face of a cathode ray tube which is then photographed. Results of an early calculation are presented in Appendix II.

VI

CONCLUSIONS

It appears that the effects of gas motion upon heterogeneous combustion may be determined using any of several types of experimental apparatus, each of which will have certain advantages and disadvantages. The quartz fibre type of apparatus permits absolute values for burning rate per unit of fuel surface to be measured, but cannot be used at extremely high Reynolds numbers where liquid fuel is blown off the fibre. The shock tube apparatus has no obvious Reynolds number limitation, and further, the shock tube permits data to be gathered relative to the rate of response of combustion to very rapid transient changes in conditions. The absolute magnitudes of the heat and mass transport coefficients obtained in the shock tube, however, are at present somewhat in doubt, since the droplet size distribution is not accurately known.

The combustion data gathered so far seem to indicate that in the region of low and moderate Reynolds number, combustion responds to Reynolds number in the same manner as do heat and mass transfer. At high Reynolds number, combustion of liquid droplets may be enhanced even further due to the shattering of the droplets. It does not seem to matter much whether the Reynolds number is produced by a steady flow of gas, by the action of an acoustic standing wave, or by a shock wave.

It is reasonably certain then that the rate determining steps in rocket engine combustion (with liquid oxygen as the oxidizer), are the heat and mass transfer processes associated with the individual propellant droplets. Accurate knowledge of the relationship of these processes to Reynolds number and other pertinent parameters should permit rocket engine combustion behavior to be computed for steady-state, transient, or oscillatory conditions if sufficiently powerful computing methods are employed.

VII

RECOMMENDATIONS

It has been shown here that with suitable techniques, heterogeneous combustion may be studied under the extreme conditions typical of rocket engine combustion (i.e., pure oxygen oxidizer, high pressure, high Reynolds number). Although the feasibility of doing this has been demonstrated, there still remains the task of collecting large amounts of data under systematically varied conditions, and the improvement of the accuracy of the data obtained. This certainly must be done before rocket combustion can become truly amenable to scientific methods.

Related to the problem of heterogeneous combustion of fuel sprays is the still unsolved problem of the production of the spray. Little is at present known about the effects of propellant stream Reynolds number, Weber number, or impingement angles upon the droplet sizes of the spray produced by rocket injector elements. Neither is there sufficient information about the rapidity of the atomization process following injection or impingement. This information must be acquired before rocket engine injectors can be rationally designed, and would be of great assistance even in the design of scientific apparatus such as the shock tube described here.

Another closely related combustion process needing study is the mixing of gross fuel-rich and fuel-lean regions in their flow through the chamber. The failure of such mixing to be completed has long been a recognized cause of low engine performance and engine damage. In addition it is possible that the periodic mixing of such regions may be important in driving certain types of combustion instability. Despite this, very little is known about the rapidity of, and the conditions governing this process under either smooth or unstable conditions.

The use of storable propellant systems in which one of the propellants cannot be considered to be completely vaporized, as was done for LOX, poses a more complex problem. However, the use of similar types of test apparatus should provide the type of information from which the processes of combustion could be delineated.

Thus it is recommended that work be continued in the study of heterogeneous combustion under extreme conditions, and in addition that the related processes of liquid atomization and gas phase mixing be studied.

APPENDIX I

CONDITIONS TO BE EXPECTED IN ROCKET ENGINE COMBUSTION

STEADY COMBUSTION

The Reynolds numbers calculated in the most general sort of model of rocket engine combustion must be found by the painstaking numerical integration of droplet drag forces, evaporation rates, etc., to derive the necessary relative velocities between droplets and gas. The maximum Reynolds numbers to be encountered, however, may be readily estimated. In Reference 2 it was shown that the acceleration of a large diameter droplet, say of diameter 500 to 600 micron is quite small, and thus the droplet velocity always remains small relative to the gas. In this case the relative velocity may be set equal to the gas velocity without introducing great error. The Reynolds number may then be written in the form:

$$Re = \frac{\rho_{gas} \; V_{gas} \; D_{drop}}{\mu_{gas}}$$

where

$$\rho_{gas} \times V_{gas} = \frac{\dot{M}_{gas}}{A}$$

If the mass flowrate through the engine, the cross-sectional area of the thrust chamber, and the fraction of total propellant which is combusted is known or estimated at some axial station, then the maximum Reynolds number per centimeter of droplet diameter may be estimated:

$$\frac{Re}{cm} = \frac{\dfrac{\dot{M}_{Total\ Propellant}}{Area} \times Z}{\mu_{gas}}$$

where Z is the fraction of total propellant which is combusted and in the gas phase. If μ is taken to be 2.0×10^{-4} poise, then:

$$\frac{Re}{cm} = 350{,}000 \times Z \times \frac{\dot{M}}{A}$$

where $\frac{\dot{M}}{A}$ is expressed in pounds per square inch per second.

The mass velocity, $\frac{\dot{M}}{A}$, lies between 1.0 and 10.0 pounds per square inch per second for engines built with today's technology. Thus, for a station where Z has a value near to one, reasonable values for $\frac{Re}{cm}$ would lie in the range of 350,000 to 3,500,000. For 500 micron drops the corresponding Reynolds numbers would be 17,500 to 175,000.

Assuming that combustion is largely completed by the time the propellant flows through the throat, it is at this point that the highest values for $\frac{Re}{cm}$ will be attained. At the throat

$$\frac{\dot{M}}{A} = \frac{P_c \times g}{C^*}$$

where $\frac{\dot{M}}{A}$ is expressed in pounds per square inch per second, P_c is chamber pressure in pounds per square inch, g is 32.2 feet/sec^2 and C* is the characteristic velocity in feet per second.

If C* = 5,000 feet/sec, then at the throat:

$$\frac{Re}{cm} = 2250 \times P_c$$

when P_c is expressed in pounds per square inch.

Thus, for any engine having a chamber pressure of 450 psi the conditions at the throat will be such that the value of Reynolds number per centimeter will be in the neighborhood of 1,000,000. Obviously, if some small fraction of the propellant, perhaps in the form of very large drops, reaches the throat of the engine unburned, its combustion will be greatly accelerated by the action of the high gas velocities.

Unstable Combustion

From the classic acoustic equations for a standing wave (see page 10) it may be shown that at a velocity loop the time average value for Reynolds number per centimeter is:

$$Re/cm = \frac{P_{max}}{\pi \mu c}$$

For a wave form which is sinusoidal.

If the typical values are chosen $\mu = 2.0 \times 10^{-4}$ poise and $a = 100{,}000$ cm/sec for the speed of sound in the hot combustion products, then

$$\overline{Re/cm} = P_{max} \times 3{,}400$$

where P_{max} is the peak-to-peak pressure amplitude measured at a pressure loop in pounds per square inches. Thus if $P_{max} = 200$ psi the mean value for Reynolds number per centimeter would be:

$$\overline{Re/cm} = 680{,}000$$

The maximum value for $\frac{Re}{cm}$ attained during a cycle would be about 1.4 times this value, or:

$$Re/cm_{(max)} = 950{,}000$$

APPENDIX II

COMPUTATIONS USED TO REDUCE SHOCK TUBE DATA

Assume that a wave disturbance is passing down an oxygen and fuel-spray filled tube. If the pressure profile in the tube has the appearance shown in Fig. 31A at some initial time, then barring reflection, attenuation, or growth it would be expected to appear as in Fig. 31B a time interval Δt later, i.e., it would just be expected to have moved a distance $C\Delta t$ where C is the wave velocity. If instead of simply translating a distance $C\Delta t$ unchanged the wave ends up larger than it initially was, as in Fig. 31C this growth must be due to combustion which takes place at the position of the wave, and which adds to its pressure as it moves along. If the rigorous but insoluble exact equations which describe the wave's action are ignored for the sake of an answer, and it is assumed that the cross-hatched pressure-volume in Fig31C is derived from the combustion which took place at the location of the wave during the time interval Δt, the pressure rise due to combustion (Fig. 25) can be related to the amount of fuel consumed. For example, assume that the channel of the tube initially contains 2/3 gram of oxygen and 3/4 gram of fuel per foot of length. Assume that a pulse is introduced which is about one foot long and of 2.0 atmospheres average absolute pressure, and that after a time interval of one millisecond the pulse has grown to 4.0 atmospheres absolute pressure. From Fig. 25 it may be seen that a 2.0 atmosphere rise in pressure corresponds to the combustion of about .02 grams of fuel per gram of oxygen initially present. If only the 2/3 gram of oxygen per foot initially present in the tube before the arrival of the wave is considered, then it would appear that the pressure rise corresponds to the combustion of .0133 gram of fuel at the position of the wave during the one millisecond period. (If an attempt were made to base the computation upon the oxygen initially present plus the amount presumed to have flowed in due to the action of the wave, a very similar value would be obtained for the amount of fuel consumed due to the nearly linear nature of the curve in the fuel-lean region.) The absolute time-average value for the combustion rate may now be computed to be 13.3 grams of fuel per second per foot of tube. The specific combustion rate would be computed as 17.8 grams of fuel per second per gram of fuel present. If a second wave were immediately to pass the same point in the tube the specific combustion rate for it would be based upon the remaining amount of fuel per foot instead of the initial .750. Where plots of specific combustion rate versus Reynolds number are shown the value for Reynolds number is obtained from Fig. 29, and the pressure ratio used was the mean value for the wave at the end of the time period under consideration. On this basis the wave just discussed would be assigned a pressure ratio of 4.0 which would correspond to a Reynolds number of about 480,000 per centimeter. Rather than trying to justify much distance and time-averaging for the waves, it is better to break down the wave into a series of sufficiently short axial segments and to consider the growth of each of these segments over a sufficiently short time interval that little averaging is necessary.

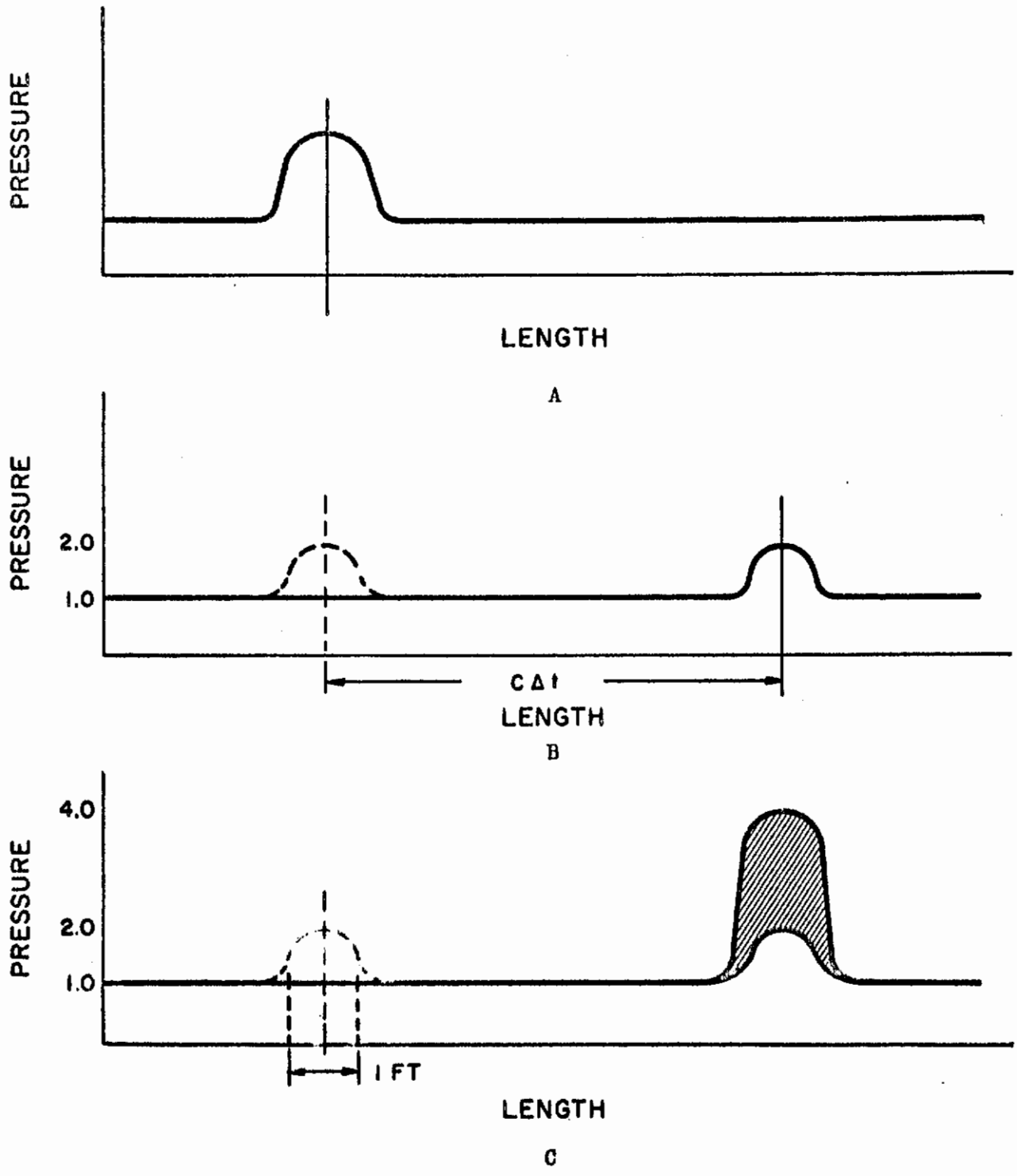

Figure 31. Shock Tube Pressure Profiles

This rather crude method of approximate computation has two great advantages. First, since large errors are introduced at the very start, small errors can be cheerfully ignored later on. Second, rough information is obtained which could not at present be obtained otherwise. This rough information will be invaluable in indicating the sort of combustion model needed in the numerical model, which we trust can be used to fit the pressure profile data exactly and with rigor.

APPENDIX III

TEST SUMMARIES

TABLE 1

TEST SUMMARY - QUARTZ FIBRE STUDIES

Test No.	Absolute Chamber Pressure, atm	Gas Flow Velocity, cm/sec	Cylinder Diameter, cm	Cylinder Length, cm	Fuel Flow Rate, gm/sec	Fuel Consumption Rate, $_2$ moles/cm^2-sec	Reynolds Number
1	0.9	0	0.070	1.78	0.0022	0.00018	....
2	0.9	0	0.065	1.85	0.0022	0.00018	....
3	0.9	0	0.050	1.50	0.0012	0.00016	....
4	3.4	0	0.055	1.92	0.0032	0.00030	....
5	3.4	0	0.060	2.10	0.0043	0.00034	....
6	6.8	0	0.060	2.05	0.0056	0.00045	....
7	6.8	0	0.065	2.32	0.0075	0.00049	....
8	10.2	0	0.065	1.78	0.0067	0.00058	....
9	10.2	0	0.065	1.92	0.0076	0.00061	....
10	3.4	200	0.070	2.50	0.0125	0.00071	340
11	3.4	600	0.070	2.02	0.0256	0.00182	1020
12	3.4	1000	0.065	1.51	0.0225	0.00227	1580
13	6.8	200	0.055	2.01	0.0134	0.00119	540
14	6.8	600	0.060	1.78	0.0242	0.00223	1750
15	6.8	1000	0.060	1.85	0.0348	0.00310	2920
16	10.2	200	0.070	2.61	0.0208	0.00114	1020
17	10.2	600	0.050	1.34	0.0169	0.00252	2140
18	10.2	1000	0.055	1.61	0.0268	0.00300	4020
19	3.4	*1690	0.070	1.34	0.0293	0.00316	*2460
20	5.1	*1500	0.065	1.82	0.0485	0.00408	*3570
21	6.8	*1570	0.070	1.21	0.0369	0.00434	*5340

*Estimated average velocity for oscillating flow in acoustic field.

TABLE 2

TEST SUMMARY - SHOCK TUBE STUDIES

Position in Tube, ft and Time Interval, m.s.	Average $\frac{\dot{M}}{M}$	Average Pressure Atmospheres (Abs)	Average Reynolds No/cm	Average Reynolds Number (based on 1000 micron drop)
First 1.9 ft segment t = 0 to t = 1.0	18.5	2.2	200,000	20,000
First 1.9 ft segment t = 1.0 to t = 2.0	25.1	1.8	135,000	13,500
First 1.9 ft segment t = 2.0 to t = 3.0	42.0	2.6	255,000	25,500
First 1.9 ft segment t = 3.0 to t = 4.0	32.5	2.2	200,000	20,000
Second 1.9 ft segment t = 1.0 to t = 2.0	20.5	3.6	412,000	41,200
Second 1.9 ft segment t = 2.0 to t = 3.0	86.0	7.6	850,000	85,000
Second 1.9 ft segment t = 3.0 to t = 4.0	48.2	5.8	685,000	68,500
Third 1.9 ft segment t = 2.0 to t = 3.0	215.5	18.4	1,287,000	128,700
Third 1.9 ft segment t = 3.0 to t = 4.0	151.0	12.2	1,120,000	112,000
Fourth 1.9 ft segment t = 3.0 to t = 4.0	99.0	25.0	1,416,000	141,600

APPENDIX IV

TABULATIONS OF COMPUTED WAVE PARAMETERS

The following tabulated values and their photographic analog representations are the results of an early wave-model computation. The tube, 255 cm long is divided into 24 segments for the purposes of computation. The pipe length is represented as 2.550E 02 on the machine print, which should be read as $2.550 \times 10^{+2}$ or 2.55 times ten raised to the exponent 2. The time interval between successive computations is printed as 3.333E -06 and thus is only one three hundredth of a millisecond. The gas properties and other pertinent input data are also listed in the heading of the printout.

The values of nine important variables for each of the twenty-four segments are listed in the columns under the heading "1" which stands for the first computational period.

The heading DIST is the distance along the tube of the twenty-four movable segment boundaries. Under the heading PRES is listed the pressures in each of the segments. VOL refers to the volume of each segment while VEL refers to the velocity of its centroid;i.e., the particle velocity. MASSG is the mass of gas in each segment and MASSL is the mass of liquid. REYN is the droplet Reynolds number as defined in the body of this report. DIAM refers to droplet diameter of the liquid phase, and MDOT is mass rate of combustion as given in Equation 6.

Obviously the computation is for a system which is initially at rest, and in which no liquid or combustion is present. The pressures of 1.667×10^6 dynes per square centimeter or about 24.2 psia in the first four segments (37.2 cm or 14.6 inches) of the tube and 1.000×10^6 dynes per square centimeter or 14.5 psia in the remainder of the tube roughly correspond to the pressures which are just sufficient to produce detonation when passed through a burning spray in the real shock tube.

The next block of tabulated values are under the heading (.90) which indicates that they are for a time .90 millisecond after initiation of the action in the tube. The two hundred and seventy intervening computed profiles are not presented, as the sequential changes would be too slight. Obviously even with the computational time period this short, there is excessive computational instability. Techniques are known (Ref. 12) by which an artificial damping force may be applied to any segment which is being rapidly compressed in order to overcome this instability. The use of such techniques will doubtless be necessary before adequate computations may be performed for high-pressure-ratio waves. The first seven photographs are machine-made plots of pressure vs distance along the tube at the same time-instants for which the values are printed. Photographs 8 through 14 show the particle velocities as the same function of time and distance along the tube.

RUN NO	TUBE	PH CH	NU CH	DRAG
1	1	0	0	1

PIPE LENGTH	PIPE AREA	PIPE PERI	DELTA TIME	WEBER CRIT
2.550E 02	2.025E 01	1.600E 01	3.333E-06	1.000E 01

SURF TENS	EVAP CONST	GAMMA	GAS LAW CONST	VISCOSITY
2.000E 01	1.875E-02	1.400E 00	3.740E 09	1.800E-04

1

DIST	PRES	VOL	VEL	MASSG	MASSL	REYN	DIAM	MDO
5.312E 00	8.333E 06	2.152E 02	0.	4.081E 00	0.	0.	0.	0.
1.594E 01	8.333E 06	2.152E 02	0.	4.081E 00	0.	0.	0.	0.
2.656E 01	8.333E 06	2.152E 02	0.	4.081E 00	0.	0.	0.	0.
3.719E 01	8.333E 06	2.152E 02	0.	4.081E 00	0.	0.	0.	0.
4.781E 01	1.000E 06	2.152E 02	0.	4.898E-01	0.	0.	0.	0.
5.844E 01	1.000E 06	2.152E 02	0.	4.898E-01	0.	0.	0.	0.
6.906E 01	1.000E 06	2.152E 02	0.	4.898E-01	0.	0.	0.	0.
7.969E 01	1.000E 06	2.152E 02	0.	4.898E-01	0.	0.	0.	0.
9.031E 01	1.000E 06	2.152E 02	0.	4.898E-01	0.	0.	0.	0.
1.009E 02	1.000E 06	2.152E 02	0.	4.898E-01	0.	0.	0.	0.
1.116E 02	1.000E 06	2.152E 02	0.	4.898E-01	0.	0.	0.	0.
1.222E 02	1.000E 06	2.152E 02	0.	4.898E-01	0.	0.	0.	0.
1.328E 02	1.000E 06	2.152E 02	0.	4.898E-01	0.	0.	0.	0.
1.434E 02	1.000E 06	2.152E 02	0.	4.898E-01	0.	0.	0.	0.
1.541E 02	1.000E 06	2.152E 02	0.	4.898E-01	0.	0.	0.	0.
1.647E 02	1.000E 06	2.152E 02	0.	4.898E-01	0.	0.	0.	0.
1.753E 02	1.000E 06	2.152E 02	0.	4.898E-01	0.	0.	0.	0.
1.859E 02	1.000E 06	2.152E 02	0.	4.898E-01	0.	0.	0.	0.
1.966E 02	1.000E 06	2.152E 02	0.	4.898E-01	0.	0.	0.	0.
2.072E 02	1.000E 06	2.152E 02	0.	4.898E-01	0.	0.	0.	0.
2.178E 02	1.000E 06	2.152E 02	0.	4.898E-01	0.	0.	0.	0.
2.284E 02	1.000E 06	2.152E 02	0.	4.898E-01	0.	0.	0.	0.
2.391E 02	1.000E 06	2.152E 02	0.	4.898E-01	0.	0.	0.	0.
2.497E 02	1.000E 06	2.152E 02	0.	4.898E-01	0.	0.	0.	0.

t = .90

DIST	PRES	VOL	VEL	MASSG	MASSL	REYN	DIAM	MDOT
5.337E 00	8.223E 06	2.162E 02	1.882E 02	4.081E 00	0.	0.	0.	0.
1.623E 01	7.765E 06	2.252E 02	1.568E 03	4.081E 00	0.	0.	0.	0.
2.858E 01	5.876E 06	2.748E 02	6.644E 03	4.081E 00	0.	0.	0.	0.
4.674E 01	2.850E 06	4.607E 02	1.635E 04	4.081E 00	0.	0.	0.	0.
6.071E 01	2.709E 06	1.051E 02	2.183E 04	4.898E-01	0.	0.	0.	0.
6.492E 01	5.232E 06	6.566E 01	2.318E 04	4.898E-01	0.	0.	0.	0.
7.053E 01	1.495E 06	1.615E 02	1.327E 04	4.898E-01	0.	0.	0.	0.
7.976E 01	1.012E 06	2.123E 02	8.626E 02	4.898E-01	0.	0.	0.	0.
9.032E 01	3.938E 05	2.151E 02	3.229E 01	4.898E-01	0.	0.	0.	0.
1.008E 02	9.932E 05	2.152E 02	9.692E-01	4.898E-01	0.	0.	0.	0.
1.116E 02	9.932E 05	2.152E 02	1.078E-02	4.898E-01	0.	0.	0.	0.
1.222E 02	9.932E 05	2.152E 02	-0.	4.898E-01	0.	0.	0.	0.
1.328E 02	9.932E 05	2.152E 02	-0.	4.898E-01	0.	0.	0.	0.
1.434E 02	9.932E 05	2.152E 02	-0.	4.898E-01	0.	0.	0.	0.
1.541E 02	9.932E 05	2.152E 02	-0.	4.898E-01	0.	0.	0.	0.
1.647E 02	9.932E 05	2.152E 02	-0.	4.898E-01	0.	0.	0.	0.
1.753E 02	9.932E 05	2.152E 02	-0.	4.898E-01	0.	0.	0.	0.
1.859E 02	9.932E 05	2.152E 02	-0.	4.898E-01	0.	0.	0.	0.
1.966E 02	9.932E 05	2.152E 02	-0.	4.898E-01	0.	0.	0.	0.
2.072E 02	9.932E 05	2.152E 02	-0.	4.898E-01	0.	0.	0.	0.
2.178E 02	9.932E 05	2.152E 02	-0.	4.898E-01	0.	0.	0.	0.
2.284E 02	9.932E 05	2.152E 02	-0.	4.898E-01	0.	0.	0.	0.
2.391E 02	9.932E 05	2.152E 02	-0.	4.898E-01	0.	0.	0.	0.
2.497E 02	9.932E 05	2.152E 02	-0.	4.898E-01	0.	0.	0.	0.

t = 1.8

DIST	PRES	VOL	VEL	MASSG	MASSL	REYN	DIAM	MDOT
6.504E 00	6.235E 06	2.634E 02	2.761E 03	4.081E 00	0.	0.	0.	0.
2.071E 01	4.917E 06	3.121E 02	8.584E 03	4.081E 00	0.	0.	0.	0.
3.875E 01	3.262E 06	4.184E 02	1.499E 04	4.081E 00	0.	0.	0.	0.
6.230E 01	2.310E 06	5.353E 02	1.736E 04	4.081E 00	0.	0.	0.	0.
7.805E 01	2.804E 06	1.025E 02	1.946E 04	4.898E-01	0.	0.	0.	0.
8.339E 01	2.427E 06	1.137E 02	1.521E 04	4.898E-01	0.	0.	0.	0.
8.899E 01	2.442E 06	1.132E 02	2.053E 04	4.898E-01	0.	0.	0.	0.
9.420E 01	2.991E 06	9.789E 01	1.939E 04	4.898E-01	0.	0.	0.	0.
1.006E 02	1.497E 06	1.605E 02	1.873E 04	4.898E-01	0.	0.	0.	0.
1.059E 02	6.766E 06	5.464E 01	2.384E 04	4.898E-01	0.	0.	0.	0.
1.121E 02	1.136E 06	1.955E 02	8.074E 03	4.898E-01	0.	0.	0.	0.
1.222E 02	9.958E 05	2.148E 02	1.697E 02	4.898E-01	0.	0.	0.	0.
1.328E 02	9.932E 05	2.151E 02	3.265E 00	4.898E-01	0.	0.	0.	0.
1.434E 02	9.932E 05	2.152E 02	4.969E-02	4.898E-01	0.	0.	0.	0.
1.541E 02	9.932E 05	2.152E 02	0.	4.898E-01	0.	0.	0.	0.
1.647E 02	9.932E 05	2.152E 02	0.	4.898E-01	0.	0.	0.	0.
1.753E 02	9.932E 05	2.152E 02	0.	4.898E-01	0.	0.	0.	0.
1.859E 02	9.932E 05	2.152E 02	0.	4.898E-01	0.	0.	0.	0.
1.966E 02	9.932E 05	2.152E 02	0.	4.898E-01	0.	0.	0.	0.
2.072E 02	9.932E 05	2.152E 02	0.	4.898E-01	0.	0.	0.	0.
2.178E 02	9.932E 05	2.152E 02	0.	4.898E-01	0.	0.	0.	0.
2.284E 02	9.932E 05	2.152E 02	0.	4.898E-01	0.	0.	0.	0.
2.391E 02	9.932E 05	2.152E 02	0.	4.898E-01	0.	0.	0.	0.
2.497E 02	9.932E 05	2.152E 02	0.	4.898E-01	0.	0.	0.	0.

t = 2.7

DIST	PRES	VOL	VEL	MASSG	MASSL	REYN	DIAM	MDOT
9.924E 00	3.451E 06	4.019E 02	4.455E 03	4.081E 00	0.	0.	0.	0.
3.055E 01	3.106E 06	4.333E 02	1.247E 04	4.081E 00	0.	0.	0.	0.
5.370E 01	2.511E 06	5.044E 02	1.738E 04	4.081E 00	0.	0.	0.	0.
7.788E 01	2.734E 06	4.747E 02	1.719E 04	4.081E 00	0.	0.	0.	0.
9.238E 01	2.459E 06	1.126E 02	1.329E 04	4.898E-01	0.	0.	0.	0.
9.779E 01	2.653E 06	1.067E 02	1.687E 04	4.898E-01	0.	0.	0.	0.
1.034E 02	2.211E 06	1.215E 02	1.353E 04	4.898E-01	0.	0.	0.	0.
1.097E 02	1.928E 06	1.339E 02	1.649E 04	4.898E-01	0.	0.	0.	0.
1.153E 02	3.210E 06	9.308E 01	1.679E 04	4.898E-01	0.	0.	0.	0.
1.224E 02	1.152E 06	1.936E 02	9.671E 03	4.898E-01	0.	0.	0.	0.
1.286E 02	6.231E 06	5.795E 01	2.063E 04	4.898E-01	0.	0.	0.	0.
1.344E 02	1.321E 06	1.755E 02	1.351E 04	4.898E-01	0.	0.	0.	0.
1.426E 02	1.547E 06	1.568E 02	1.869E 04	4.898E-01	0.	0.	0.	0.
1.479E 02	5.956E 06	5.985E 01	2.452E 04	4.898E-01	0.	0.	0.	0.
1.544E 02	1.087E 06	2.018E 02	6.044E 03	4.898E-01	0.	0.	0.	0.
1.647E 02	9.945E 05	2.149E 02	1.015E 02	4.898E-01	0.	0.	0.	0.
1.753E 02	9.932E 05	2.152E 02	1.426E 00	4.898E-01	0.	0.	0.	0.
1.859E 02	9.932E 05	2.152E 02	6.744E-03	4.898E-01	0.	0.	0.	0.
1.966E 02	9.932E 05	2.152E 02	-0.	4.898E-01	0.	0.	0.	0.
2.072E 02	9.932E 05	2.152E 02	-0.	4.898E-01	0.	0.	0.	0.
2.178E 02	9.932E 05	2.152E 02	-0.	4.898E-01	0.	0.	0.	0.
2.284E 02	9.932E 05	2.152E 02	-0.	4.898E-01	0.	0.	0.	0.
2.391E 02	9.932E 05	2.152E 02	-0.	4.898E-01	0.	0.	0.	0.
2.497E 02	9.932E 05	2.152E 02	-0.	4.898E-01	0.	0.	0.	0.

t = 3.6

DIST	PRES	VOL	VEL	MASSG	MASSL	REYN	DIAM	ME
1.406E 01	2.120E 06	5.693E 02	4.588E 03	4.081E 00	0.	0.	0.	0.
4.202E 01	2.151E 06	5.633E 02	1.258E 04	4.081E 00	0.	0.	0.	0.
6.886E 01	2.383E 06	5.236E 02	1.587E 04	4.081E 00	0.	0.	0.	0.
9.288E 01	2.951E 06	4.494E 02	1.598E 04	4.081E 00	0.	0.	0.	0.
1.064E 02	2.899E 06	1.001E 02	1.833E 04	4.898E-01	0.	0.	0.	0.
1.117E 02	2.428E 06	1.136E 02	1.432E 04	4.898E-01	0.	0.	0.	0.
1.170E 02	2.850E 06	1.013E 02	1.660E 04	4.898E-01	0.	0.	0.	0.
1.227E 02	2.050E 06	1.282E 02	1.410E 04	4.898E-01	0.	0.	0.	0.
1.288E 02	2.262E 06	1.195E 02	1.577E 04	4.898E-01	0.	0.	0.	0.
1.346E 02	2.379E 06	1.153E 02	1.475E 04	4.898E-01	0.	0.	0.	0.
1.420E 02	1.247E 06	1.829E 02	1.126E 04	4.898E-01	0.	0.	0.	0.
1.481E 02	5.546E 06	6.298E 01	1.786E 04	4.898E-01	0.	0.	0.	0.
1.546E 02	1.086E 06	2.019E 02	6.513E 03	4.898E-01	0.	0.	0.	0.
1.633E 02	1.662E 06	1.489E 02	1.678E 04	4.898E-01	0.	0.	0.	0.
1.688E 02	4.217E 06	7.660E 01	2.079E 04	4.898E-01	0.	0.	0.	0.
1.760E 02	1.010E 06	2.126E 02	2.957E 03	4.898E-01	0.	0.	0.	0.
1.852E 02	1.505E 06	1.599E 02	1.867E 04	4.898E-01	0.	0.	0.	0.
1.905E 02	6.401E 06	5.685E 01	2.523E 04	4.898E-01	0.	0.	0.	0.
1.969E 02	1.086E 06	2.019E 02	6.258E 03	4.898E-01	0.	0.	0.	0.
2.072E 02	9.944E 05	2.150E 02	9.617E 01	4.898E-01	0.	0.	0.	0.
2.178E 02	9.932E 05	2.152E 02	1.224E 00	4.898E-01	0.	0.	0.	0.
2.284E 02	9.932E 05	2.152E 02	4.741E-03	4.898E-01	0.	0.	0.	0.
2.391E 02	9.932E 05	2.152E 02	0.	4.898E-01	0.	0.	0.	0.
2.497E 02	9.932E 05	2.152E 02	0.	4.898E-01	0.	0.	0.	0.

1081

1351 t = 4.5

DIST	PRES	VOL	VEL	MASSG	MASSL	REYN	DIAM	MDOT
1.803E 01	1.496E 06	7.303E 02	4.190E 03	4.081E 00	0.	0.	0.	0.
5.260E 01	1.688E 06	6.699E 02	1.070E 04	4.081E 00	0.	0.	0.	0.
8.193E 01	2.419E 06	5.180E 02	1.315E 04	4.081E 00	0.	0.	0.	0.
1.067E 02	2.668E 06	4.830E 02	1.457E 04	4.081E 00	0.	0.	0.	0.
1.210E 02	2.928E 06	9.939E 01	1.302E 04	4.898E-01	0.	0.	0.	0.
1.262E 02	2.534E 06	1.102E 02	1.775E 04	4.898E-01	0.	0.	0.	0.
1.315E 02	2.752E 06	1.039E 02	1.491E 04	4.898E-01	0.	0.	0.	0.
1.369E 02	2.415E 06	1.141E 02	1.652E 04	4.898E-01	0.	0.	0.	0.
1.425E 02	2.382E 06	1.152E 02	1.551E 04	4.898E-01	0.	0.	0.	0.
1.482E 02	2.351E 06	1.163E 02	1.622E 04	4.898E-01	0.	0.	0.	0.
1.540E 02	2.294E 06	1.183E 02	1.523E 04	4.898E-01	0.	0.	0.	0.
1.607E 02	1.650E 06	1.497E 02	1.473E 04	4.898E-01	0.	0.	0.	0.
1.665E 02	3.483E 06	8.781E 01	1.620E 04	4.898E-01	0.	0.	0.	0.
1.739E 02	1.010E 06	2.126E 02	4.422E 03	4.898E-01	0.	0.	0.	0.
1.811E 02	4.163E 06	7.730E 01	1.772E 04	4.898E-01	0.	0.	0.	0.
1.869E 02	1.517E 06	1.590E 02	1.395E 04	4.898E-01	0.	0.	0.	0.
1.963E 02	9.507E 05	2.220E 02	7.245E 02	4.898E-01	0.	0.	0.	0.
2.039E 02	3.701E 06	8.408E 01	2.046E 04	4.898E-01	0.	0.	0.	0.
2.094E 02	1.867E 06	1.371E 02	1.866E 04	4.898E-01	0.	0.	0.	0.
2.182E 02	9.504E 05	2.220E 02	-7.875E 02	4.898E-01	0.	0.	0.	0.
2.281E 02	1.292E 06	1.783E 02	1.607E 04	4.898E-01	0.	0.	0.	0.
2.336E 02	9.005E 06	4.455E 01	2.609E 04	4.898E-01	0.	0.	0.	0.
2.396E 02	1.133E 06	1.959E 02	9.369E 03	4.898E-01	0.	0.	0.	0.
2.497E 02	9.949E 05	2.149E 02	1.361E 02	4.898E-01	0.	0.	0.	0.

1621 t = 5.4

DIST	PRES	VOL	VEL	MASSG	MASSL	REYN	DIAM	MDOT
2.151E 01	1.168E 06	8.712E 02	3.495E 03	4.081E 00	0.	0.	0.	0.
6.106E 01	1.494E 06	7.307E 02	8.058E 03	4.081E 00	0.	0.	0.	0.
9.258E 01	2.248E 06	5.458E 02	1.055E 04	4.081E 00	0.	0.	0.	0.
1.188E 02	2.445E 06	5.140E 02	1.235E 04	4.081E 00	0.	0.	0.	0.
1.342E 02	2.455E 06	1.127E 02	1.606E 04	4.898E-01	0.	0.	0.	0.
1.393E 02	3.152E 06	9.430E 01	1.187E 04	4.898E-01	0.	0.	0.	0.
1.451E 02	1.831E 06	1.390E 02	1.528E 04	4.898E-01	0.	0.	0.	0.
1.508E 02	3.318E 06	9.090E 01	1.400E 04	4.898E-01	0.	0.	0.	0.
1.566E 02	1.735E 06	1.444E 02	1.510E 04	4.898E-01	0.	0.	0.	0.
1.625E 02	3.194E 06	9.342E 01	1.495E 04	4.898E-01	0.	0.	0.	0.
1.682E 02	1.800E 06	1.407E 02	1.584E 04	4.898E-01	0.	0.	0.	0.
1.741E 02	3.067E 06	9.616E 01	1.562E 04	4.898E-01	0.	0.	0.	0.
1.802E 02	1.604E 06	1.528E 02	1.559E 04	4.898E-01	0.	0.	0.	0.
1.861E 02	3.708E 06	8.397E 01	1.643E 04	4.898E-01	0.	0.	0.	0.
1.928E 02	1.188E 06	1.893E 02	1.154E 04	4.898E-01	0.	0.	0.	0.
1.990E 02	6.091E 06	5.890E 01	1.725E 04	4.898E-01	0.	0.	0.	0.
2.056E 02	1.041E 06	2.080E 02	5.780E 03	4.898E-01	0.	0.	0.	0.
2.142E 02	1.757E 06	1.431E 02	1.518E 04	4.898E-01	0.	0.	0.	0.
2.200E 02	3.374E 06	8.983E 01	1.731E 04	4.898E-01	0.	0.	0.	0.
2.248E 02	2.644E 06	1.069E 02	-5.563E 04	4.898E-01	0.	0.	0.	0.
2.305E 02	2.158E 06	1.236E 02	-4.772E 04	4.898E-01	0.	0.	0.	0.
2.386E 02	1.072E 06	2.038E 02	4.492E 03	4.898E-01	0.	0.	0.	0.
2.455E 02	4.196E 06	7.687E 01	3.525E 04	4.898E-01	0.	0.	0.	0.
2.512E 02	1.598E 06	1.532E 02	3.952E 04	4.898E-01	0.	0.	0.	0.

RESULTS OF NUMERICAL WAVE MODEL

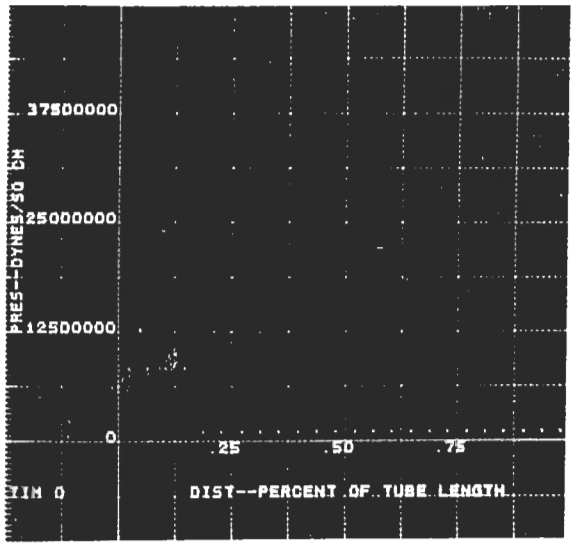

t = 0 ms

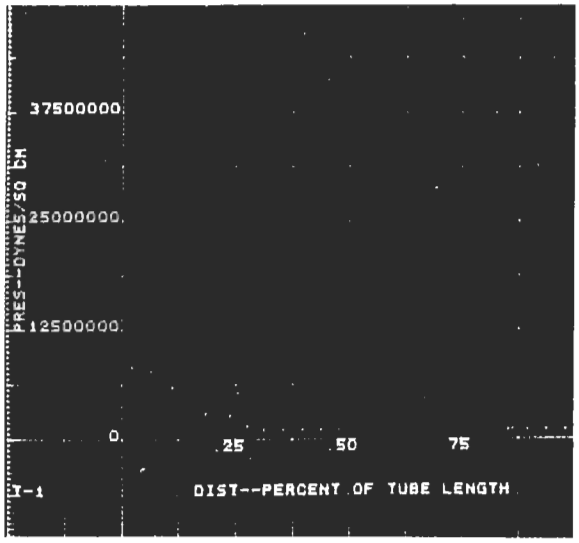

t = .90 ms

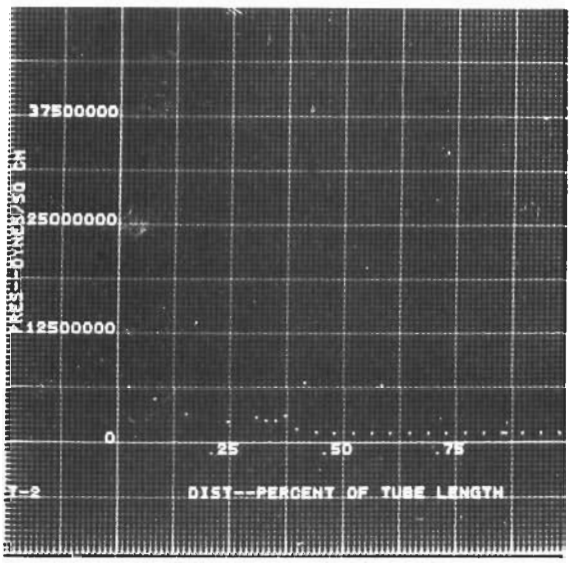

t = 1.8 ms

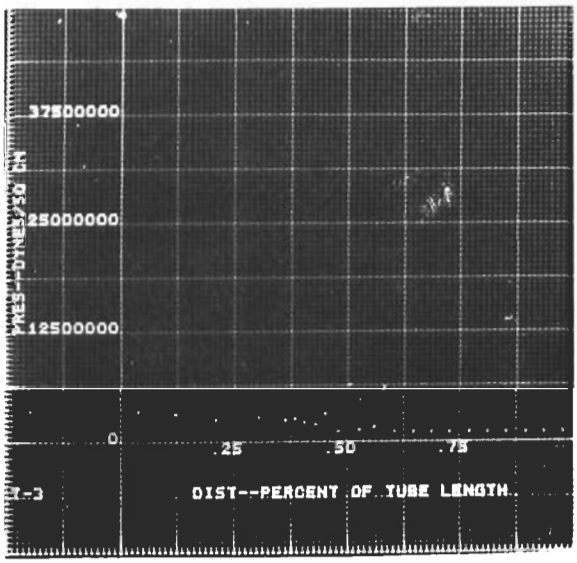

t = 2.7 ms

Figure 32. Computed Pressure vs Length of Tube

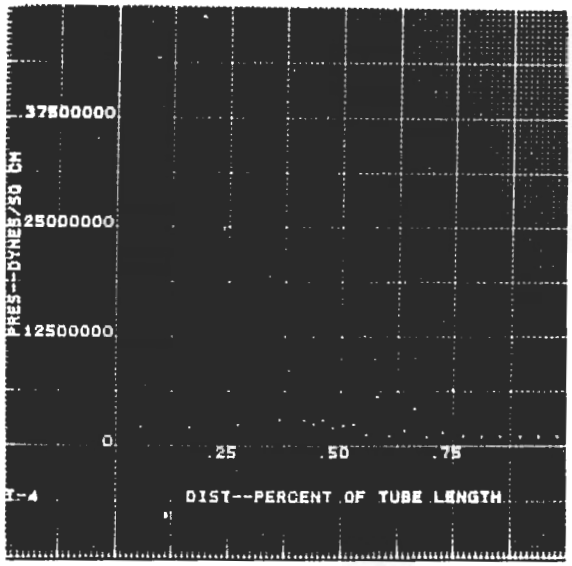

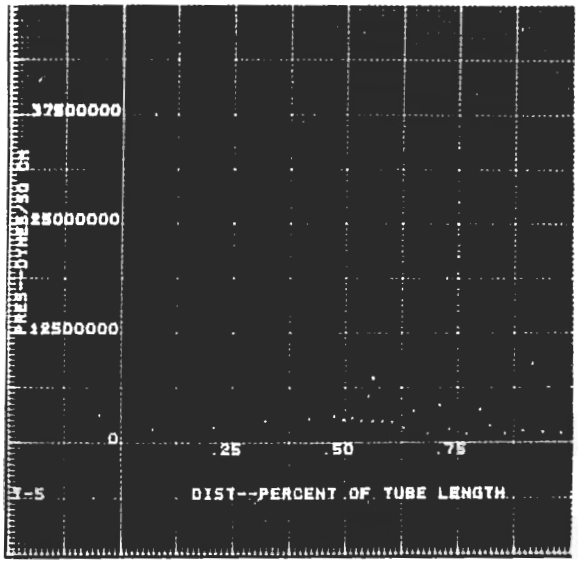

t = 4.5 ms

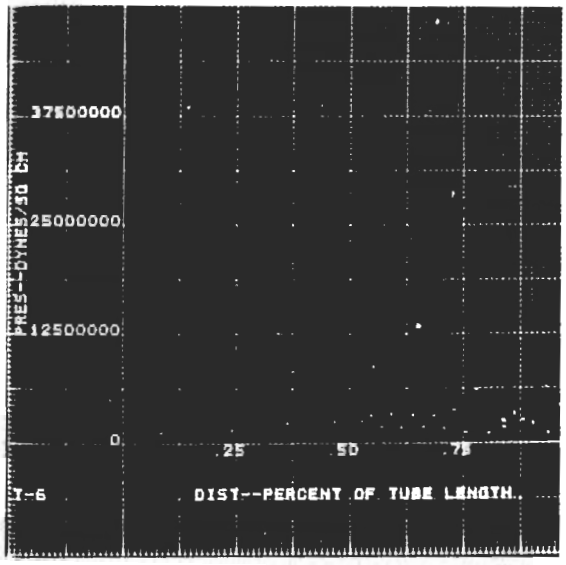

t = 5.4 ms

Figure 32 (Continued)

RESULTS OF NUMERICAL WAVE MODEL

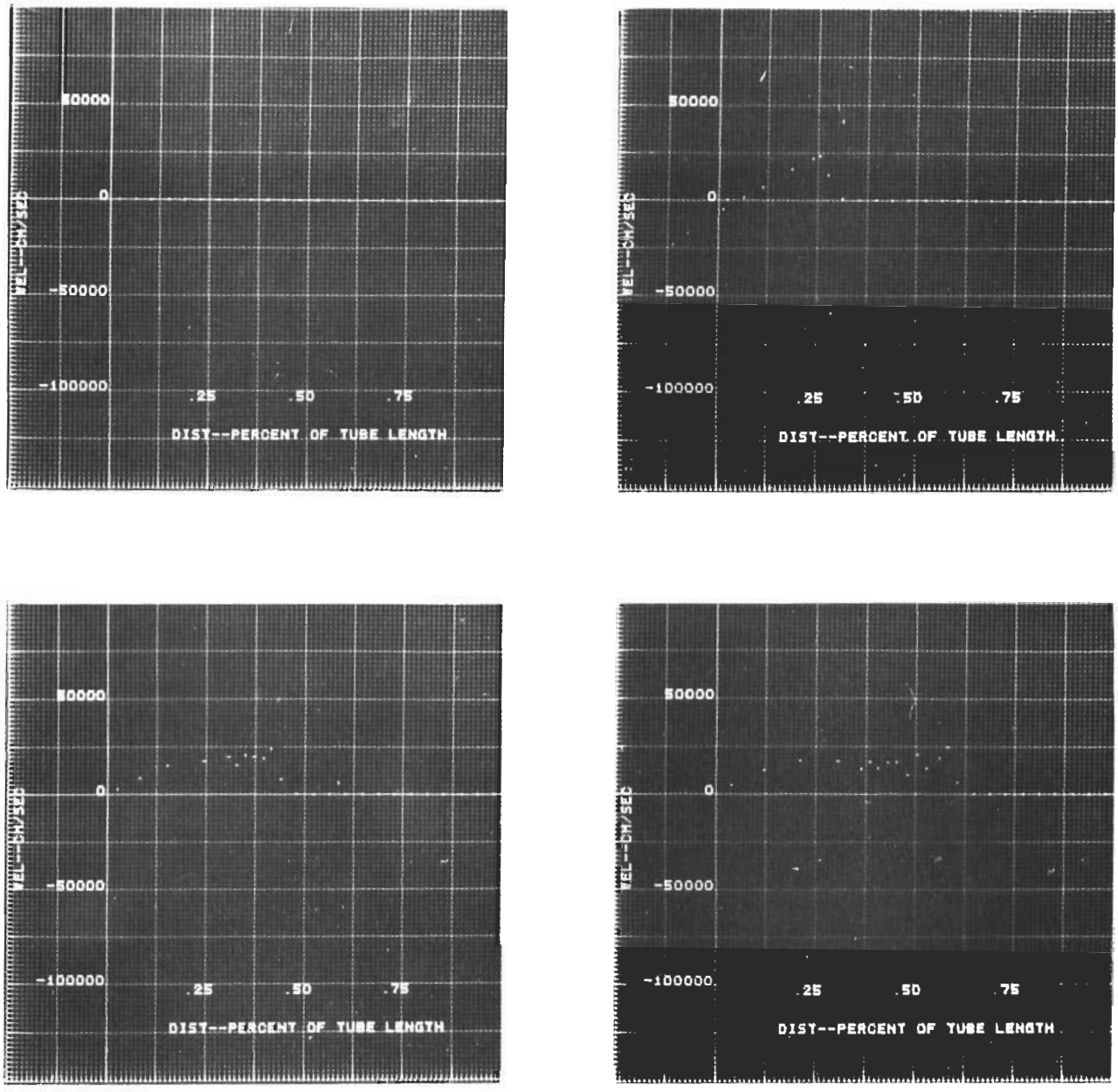

t = 1.8 ms

t = 2.7 ms

Figure 33. Computed Particle Velocity vs Length of Tube

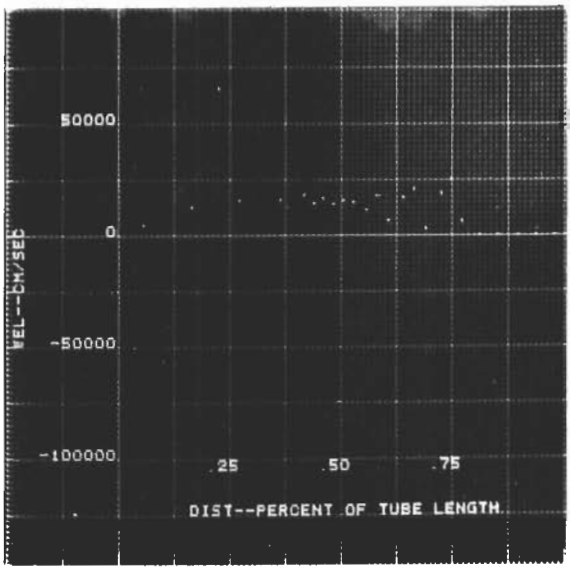

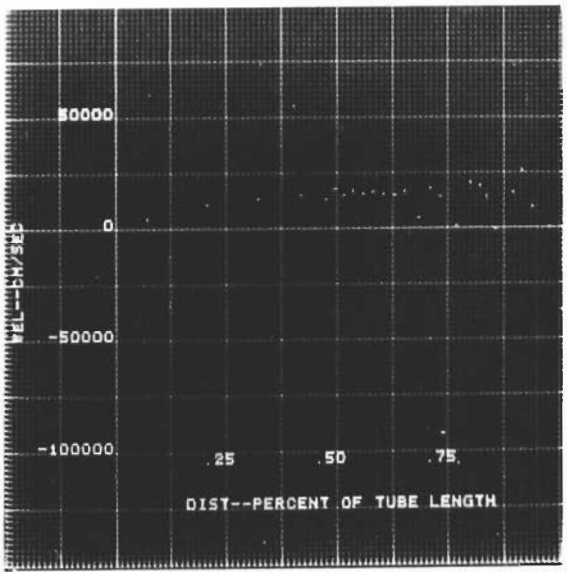

t = 4.5 ms

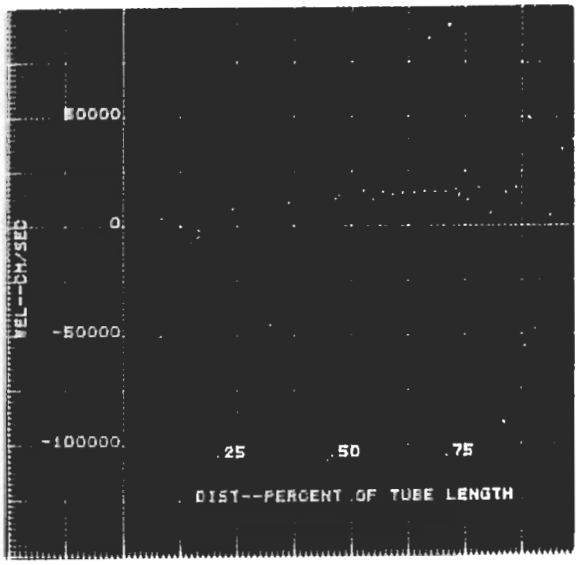

t = 5.4 ms

Figure 33 (Continued)

VIII BIBLIOGRAPHY

1. McAdams, W. H., Heat Transmission (Third Edition), McGraw-Hill, Inc., New York, 1954.

2. Cramer, F. B., Webber, W. T., and Lawhead, R. B., Research on the Basic Fluid Dynamic Phenomena Related to Rocket Combustion Instability, Summary Technical Note, WADC Technical Note 57-426, Wright Air Development Center, ASTIA A.D. 142255, Wright-Patterson Air Force Base, Ohio, 1958.

3. Treybal, R. E., Mass Transfer Operations, McGraw-Hill, Inc., New York, 1955.

4. Priem, R. J., Propellant Vaporization as a Criterion for Rocket Engine Design: Calculations of Chamber Length to Vaporize a Single n-Heptane Drop, NACA Technical Note 3985, National Advisory Committee for Aeronautics, Washington, D. C., 1957.

5. Priem, R. J., Propellant Vaporization as a Criterion for Rocket Engine Design: Calculations Using Various Log-Probability Distributions of Heptane Drops, NACA Technical Note 4098, National Advisory Committee for Aeronautics, Washington, D. C., 1957.

6. Miesse, C. C., "On the Combustion of a Liquid Fuel Spray," Sixth Symposium on Combustion, Reinhold Publishing Company, New York, 1957, p. 732.

7. Williams, F. A., Penner, S. S., Gill, G., and Eckel, E. F., Heterogeneous Burning in a Diverging Reactor, To be published.

8. Torda, T. P., Aerothermochemistry of Liquid Propellant Rocket Combustion Chambers, Brooklyn Polytechnic Institute TR-5-R850X-713428, 8 October 1958.

9. Mayer, E., On Vaporization Rate-Limited Combustion in Bipropellant Rocket Chambers, American Rocket Society Preprint No. 676-58, November 1958.

10. Spalding, D. B., A One-Dimensional Theory of Liquid-Fuel Rocket Combustion, Imperial College London, Aeronautical Research Council, A.R.C. 20, 175 - C.F. 440 - R. 435, May 1958.

11. Lawhead, R. B., Levine, R. S., and Webber, W. T., Liquid-Propellant Rocket Combustion Instability Studies, Final Summary Report Covering the Period 1 June 1954 to 30 November 1955, Rocketdyne Report No. R-122, Rocketdyne, A Division of North American Aviation, Inc., Canoga Park, Calif., January 1956.

12. Study of Detonation Behavior of Solid Propellants, Aeronutronic Systems, Inc. Publication Number U-154, Contract No. NOrd-17945, Navy Bureau of Ordnance.

13. Wachtell, G. P., "A Theory of the Spread of Flame in a Propellant Bed," Proceedings of the Gas Dynamics Symposium on Aerothermochemistry, Northwestern University, Evanston, Illinois, 1955.

14. Godsave, G. A. E., "Studies of the Combustion of Drops in a Fuel Spray -- The Burning of Single Drops of Fuel," Fourth Symposium on Combustion, Williams and Wilkins, Baltimore, Md., 1953, p. 818.

15. Goldsmith, M., and Penner, S. S., "On the Burning of Single Drops of Fuel in an Oxidizing Atmosphere," Jet Propulsion, Vol. 24, July-August 1954, p. 245.

16. Smith, A. L. and Graves, C. C., Drop Burning Rates of Hydrocarbon and Non-Hydrocarbon Fuels, NACA R.M. E 57 F 11, National Advisory Committee for Aeronautics, Washington, D. C., 1957.

17. Goldsmith, M., "Experiments on the Burning of Single Drops of Fuel," Jet Propulsion, Vol. 26, No. 3, March 1956, p. 172.

18. Spalding, D. B., Some Fundamentals of Combustion, Butterworth's Scientific Publications, London, 1955, p. 122.

19. Ranz, W. E. and Marshall, W. R., Chemical Engineering Progress, 48, 141, 1952, Chemical Engineering Progress, 48, 173, 1952.

20. Ingebo, R. D., Drag Coefficients for Droplets and Solid Spheres in Clouds Accelerating in Air Streams, NACA Technical Note 3762, National Advisory Committee for Aeronautics, Washington, D. C., 1956.

21. El Wakil, M. M., Uyehara, O. A., and Myers, P. S., A Theoretical Investigation of the Heating-Up Period of Injected Fuel Droplets Vaporizing in Air, NACA Technical Note 3179, National Advisory Committee for Aeronautics, Washington, D. C., 1954.

22. Miesse, C. C., "Ballistics of an Evaporating Droplet," Jet Propulsion, Vol. 24, July-August 1954, p. 237.

23. Lane, W. R., "Shatter of Drops in Streams of Air," Industrial Engineering and Chemistry, 43, No. 6, 1951, p. 1312.

24. Hanson, A. R., Romich, F. G., and Adams, H. S., An Experimental Investigation of Impact and Shock Wave Break-Up of Liquid Drops, Research Report 125, University of Minnesota, Institute of Technology, Department of Aeronautical Engineering, January 1956.

25. Rabin, E., and Cramer, F. B., Shattering of Burning and Non-Burning Propellant Droplets by Shock Waves, AFOSR Technical Note 58-62, ASTIA No. 148 104, Air Force Office of Scientific Research, Washington, D. C., 1958.

26. Rabin, E., and Lawhead, R. B., The Motion and Shattering of Burning and Non-Burning Propellant Droplets, WADC Technical Note 59-129, ASTIA 210-768, Wright Air Development Center, Wright-Patterson Air Force Base, Ohio, 1959.